

**SPATIOTEMPORAL DYNAMICS OF
HUMAN EPIDERMAL GROWTH FACTOR RECEPTOR 2 (HER2)
PROTRUSION SIGNALING**

By

Wai Yan Lam

A DISSERTATION

Presented to the Department of Biomedical Engineering
and the Oregon Health & Science University
School of Medicine
in partial fulfillment
of the requirements for the degree of

Doctor of Philosophy

September 2017

School of Medicine
Oregon Health & Science University

CERTIFICATE OF APPROVAL

This is to certify that the PhD dissertation of
Wai Yan Lam
has been approved

Mentor/Advisor – Tania Vu, PhD

Committee Chair – Jeffrey Tyner, PhD

Committee Member – Jim Korkola, PhD

Committee Member – Summer Gibbs, PhD

Committee Member – Young Hwan Chang, PhD

TABLE OF CONTENTS

CHAPTER 1: INTRODUCTION AND BACKGROUND	1
1.0 Breast Cancer	1
1.1 Membrane Protrusions and Actin	1
1.1.1 Lamellipodia: Structure and Molecular Components	4
1.1.2 Filopodia: Structure and Molecular Components	5
1.1.3 Signaling in Protrusions	8
1.1.4 Protrusions in Cancer	10
1.2 HER2 and HER Family Receptors	13
1.2.1 HER Family Receptors	13
1.2.2 HER2 Amplification and Overexpression	14
1.2.3 HER2 is the Preferred Dimer Partner	15
1.2.4 PI3K-AKT Pathway	17
1.2.5 HER2 Targeted Therapy	18
1.2.6 HER2 and Protrusions	21
1.3 Membrane Compartmentalization by Actin	22
1.3.1 Actin Modulation of Protein Dynamics Influences Signaling	24
1.4 Studying Protein Spatiotemporal Dynamics by Quantum Dots	25
1.5 Thesis Overview	27
CHAPTER 2: SENSITIVE METHOD FOR DETECTING PROTEIN QUANTITY AND LOCATION WITHIN THE SPATIAL ARCHITECTURE OF SINGLE CELLS	28
2.1 Introduction	28
2.2 Materials and Methods	29
2.2.1 Cell Culture	29
2.2.2 Wide-Field Fluorescence Microscopy	29
2.2.3 Characterization of HER2-affiFAP-MG-QD Probe	30
2.2.4 Immunolabeling of HER2 and pAKT in Fixed Cells	31
2.2.5 Cell Treatment with NRG1- β 1 and Latrunculin B	32
2.2.6 HER2-siRNA Transfection	32

2.2.7	HER2-QD Quantification.....	32
2.2.8	Western Blot.....	33
2.2.9	Quantification of Western Blot.....	33
2.2.10	Spatial Localization of pAKT-QD using Whole Cell Marker.....	34
2.2.11	Spatial Localization of pAKT-QD using Subcellular Markers	34
2.2.12	Spatial Distribution of pAKT-QD by 1D Probability Density Plots	35
2.2.13	Spatial Distribution of pAKT-QD by 2D Probability Density Plots	35
2.2.14	Classification of Membrane-Adjacent (Narrow) and Membrane-Distant (Broad) States	35
2.2.15	Statistical Analyses	36
2.3	Results.....	36
2.3.1	QDs Bind Specifically to Protein Target.....	36
2.3.2	Increased Sensitivity of Protein Quantification by QD for Single Cells.....	41
2.3.3	Discrete QD Enables Quantitative Spatial Localization of Proteins in Single Cells	43
2.4	Discussion	52
2.4.1	Sensitive Detection of HER2-QD in Single Cells Reveal Increased HER2 with HER3 Knockdown	52
2.4.2	Quantitative Analysis of pAKT-QD Spatial Organization Underscore Cell Heterogeneity and Protein Localization Time Course.....	53
CHAPTER 3: SPATIOTEMPORAL DYNAMICS OF HER2 SIGNALING IN PROTRUSION IS MEDIATED BY ACTIN		56
3.1	Introduction.....	56
3.2	Materials and Methods.....	59
3.2.1	Cell Culture.....	59
3.2.2	Live Cell Microscopy	59
3.2.3	Wide-Field Fluorescence Microscopy.....	60
3.2.4	Scanning Electron Microscopy.....	61
3.2.5	Structured Illumination Microscopy	61
3.2.6	2D STORM Imaging	62
3.2.7	Double-Helix 3D Super-Resolution Imaging.....	62
3.2.8	Volume Electron Microscopy Sample Preparation	63

3.2.9	Volume Electron Microscopy Imaging.....	64
3.2.10	HER2 Labeling using affiFAP-MG-QD for Live Single QD Imaging.....	65
3.2.11	Immunolabeling of HER2, pAKT, and Actin in Fixed Cells.....	65
3.2.12	Immunolabeling of HER2 in Membrane or Cytoplasm.....	67
3.2.13	HER2 staining for 2D STORM	67
3.2.14	Actin staining for 3D Super-Resolution	68
3.2.15	Cell Treatment with NRG1- β 1 and Latrunculin B.....	68
3.2.16	HER2-siRNA Transfection.....	69
3.2.17	Assessment of Filopodia from Cell Images	70
3.2.18	HER2-QD Quantification.....	70
3.2.19	pAKT-Alexa Quantification in Protrusions.....	71
3.2.20	Protrusion to Entire Cell Ratio Measurement	71
3.2.21	Western Blot.....	72
3.2.22	Single QD Tracking	72
3.2.23	Dynamic Analysis of HER2-QD Trajectories	74
3.2.24	Statistical Analyses	74
3.3	Results.....	75
3.3.1	Breast Cancer Cell Protrusion Exhibit Similar Nanoscale Morphology <i>In Vitro</i> and <i>In Vivo</i>	75
3.3.2	HER2 Signaling of Protrusion Growth is Rapid and Spatially Localized.....	80
3.3.3	Protrusions are the Primary Site of HER2 and pAKT Signaling.....	83
3.3.4	Enhanced Mobility of HER2-QDs in Filopodia	88
3.3.5	Disruption of Actin Linear Geometry Reduces HER2 Mobility and Inhibits Signaling	96
3.4	Discussion	102
3.4.1	Cellular Protrusions are the Primary Site of Protrusion Growth Regulation.....	102
3.4.2	Rapid HER2 Transport along Protrusions Enabled by Actin	103
CHAPTER 4: SUMMARY, CONCLUSIONS, AND FUTURE DIRECTIONS		105
4.1	Discrete Quantification and Spatial Localization of HER2 and pAKT by QD	105
4.2	HER2 Signaling is Localized to Protrusions and Mediated by Actin.....	106
4.3	HER2 Signaling is Spatially Regulated in Protrusions	108

4.4	Linear Actin Structure Facilitates Rapid Signaling of HER2 through Diffusion.....	109
4.5	Future Directions	112
4.5.1	Filopodial-specific Cytoskeletal Targeting of HER2 Signaling by Fascin Inhibitors ...	112
4.5.2	HER2 Directionality and Influence of Protrusion Geometry on Mobility	113
4.5.3	HER2-HER3 Dimer Dynamics in Protrusions.....	114
4.5.4	Spatial Targeting of HER2 in Filopodial Protrusions.....	114
	REFERENCES	116

LIST OF FIGURES

Figure 2.1: Characterization of HER2 affibody-FAP-MG-QD probe for monovalent and specific HER2 label.	39
Figure 2.2: Characterization of HER2 affibody-FAP-MG for specific HER2 label.	40
Figure 2.3: pAKT-QD probe shows specific labeling for pAKT.	41
Figure 2.4: Quantification of HER2 by QD labeling demonstrates increased sensitivity for single cells compared to quantification by Western blot.	43
Figure 2.5: Quantitative spatial distribution of pAKT-QD in single cells.	47
Figure 2.6: Quantitative spatial localization of pAKT-QD in subcellular regions of single cells.	50
Figure 2.7: Additional spatial maps of SKBR3 cells from Starved conditions, 30 sec and 5 min post- NRG1 stimulation.	51
Figure 3.1: Morphology of filopodial and lamellipodial protrusions in <i>in vitro</i> and <i>in vivo</i> breast cancer epithelial cells.	78
Figure 3.2: SEM of filopodia and lamellipodia in additional breast cancer epithelial cell types.	79
Figure 3.3: Toluidine-blue stained 600 nm thick resin section of the <i>in vivo</i> HER2-positive breast tumor cell obtained from a biopsy of a metastatic bone lesion that was prepared for Volume EM. .	79
Figure 3.4: SEM of filopodia and lamellipodia in NRG1-stimulated SKBR3 breast cancer cells.	80
Figure 3.5: Rapid, spatially localized nature of HER2-evoked protrusion growth.	82
Figure 3.6: Protrusions are the primary site of HER2-HER3 pathway activation and downstream pAKT signaling of protrusion growth.	85
Figure 3.7: Activated HER2 receptors localize to membrane protrusions and remain primarily membrane bound.	87
Figure 3.8: Rapid dynamics of HER2-QDs along filopodia compared to other cellular regions.	91
Figure 3.9: HER2 dynamics increase in mobility and instantaneous velocity upon NRG1 stimulation.	93
Figure 3.10: HER2 motion along longitudinal axis of filopodia is diffusive Brownian motion.	95
Figure 3.11: Actin Modulates HER2 Mobility and Downstream Protrusion Signaling.	99

LIST OF TABLES

Table 3.1: Comparison of diffusion constants of HER2 amongst different cellular regions as well as compared to other membrane receptor proteins.	94
Table 3.2: Test of significance for HER2 expression and filopodial growth; HER2 and pAKT density in cellular regions; HER2 dynamics in subcellular regions.....	101

LIST OF ABBREVIATIONS

4E-BP1	eIF4E-binding proteins
ADCC	Antibody-dependent cell-mediated cytotoxicity
ARP2/3	Actin-related proteins 2/3
ATP	Adenosine Triphosphate
BCR	B cell receptor
CD36	Cluster of differentiation 36
CDC42	Cell division control protein 42
Dpp	Decapentaplegic
ECM	Extracellular matrix
EGF	Epidermal growth factor
EGFR	Epidermal growth factor receptor
EM	Electron microscopy
EMT	Epithelial-to-mesenchymal transition
ERK	Extracellular signal-regulated kinases
FAK	Focal adhesion kinase
Fc	Fragment crystallizable
FcεRI	High-affinity IgE receptor
FDA	Food and Drug Administration
FGF	Fibroblast growth factors
FLP	Filopodium-like protrusion
GAP	GTPase activating protein
GDP	Guanosine diphosphate
GEF	Guanine nucleotide exchange factor
GRB2	Growth factor receptor-bound protein 2
GTP	Guanosine-5'-triphosphate
HB-EGF	Heparin-binding EGF-like growth factor
HER	Human epidermal growth factor receptor
HER2	Human epidermal growth factor receptor 2
HER3	Human epidermal growth factor receptor 3
HER4	Human epidermal growth factor receptor 4
I-BAR	Inverse-Bin-Amphiphysin-Rvs
IRSp53	Insulin receptor substrate p53
MAPK	Mitogen-activated protein kinase
mDIA2	Mammalian Diaphanous-related formin-2
mTORC2	Mammalian target of rapamycin complex 2
NPF	Nucleation promoting factor
NRG	Neuregulin
N-WASP	Neuronal Wiskott-Aldrich syndrome protein
PDK1	Phosphoinositide-dependent kinase-1
PH	Pleckstrin homology

PHLPP	PH domain and Leucine rich repeat protein phosphatases
PI3K	Phosphatidylinositol-3-kinase
PIP2	Phosphatidylinositol (4,5)-bisphosphate
PIP3	Phosphatidylinositol (3,4,5)-trisphosphate
PKB	Protein kinase B
PP2A	Protein phosphatase 2
PTEN	Phosphatase and tensin homolog
QD	Quantum dot
RTK	Receptor tyrosine kinase
S6RP	S6 ribosomal protein
SHC	SH2-containing collagen-related proteins
Shh	Sonic hedgehog protein
SPT	Single-particle tracking
T-DM1	Trastuzumab emtansine
TGF α	Transforming growth factor alpha
TKI	Tyrosine kinase inhibitor
VASP	Vasodilator-stimulated phosphoprotein
WASP	Wiskott-Aldrich syndrome protein
WAVE	WASP-family verprolin homologous protein
Wnt	Wingless-type MMTV integration site family member

ACKNOWLEDGEMENTS

Grad school is truly a group endeavor, and I am fortunate to have had a “village” of faculty, lab mates, admin, students, friends, and family supporting me through this process.

First, I want to thank my advisor and mentor Dr. Tania Vu for her guidance and support throughout these years. Without her expertise and direction, this project could never have moved forward. I have learned so much from her about not only how to be a good scientist, but how to approach life meaningfully. She has been a valuable source of encouragement and wisdom during the many times I felt lost and discouraged. During moments when I felt my challenges were insurmountable, she was always there to dispense some much needed perspective (“One failed experiment is not the end of your PhD!”). And most importantly, she consistently believed in me and affirmed my capability and self-worth when I consistently saw myself as an impostor. It is not an exaggeration to say that I could not have accomplished this without her.

I am grateful to the members of my dissertation committee: Dr. Jeffrey Tyner, Dr. Summer Gibbs, Dr. Jim Korkola, and most recently Dr. Young Hwan Chang for their expert scientific advice and helpful suggestions during the progression of this project. I am especially thankful to my DAC chair Dr. Jeffrey Tyner who sacrificed time from his busy schedule to meet with me weekly during the last few difficult months, to offer suggestions and encouragement, and to give me the push that I needed to bring this to completion.

I am indebted to members of the BME department, especially Dr. Monica Hinds and Dr. Owen McCarty for motivating me during various stages of grad school. Thank you to Dr. Owen McCarty for popping in at the exact moments when I needed those unexpected, but always welcomed pep talks to nudge me forward. Thank you especially to Dr. Monica Hinds for being my cheerleader during the most difficult months of writing, for ensuring that I had the time and support I needed, and for reaching out to me weekly despite her busy schedule to make sure I was on the right track.

Thank you to current and past members of the Vu Lab: Thomas, Damien, and Anke, who taught me everything about microscopes, cells, and software that I needed to learn, but who were also the best lab mates a grad student could ask for. I am fortunate for Thomas’s expert skills at troubleshooting my experimental issues, for Damien’s “tough love” approach to teaching me MATLAB, and for Anke’s creative experimental solutions to my biology problems. But most importantly, I’m thankful for their patience and friendship.

Thank you to the administrative members of the BME department, especially Nermina and Virginia. I appreciate Nermina for always diligently responding to my emails and keeping up with my paperwork, scheduling etc. even when I didn’t always reciprocate in a timely manner. Thank

you to Virginia for accommodating my always last-minute order requests for lab supplies, but also for her simple gestures of kindness throughout my time here.

I want to express my gratitude for the ARCS Foundation, who have extended financial and social support to me throughout the years. Members of the ARCS foundation have been some of the most passionate cheerleaders of my work. I am particularly grateful to Barbara and Phil Silvers who have been excited about my work and embraced me into Portland from the very beginning.

I am thankful for my family and friends who have been instrumental in providing the foundation of support I needed to complete this journey. Thank you to my mom, dad, sister, and brothers for sacrificing so much all these years to support me; to my best friends Wendy, Rose, Helen, Lexi, Alex, and Taryn for so many shoulders to cry and laugh on; to Ying, Li-Jung, Andrew, Tao, and Jing for the happy hours and moments of commiserating.

Finally, thank you to the MVP of this entire process, my boyfriend Thomas, who has supported me through blood, sweat, and tears all these years to get me to this point. If there is anyone who deserves this PhD more than me, it is this guy, who has had to endure me at my worst. From housekeeping, cooking, chauffeuring me to and from lab at all hours, to comforting me through my stresses and tears, he has undeniably kept me sane, loved, and well-fed through this chaos. There are no number of words that will justifiably acknowledge all that he has done for me, and no words to express how lucky I am to have him in my life. All I can say is: he's the real MVP.

ABSTRACT

Signal transduction entails the precise interaction of relevant proteins for transmission of signaling pathways that carry out essential functions. Spatial arrangement and dynamics of these signaling molecules in a complex cellular environment is a critical mechanism by which signaling is precisely and rapidly regulated. Modulation of these spatial arrangements can occur through membrane topology and underlying cytoskeletal structures that confine and regulate protein dynamics to influence signaling. Cellular protrusions are peripheral elaborations that mediate fundamental physiological processes such as chemosensory and motility functions. In cancer, dysregulated protrusion growth underlies metastasis and disease progression. Breast cancer cell protrusions express HER2 and HER2 has been linked to protrusion growth, but details of how HER2 signaling is conducted in protrusions remains unclear. Here, I demonstrate a sensitive and quantitative method for analyzing the expression and spatial localization of HER2 and pAKT using quantum dots (QDs). I also employ novel monovalent HER2-QD probes using various imaging modalities (single particle tracking, EM, and super-resolution) to characterize the spatiotemporal features of HER2 signaling in breast cancer cell protrusions. I found that HER2 and downstream pAKT molecules are primarily localized in protrusions. In protrusions, HER2 motion is diffusive with mobility in filopodia that is faster than in lamellipodia and non-protrusive membrane regions; this is one of the fastest mobilities reported for membrane receptors. When the linear geometry of filopodial actin is perturbed, HER2 motion resembles areas of membrane absent of protrusions and downstream signaling is reduced. I propose that the linear actin structure creates a local environment for efficient movement of HER2 in filopodia that does not require active transport. This implicates the behavior of signaling molecules and their local environment in filopodia in shaping rapid, localized signaling of protrusion growth.

CHAPTER 1: INTRODUCTION AND BACKGROUND

1.0 Breast Cancer

Breast cancer is the most common cancer in women, and the second most common cause of death for women in the United States. In 2014 alone, 236,968 women were diagnosed with, and 41,211 women and 465 men died from breast cancer in the US (CDC, 2014). The magnitude and impact of this disease is staggering and raises the crucial need for improved treatment strategies through better understanding of the cancer's biology.

In this first chapter, I provide an overview of aspects of cellular function including: (1) protrusion biology, (2) HER2 signaling, and (3) actin regulation of signaling, that when dysregulated, operate in an aberrant and integrated manner within the cellular environment to drive disease progression.

1.1 Membrane Protrusions and Actin

The plasma membrane is a dynamic structure that connects the extracellular environment to the intracellular world of the cell. Arrangement and organization of signaling components at relevant spatial compartments on the membrane is necessary for enabling the extra- and intra-cellular communication that direct and initiate signal transduction (Kholodenko, 2006; Scott and Pawson, 2009; Groves and Kuriyan, 2010). These cellular signals are critical for effecting processes from cell proliferation, metabolism, to motility (Ridley, 2011). Functional organization of the membrane is enabled by the formation of distinct cellular projections occurring in the form of membrane elaborations. Two major types of protrusion structures are filopodia and lamellipodia,

which serve as the main membrane extensions that orchestrate one of their primary functions of cell motility (Ridley, 2011; Krause and Gautreau, 2014). The lipid membrane is supported by an actin framework that defines cell shape and polarity, and their dynamic assembly and disassembly provides the driving force for cell locomotion (Hall, 1998). The dynamic coordination of the fluid membrane with this underlying cytoskeleton is critical for formation of membrane protrusions, and is reflected in their distinct morphological and molecular components.

Actin filaments serve as the major structural component for lamellipodia and filopodia (Pollard and Borisy, 2003). These filaments are polymers of globular actin (G-actin) that assemble to form right-handed helices approximately 8 nm in width (Clarke *et al.*, 1975; Pollard and Borisy, 2003). Such assemblies of filamentous actin (F-actin) maintain a polarity during polymerization with a barbed end (+) oriented towards the cell membrane where subunits are rapidly added, and a pointed end (-) towards the cell cytoplasm with slower dynamics that favor depolymerization (Carlier and Pantaloni, 1997; Pollard and Borisy, 2003). Actin polymerization is associated with ATP hydrolysis which drives the treadmilling of actin (Carlier and Pantaloni, 1997). This process of actin assembly is fast as revealed by measurements *in vivo* in systems from bacteria to fish keratocytes where variable rates of 1 $\mu\text{m}/\text{min}$ to 60 $\mu\text{m}/\text{min}$ of the moving leading edge have been observed (Carlier and Pantaloni, 1997). In addition to the longitudinal polymerization of subunits, fine helical actin filaments are structurally strengthened by organization into linear bundles, assembled into two-dimensional networks, or a thicker, three-dimensional organization of cross-linked actin filaments with less polarized organization (Mitchison and Cramer, 1996).

Protrusion of the cell membrane and subsequent cell motility is primarily coordinated by the activity of monomeric GTPases of the RHO family (Nobes and Hall, 1995). These RHO GTPases are involved in coordination of the front and back ends of the cell, as well as in mediating actin dynamics by control of distinct molecular populations at different spatial locations in the cell. RHO GTPases are activated by guanine nucleotide exchange factors (GEFs) which facilitate the exchange of GDP for GTP, and are inactivated by GTPase activating proteins (GAPs) that catalyze the hydrolysis of GTP to GDP on RHO (Ridley, 2015). The activity of RHO GTPases thus cycles between an active GTP-bound state and an inactive GDP-bound state (Ridley, 2011). Three major RHO proteins that regulate the actin cytoskeleton and cell migration are the RHO, RAC and CDC42 (Hall, 1998; Ridley, 2015). Activation of CDC42 triggers actin polymerization and bundling that induces filopodia formation; activation of RAC induces actin polymerization at the cell periphery that results in lamellipodia formation, and activation of RHO regulates formation of actin stress fibers and focal adhesions that provide mechanical traction to the cell during cell motility (Ridley *et al.*, 1992; Nobes and Hall, 1995, 1999). Moreover, these RHO GTPases are intimately linked, as one RHO protein is capable of activating another RHO to elicit a diversity of cellular protrusion outcomes. For example, CDC42 can activate RAC leading to close association of filopodia with lamellipodia, and RAC can activate RHO producing focal adhesions and contractile actin bundles along the lamellipodia (Hall, 1998; Nobes and Hall, 1999). This may explain the presence of filopodia protruding from lamellipodia in some instances. Thus, RHO GTPases play a central role in regulating cell motility, and this is effected by their activation of downstream signaling targets that dictate the protrusion fate of the subcellular spatial region.

1.1.1 Lamellipodia: Structure and Molecular Components

Lamellipodia are broad, sheet-like projections extending from the cell margin that direct cell locomotion (Adams, 2001). These broad, fan-like outgrowths are thin, 0.1-0.2 μm in thickness, and vary in widths of several microns (Rovensky, 2011), and are found in a variety of cell types in vivo from chick fibroblasts to fish epidermal keratocytes (Abercrombie *et al.*, 1971; Svitkina *et al.*, 1997). Their flat morphology of lamellipodia are supported by a dendritic network of branched actin filaments (Le Clainche and Carlier, 2008). During migration, the leading edge of the lamellipodia may contain filopodial extensions that guide directionality (Adams, 2001). Apart from their common two-dimensional appearance, lamellipodia are also present as ruffles (Adams, 2001; Rovensky, 2011). These ruffles are folded invaginations protruding vertically from the cell body that dynamically elaborate and fall back onto the cell body (Adams, 2001).

Lamellipodia extension is driven by actin polymerization at the leading edge of the cell by actin modulating proteins that nucleate and elongate actin to drive formation of the protrusion (Le Clainche and Carlier, 2008). The addition of actin monomers between the barbed end of actin filaments and the membrane interface produces the driving force that pushes growth of the lamellipodia edge forward (Bisi *et al.*, 2013). Initiation of the lamellipodia occurs by a branching addition in which nascent actin filaments are nucleated upon existing filaments by the “Y-branching nucleator” called the ARP2/3 complex (Mullins *et al.*, 1998; Campellone and Welch, 2010). Nucleation promoting factors (NPF) such as WASP/N-WASP and WAVE act downstream of RHO GTPases RAC and CDC42 to stimulate ARP2/3 nucleation of actin polymerization (Campellone and Welch, 2010). Additionally, interaction of WAVE with actin elongating proteins such as VASP

promotes extension of actin filaments (Chen *et al.*, 2014). Aside from ARP2/3, all other actin nucleators produce unbranched filaments (Campellone and Welch, 2010). A major actin nucleator and elongator is formin, a RAC (also CDC42) target that works in concert with ENA/VASP to polymerize actin filaments by the addition of profilin-bound actin monomers (Barzik *et al.*, 2005). The ability of formin to nucleate actin filaments by stabilizing the barbed ends and facilitating the addition of actin subunits enables them to nucleate unbranched actin independent of ARP2/3 while elongating actin filaments (Chesarone and Goode, 2009). Together, formin and ENA/VASP act as the major actin elongating proteins that help to associate with the barbed ends of filaments, shielding them from capping proteins and regulating the rate of elongation at the leading edge of cells (Chesarone and Goode, 2009; Krause and Gautreau, 2014).

1.1.2 Filopodia: Structure and Molecular Components

Filopodia are slender, finger-like projections extending from the cell surface that enable exploratory sensing of the environment (Mattila and Lappalainen, 2008). Each filopodium consists of a 0.1-0.3 μm diameter core (Adams, 2001; Mattila and Lappalainen, 2008), composed of 15-20 parallel and unbranched actin filaments tightly packed in a parallel bundle (Fowler and Aebi, 1983; Le Clainche and Carlier, 2008), and can reach lengths of up to tens of microns (Rovensky, 2011). Filopodia typically extend from the leading edge of lamellipodia, but can form independent of lamellipodia (Ridley, 2011). Characterized as the antennae of a cell, filopodia enable cells to rapidly scan the environment for chemoattractants (Rovensky, 2011), for instance, in locating pathogens by macrophages (Mattila and Lappalainen, 2008), then to direct motility efforts towards the source. In

addition to these cell migratory roles, filopodia can initiate cell-cell contacts (Blanchoin *et al.*, 2014), form selective adhesion (Adams, 2001), as well as transmit cellular signals (Fairchild and Barna, 2014; Prols *et al.*, 2016). As a result, filopodia are critical for a number of cellular processes such as wound healing (Redd *et al.*, 2004), embryonic development (Miller *et al.*, 1995), and neuronal growth cone path finding (Dent *et al.*, 2011).

The formation of filopodia is driven by linear polymerization of actin at the filopodial tip by actin modulating proteins that nucleate, elongate, and bundle actin to drive formation of the protrusion (Leijnse *et al.*, 2015). A major point of contention in the field is the origin of the filopodial filament during initiation; it is unclear whether filopodia derive from lamellipodia or whether they are nucleated *de novo* (Faix and Rottner, 2006; Yang and Svitkina, 2011; Steffen *et al.*, 2017). Generally, initiation of filopodia formation is enabled by the I-BAR domain containing protein IRSp53 which induces membrane curvature and recruits RHO GTPase CDC42, the formin mDIA2, and WASP/N-WASP to stimulate actin polymerization (Ahmed *et al.*, 2010). The actin nucleator and elongation factor formin and the actin elongation factor ENA/VASP serve similar but critical roles in the formation of linear and unbranched actin filaments. Addition of actin monomers to F-actin results in the persistence of long strands of actin filaments enabled by formins (such as mDIA2) and actin elongating proteins such as ENA/VASP (Ridley, 2011). The formin, mDIA2, is a target of CDC42, and upon activation, nucleates actin polymerization, localizes with ENA/VASP to the filopodial tip to stabilize and protect filament ends from capping, and recruits profilin-bound monomeric actin for processive polymerization (Applewhite *et al.*, 2007; Bear and Gertler, 2009; Mellor, 2010). Though both serve similar actin elongating functions, formins are important in the

initiation of filaments, while ENA/VASP are crucial in regulating elongation rates (Chesarone and Goode, 2009). Additionally, the motor protein Myosin-X has been found to localize to the filopodial tip and may facilitate actin filament elongation through delivery of actin monomer cargoes to the tip, and/or by physically pushing the plasma membrane from the barbed end of filaments to generate space for additional monomer additions (Sousa and Cheney, 2005; Zhuravlev *et al.*, 2010). Another role proposed for Myosin-X is that it induces filopodium assembly by converging actin filaments at the leading edge to initiate filopodium extension (Bohil *et al.*, 2006; Watanabe *et al.*, 2010; Kerber and Cheney, 2011). A distinctive characteristic of filopodia is the bundle of parallel actin filaments that make up the core of the protrusion. The major actin-linking protein in filopodia, fascin, which localizes over the entire length of the protrusion, is found to be responsible for the tight bundling that provides stiffness and stability to filopodia (Vignjevic *et al.*, 2006; Machesky and Li, 2010; Zanet *et al.*, 2012). Myosin-X has been shown to selectively traffic along filopodia to the tip; this selectivity is attributed to its preference for movement along fascin-actin bundles (Nagy *et al.*, 2008).

Together, these molecular components give rise to the protrusion of the cell membrane. Forward movement of the cell is executed by coordination with the extracellular matrix (ECM) to drive advancement of the cell membrane during migration. This coordinated action involves: protrusion, adhesion, and contraction of the trailing edge (Parsons *et al.*, 2010). To advance the leading edge of the cell, protrusion of the cell must be coupled to adhesion of the cell front and deadhesion at the back (Ridley *et al.*, 2003). Attachment to the ECM by the cell is enabled by

formation of focal adhesions, dynamic assemblies of proteins that link the actin cytoskeleton to the substratum (Gardel *et al.*, 2010). Prominent amongst focal adhesions are a family of transmembrane receptors called integrins, which connect actin filaments to the ECM through actin binding proteins such as talin and vinculin, as well as mediates mechanical and chemical signals from the ECM (Ziegler *et al.*, 2008; Parsons *et al.*, 2010). In cells spreading lamellipodia, integrins are found at points along the edge of the lamellipodia and at stress fibers, adhered to the ECM to provide traction during movement; in filopodia, integrins have been found localized at their tips to promote cell adhesion (Giancotti and Ruoslahti, 1999; Mattila and Lappalainen, 2008).

1.1.3 Signaling in Protrusions

In addition to the role of protrusions in cell migration, there is accumulating evidence indicating that protrusions can serve as a platform that houses components of signaling pathways that dictate non-motility processes such as cell survival and differentiation (Harburger and Calderwood, 2009). For instance, integrins, receptors known to conduct signaling through spatial and temporally regulated recruitment of signaling proteins, can initiate pro-survival mechanisms through binding to ECM ligands or trigger apoptosis through lack of ECM adhesion (Hood and Cheresh, 2002; Harburger and Calderwood, 2009). Integrins can transmit signals received at the extracellular domain (outside-in signaling) to activate intracellular signaling through FAK, which recruits complex, multi-protein units formed at focal adhesions of components such as GRB2, SHC, and SRC to activate downstream effectors such as RAS and ERK to effect changes to the cytoskeletal organization (Hood and Cheresh, 2002). Alternatively, integrins can also receive intracellular signals

from its cytoskeletal domain that induce different integrin heterodimerization, integrin clustering, or integrin alterations to regulate the strength of adhesion to the ECM (Calderwood *et al.*, 2000).

Recently, emerging studies have brought to light the existence of “specialized” filopodia which direct specific signaling functions through delivery of signaling molecules (Fairchild and Barna, 2014; Prols *et al.*, 2016). Similar to typical filopodia, specialized filopodia are actin-based protrusions but can reach lengths of hundreds of micrometers (Prols *et al.*, 2016). Filopodia with motility-independent functions were first identified several decades ago in sea urchin embryos as cellular projections that extended across long distances (Miller *et al.*, 1995). These filopodia, which extended from distant primary mesenchymal cells through the blastocoel, across lengths of 80 μm , to cells of the ectoderm appeared to engage in signal-specific interactions, suggesting a role for them in signaling (Miller *et al.*, 1995). Since then, filopodia have emerged as a potential method of direct delivery ligands or morphogens to distant cells and numerous recent studies have identified signaling molecules in different systems that localize to filopodia (Fairchild and Barna, 2014; Kornberg and Roy, 2014; Prols *et al.*, 2016). These protrusions may aid cells in overcoming spatial barriers such as distance to initiate specific signaling programs at target cells. This has been shown to be true in various contexts such as zebrafish and *Xenopus* where delivery of ligands and/or receptors enables activation of specific developmental programs (Fairchild and Barna, 2014). In chick limb buds, the signaling molecule Shh (Sonic Hedgehog) has been observed to deliver along filopodia in an anterograde fashion to cells containing Shh receptors (Sanders *et al.*, 2013). In *Drosophila*, signaling components such as Dpp, FGF, and EGF receptors have been found to localize to cellular extensions called cytonemes that extend from *Drosophila* wing imaginal disks (Hsiung *et al.*, 2005; Roy *et al.*,

2014). These receptor-localized cytonemes are found to extend toward the ligand secreting cells (Hsiung *et al.*, 2005; Roy *et al.*, 2014). In zebrafish, the signaling molecule Wnt8a is observed to localize to filopodia of epithelial cells of the presumptive neuroectoderm and to be released through retraction of the filopodia (Luz *et al.*, 2014). And in *Xenopus*, Wnt signaling molecules were found to localize on the tips of filopodia and to transport with the moving ends of the filopodia where it was taken up by Wnt receiving cells (Holzer *et al.*, 2012). In addition to models of developmental biology, signaling in filopodia in mammalian cell lines has been observed most prominently in quantum dot (QD) studies of the EGFR (Lidke *et al.*, 2004; Lidke *et al.*, 2005a). In these studies, Lidke et al found EGF-bound EGFR to transport in a retrograde fashion towards the cell body in an actin-dependent manner, suggesting a role of filopodia in mediating signal initiation that is transduced to the cell body (Lidke *et al.*, 2004; Lidke *et al.*, 2005a). Together, these data demonstrate a role for filopodial protrusions in facilitating signal transduction through convergence of signaling components in a nanoscale environment to enable directed and localized transmission of signaling.

1.1.4 Protrusions in Cancer

Cell migration is enabled by protrusion of the cell membrane. Dysregulation of this process endows cancer cells with the ability to invade to distant sites and metastasize. This process involves the departure of cancers cells from their primary tumor, entrance into the bloodstream (intravasation), and departure out of the bloodstream (extravasation) towards a secondary tissue to establish metastasis (Sahai, 2007). A reprogramming of the cell's differentiation state by an

epithelial-to-mesenchymal transition (EMT) is central to acquiring an invasive phenotype during cancer progression. This transition is accompanied by changes in gene expression patterns that result in loss of epithelial cell-cell junctions and apical-basal polarity, and a subsequent gain in cell motility through fundamental changes in the cytoskeletal organization, front-rear polarity, and increased ability to degrade and remodel the ECM (Machesky and Li, 2010).

Progression of cells to a pathological state is enabled by aberrant modulation of molecular components that play key roles in the formation of lamellipodial and filopodial structures. In lamellipodia, actin regulatory proteins such as ARP2/3 and WAVE have been implicated to be upregulated in cancer cells displaying invasive properties (Yamaguchi and Condeelis, 2007). And in primary tumors, cancer cells extend lamellipodia-like protrusions (called pseudopodia in 3D) to crawl along the ECM (Yamaguchi *et al.*, 2005).

In cancer cells, filopodial protrusions in particular have been linked with invasiveness and disease progression. Filopodia protrusions are known to promote cell migration (Arjonen *et al.*, 2011; Jacquemet *et al.*, 2015). Consistent with this, abundant filopodia are observed in metastatic tumor cells, and their quantity has been correlated with cell invasiveness (Vignjevic *et al.*, 2007; Tan *et al.*, 2013). A variety of names have been assigned to protrusions that structurally or molecularly resemble filopodia. These range from actin spikes, filopodia-like protrusions to invadopodia (Jacquemet *et al.*, 2015). Most notably, invadopodia are a specialized protrusion frequently compared to filopodia that are found in cancer cells. These specialized actin-based protrusions form on the ventral surface of cells and are known to house proteases and adhesion molecules that aid in the degradation of ECM to facilitate invasive migration. Thus, cancer cells likely protrude

invadopodia as a method of invading the tumor microenvironment and entering the bloodstream during the course of metastasis (Yamaguchi and Condeelis, 2007). Additionally, another potential subset of protrusions labeled “filopodia-like protrusions” (FLPs) have also been shown to aid extravasated cells in their seeding at secondary tissues of the lung (Shibue *et al.*, 2012). While FLPs and filopodia contain structural similarities, their molecular similarities and distinctions have not been completely identified.

Several proteins critical for filopodia formation are found to be upregulated during cancer. In particular, the actin bundling protein fascin is upregulated in aggressive and metastatic cancer (Machesky and Li, 2010). A number of studies have shown that elevated fascin expression is correlated with poor clinical prognosis in breast, ovarian, kidney, lung, and brain cancer (Yang *et al.*, 2013; Cao *et al.*, 2014; Huang *et al.*, 2015). Furthermore, fascin expression has been correlated with downregulation of e-cadherin, suggesting fascin expression is in line with a program of epithelial-to-mesenchymal transition (EMT) that confers cells with increased motile ability (Hayashi *et al.*, 2011). Given the functional importance of filopodial protrusions in establishing migration and signaling activity, disrupting their functions in pathological conditions thus serves as a potential target for limiting disease. Thus, understanding filopodia signaling and identifying filopodial-targets such as fascin may serve as potential therapeutic targets for limiting cancer metastatic potential.

1.2 HER2 and HER Family Receptors

1.2.1 HER Family Receptors

The human epidermal growth factor receptor (HER/ERBB) family are receptor tyrosine kinases (RTK) which act as the messengers that transmit extracellular signals to the intracellular environment (Rubin and Yarden, 2001; Yarden, 2001). The HER family is composed of four homologous receptors (HER1/EGFR/ERBB1, HER2/ERBB2, HER3/ERBB3, HER4/ERBB4) that interact with a range of growth factor ligands which induce receptor homo- and heterodimerization at the plasma membrane to activate signal transduction that control cellular outcomes such as cell growth, differentiation, and survival (Rubin and Yarden, 2001; Yarden, 2001). HER receptors share a similar structure of an extracellular domain containing several cysteine-rich regions in the ligand binding domain, a lipophilic single pass transmembrane segment, and an intracellular tyrosine kinase domain (Rubin and Yarden, 2001; Yarden, 2001). These receptors exist as monomers on the plasma membrane, and are activated upon binding of growth factors such as epidermal growth factor (EGF), transforming growth factor α (TGF α), heparin binding EGF (HB-EGF), and the family of peptides called neuregulins (NRG) (Hynes and Lane, 2005). Growth factor ligands such as EGF and TGF α bind specifically to EGFR, while others such as HB-EGF can bind both EGFR and HER4, and the neuregulin family of peptides can bind both HER3 and HER4 (Hynes and Lane, 2005). In comparison to other HER receptors of the family, HER2 is a ligandless receptor, and HER3 is kinase defective (Rubin and Yarden, 2001; Yarden, 2001). After ligand binding, different HER receptors can associate to form any of the ten different receptor homo- or heterodimer combinations. This coupling activates the intrinsic kinase domain that results in phosphorylation of specific tyrosine residues on the cytoplasmic tail (Rubin and Yarden, 2001; Yarden, 2001). These

phosphorylated residues serve as docking sites for proteins, and recruitment of signaling proteins to these docking sites leads to activation of various signaling cascades such as PI3K-AKT and MAPK pathway (Baselga and Swain, 2009).

1.2.2 HER2 Amplification and Overexpression

Among the four receptors, HER2 is of particular interest as it is overexpressed in 20-30% of invasive breast carcinomas and its overexpression is correlated with poor clinical prognosis (Slamon *et al.*, 1989). HER2 overexpression serves as a major prognostic indicator of breast cancer, and its amplification and overexpression also occur in a number of other cancers including ovarian and gastric cancers (Hynes and Lane, 2005; Baselga and Swain, 2009).

HER2 is encoded by the *ERBB2* gene, a proto-oncogene mapped to chromosome 17q21 (Rubin and Yarden, 2001; Yarden, 2001). Proto-oncogenes are normal genes that express proteins regulating cellular survival, proliferation and growth. Upon activation, proto-oncogenes can become oncogenes through (1) mutations, (2) increased protein expression arising from gene amplification or elevated transcriptional activity, or (3) chromosomal translocations (Polsky and Cordon-Cardo, 2003). This activation results in transformation of cells from a normal to a pathological and cancerous state.

In HER2-positive breast cancers, overexpression of the receptor arises from gene amplification of a region on the long arm of chromosome 17 that results in increased levels of the normal HER2 protein (Moasser, 2007). This amplification results in cancer cells containing up to

25-50 copies of the *ERBB2* gene and consequently expression of up to 2 million receptors on cell surfaces (Venter *et al.*, 1987; Lohrisch and Piccart, 2001; Moasser, 2007).

Gene amplification events are likely initiated by errors in DNA replication that result in breakage and recombination of redundant DNA segments into two forms: homogeneously staining regions (HSRs) or double-minute chromosomes (DMs) (Polsky and Cordon-Cardo, 2003; Albertson, 2006). In the form of HSRs, amplification exists as an intrachromosomal region composed of head-to-tail or head-to-head repeats of the gene that are visible as homogeneously staining regions. Alternatively, in the form of DMs, amplified genes exist as extrachromosomal fragments lacking centromeres that are scattered throughout the nucleoplasm (Albertson 2006, Polsky and Cordon-Cardo 2003). Amplification of *ERBB2* has been reported to occur in the form of both DMs and HSRs (Kobayashi *et al.*, 2002; Vicario *et al.*, 2015). Regardless of the form of amplification, the outcome is an increase in the number of copies of the oncogene and thus overproduction of the HER2 protein in cancer cells (Vicario 2015, Kobayashi 2002).

1.2.3 HER2 is the Preferred Dimer Partner

HER2 is distinct from other members of the family because it lacks a known ligand; interestingly, HER3 is capable of ligand binding, but lacks intrinsic kinase activity (Rubin and Yarden, 2001; Yarden, 2001). HER2 serves as the preferred heterodimer for other HER receptors, and HER2-containing heterodimers are known to potentiate the strongest mitogenic effects (Rubin and Yarden, 2001; Yarden, 2001). The increased potency of HER2-containing heterodimers is attributed to the slow rate of ligand dissociation and to HER2's slow internalization in comparison

to the EGFR (Baulida *et al.*, 1996; Pinkas-Kramarski *et al.*, 1996). Part of this is explained by the conformation of the HER receptors in their active and inactive states (Hynes and Lane, 2005; Hynes and MacDonald, 2009). Each HER receptor consists of four domains (I-IV), and in the absence of ligand binding, the receptor assumes a “closed” conformation in which the domains responsible for ligand binding (I and III) remain apart (Hynes and Lane, 2005; Hynes and MacDonald, 2009). Upon ligand binding, receptors undergo a conformational change in which domains I and III are engaged with the ligand, and the dimerization arm (domain II) is exposed to allow receptor interaction (Holbro and Hynes, 2004). While EGFR, HER3, and HER4 undergo such conformational adjustments upon ligand activation, HER2 remains in a constitutively “open” conformation, resembling a ligand-activated state, with the dimerization arm exposed, priming the receptor for activation (Hynes and Lane, 2005; Hynes and MacDonald, 2009). Thus, HER2 provides an optimal partner to the kinase impaired HER3, which requires dimerization to another HER receptor to signal.

Given the role of HER2 as a ligandless receptor, and HER3 as a kinase defective receptor, the pairing of the two appears to be compensatory, allowing them to efficiently function as an oncogenic unit under circumstances of HER2 overexpression. Consistent with this, HER2-HER3 heterodimers effectively generates the most potent intracellular signal to promote cell proliferation and survival than all other possible dimer associations (Tzahar *et al.*, 1996).

1.2.4 PI3K-AKT Pathway

Activation of the PI3K-AKT pathway has been linked to tumor progression and cell survival (Baselga and Swain, 2009). Direct activation of PI3K can occur through HER3, which contains a binding site for the p85 subunit of PI3K (Hellyer *et al.*, 1998; Hellyer *et al.*, 2001). This direct activation is likely one reason for the potent mitogenic signaling induced by HER2-HER3 dimers (Yarden and Sliwkowski, 2001).

The serine and threonine kinase AKT, also referred to as protein kinase B (PKB), is a 56kDa protein that is activated downstream of PI3K, and is important in the regulation of cellular processes such as cell proliferation and growth (Manning and Toker, 2017). AKT exists in three isoforms in mammalian cells: AKT1 (PKB α), AKT2 (PKB β), and AKT3 (PKB γ), and is encoded by different genes (Franke, 2008b). These different isoforms have been identified as having different functions ranging from cell migration and proliferation, glucose metabolism, to brain development (Gonzalez and McGraw, 2009).

AKT activity is directed by ligand stimulation of receptor tyrosine kinases at the membrane. Ligand binding of RTK results in receptor dimerization and phosphorylation of tyrosine residues at the cytoplasmic domain. These phosphorylated residues act as docking sites that recruit and activate PI3K to the membrane, where it phosphorylates phosphoinositides to generate lipid second messengers phosphatidylinositol-3,4-bisphosphate (PI-3,4-P₂, PIP₂) and phosphatidylinositol-3,4,5-triphosphate (PI-3,4,5-P₃, PIP₃) (Franke *et al.*, 1997). The presence and accumulation of PIP₃ at the plasma membrane recruits cytoplasmic AKT to the membrane where AKT engages PIP₃ via its PH domain (Franke, 2008a; Franke, 2008b). Binding of the PH-domain to PIP₃ results in the

release of the PH and kinase domain interaction, allowing phosphorylation of AKT at T308 and S473 by PDK1 and mTORC2 respectively (Calleja *et al.*, 2009; Manning and Toker, 2017).

Modulation of AKT activity occurs through phosphatases that indirectly inactivate AKT through dephosphorylation of PIP3 by PTEN, or that directly inactivate AKT through dephosphorylation at T308 and S473 by phosphatases such as PP2A and PHLPP (Franke, 2008b; Manning and Toker, 2017). Upon signaling, AKT regulates a number of downstream targets such as 4E-BP1 and S6RP that regulate translation and metabolism (Gingras *et al.*, 1998; Hay and Sonenberg, 2004).

Together, the HER2-HER3-PI3K-AKT pathway promotes cell survival, proliferation, and growth as an avenue of signaling that tumor cells frequently depend upon to drive cancer progression.

1.2.5 HER2 Targeted Therapy

The development of HER2-directed therapies has improved the clinical treatment and outlook of patients with HER2-positive breast cancers. But despite their benefits, challenges arise due to the loss of efficacy and acquisition of drug resistance of these therapeutic interventions over time (Singh *et al.*, 2014; Parakh *et al.*, 2017). The advent of trastuzumab was a major milestone in the treatment of HER-positive breast cancer, and since then, a number of treatments have emerged and been approved to tackle HER2-positive disease. These treatments are classified as two major classes of anti-HER2 therapeutics: ectodomain-binding antibodies and small molecule inhibitors that exist in the form of tyrosine kinase inhibitors (TKIs) that block binding of ATP at the kinase domain (Hynes and Lane, 2005).

The humanized monoclonal antibody trastuzumab represents the most successful earliest approach for the targeting of HER2-positive disease and has yielded considerable improvement for delaying disease progression (Parakh *et al.*, 2017). Trastuzumab binds to the extracellular domain IV of the HER2 extracellular domain and has been shown to elicit anti-tumor activity through mechanisms that are not completely understood (Arteaga *et al.*, 2011). Its therapeutic function may be mediated by endocytic regulation and degradation of HER2 induced by antibody binding, inhibition of extracellular domain cleavage, antibody dependent cellular cytotoxicity (ADCC) arising from engagement of immune cells through the Fc region of trastuzumab, and inhibition of downstream signaling through MAPK and PI3K-AKT pathways (Arteaga *et al.*, 2011; Vu and Claret, 2012; Parakh *et al.*, 2017). The efficacy of trastuzumab has also enabled development of antibody drug conjugates for targeted drug delivery in the form of ado-trastuzumab emtansine (T-DM1) (Junttila *et al.*, 2011). T-DM1 is a conjugate of trastuzumab and the anti-mitotic agent DM1, an inhibitor of microtubule dimerization, and has been shown to be effective at inducing cytotoxic effects specifically to HER2-overexpressing cells (Junttila *et al.*, 2011).

Given the functional importance of receptor dimerization for activation of HER2 signaling, inhibition of receptor coupling would yield an effective strategy for targeting HER2 activity. As such, another monoclonal antibody developed for treatment of HER2-positive cancer and approved by the FDA is the dimerization inhibiting agent pertuzumab. Pertuzumab binds to the dimerization arm of HER2 at domain II to inhibit ligand-induced dimerization between HER2 and other HER receptors, notably HER3 (Franklin *et al.*, 2004). Since pertuzumab targets a different site of HER2 than trastuzumab, strategies combining the two antibodies demonstrated even greater efficacy for

inhibition of HER2 signaling than either antibody alone and currently represents the standard first-line of care (Arteaga *et al.*, 2011).

Another major class of HER2-directed therapy are small molecule inhibitors. Current small molecule tyrosine kinase inhibitors (TKI) approved for the treatment of HER2-positive breast cancer include lapatinib which reversibly inhibits the tyrosine kinase activity of EGFR and HER2 to reduce downstream signaling through MAPK and PI3K-AKT pathways (Arteaga *et al.*, 2011). Very recently, the irreversible EGFR and HER2 TKI neratinib was additionally approved by the FDA for treatment of HER2-positive breast cancer (Chan *et al.*, 2016). Irreversible TKIs such as neratinib have been found to have improved efficacy over TKIs such as lapatinib and to prolong target inhibition (Arteaga *et al.*, 2011). And small molecule inhibitors in general may offer better efficacy for breast cancers that have metastasized to the brain due to their smaller nature relative to antibodies which may allow penetration through the blood-brain barrier (Arteaga *et al.*, 2011; Steeg *et al.*, 2011).

Though these therapeutic interventions represent advances in treatment of HER2-positive breast cancer, a significant portion of patients eventually relapse and tumors acquire drug resistance (Baselga and Swain, 2009; Arteaga *et al.*, 2011; Parakh *et al.*, 2017). A regimen composed of trastuzumab is the current first-line therapy for HER2-positive breast cancer, but unfortunately, over 70% of these cancers eventually gain primary resistance to the antibody (Parakh *et al.*, 2017). Several mechanisms of resistance have been suggested for how cells become resistant to therapeutic treatment. Alterations in the HER2 ectodomain that affect epitope binding and truncation of HER2 lacking an extracellular domain (p95-HER2) is thought to affect targeting by trastuzumab

and trastuzumab-mediated ADCC (Parakh *et al.*, 2017). Additionally, deficiency in PTEN and mutations in PIK3CA may drive constitutive activation of the PI3K-AKT pathway; activation of this pathway is thought to drive trastuzumab resistance (Nahta and Esteva, 2006). Similarly, resistance to lapatinib is thought to be driven by loss of PTEN and PIK3CA mutations as well as by mutations in the EGFR and HER2 tyrosine kinase domain (Arteaga *et al.*, 2011; Parakh *et al.*, 2017). Overcoming resistance to HER2-targeted therapies may require improved targeting of therapeutics. Recent evidence have pointed to differences in the spatial distribution of HER2 within cells (Hommelgaard *et al.*, 2004; Peckys *et al.*, 2015; Chung *et al.*, 2016; Jeong *et al.*, 2017). Thus, spatial targeting of receptors may offer another therapeutic strategy to limit metastatic potential of cells and tumorigenic progression.

1.2.6 HER2 and Protrusions

As discussed in an earlier section, protrusions are known to house a variety of signaling components that aid in cellular motility as well as non-motility functions. In breast cancer cells, HER2 is reported to reside on membrane protrusions, ruffles, and “finger-like structures” (Hommelgaard *et al.*, 2004; Lerdrup *et al.*, 2007; Peckys *et al.*, 2015; Chung *et al.*, 2016; Jeong *et al.*, 2017). This preferential localization to protrusions is thought to serve as a mechanism that prevents endocytic downregulation of HER2 (Hommelgaard *et al.*, 2004). EGFR containing dimers are downregulated through ligand-activated internalization into endocytic vesicles destined for degradation (Lenferink *et al.*, 1998). In comparison, HER2 internalizes much less efficiently than other HER receptors, and HER2 dimerization with EGFR inhibits EGFR downregulation (Sorkin *et*

al., 1993; Hommelgaard *et al.*, 2004). This resistance to downregulation likely promotes HER2 oncogenic potential, though it is unclear whether this aspect is a consequence of efficient recycling of HER2 back to the membrane or exclusion from endocytosis (Austin *et al.*, 2004; Hommelgaard *et al.*, 2004).

HER2 residence on protrusions was first identified in EM studies of HER2 that demonstrated higher density localization along membrane invaginations compared to areas of “bulk membrane” (Hommelgaard *et al.*, 2004). Since then, other studies have also confirmed HER2 retention on protrusions and “finger-like structures” (Peckys *et al.*, 2015; Chung *et al.*, 2016; Jeong *et al.*, 2017). Recently, it has been suggested that overexpression of HER2 sterically induces membrane deformation through protein-protein and protein-lipid interactions that induce membrane bending (Chung *et al.*, 2016). Other studies have shown that HER2 signaling is linked with lamellipodia formation and growth of filopodia-like structures (Grothey *et al.*, 2000; Marone *et al.*, 2004; Yokotsuka *et al.*, 2011). Given the close relationship observed between HER2 and protrusions, there may be functional implications for HER2 retention on membrane invaginations.

1.3 Membrane Compartmentalization by Actin

The idea of the plasma membrane as a homogeneous fluid of phospholipids and proteins has evolved into a more advanced understanding of the complexity of the membrane structure. It is now understood that the membrane contains a complex and inhomogeneous organization of lipid and protein domains (lipid rafts, protein oligomers, protein islands) present as nanodomains or

microdomains arranged on the uniquely folded and dynamic membrane surface (Jaqaman and Grinstein, 2012; Kusumi *et al.*, 2012).

The arrangement of these domains is influenced in large part by the cortical cytoskeleton, which has been proposed to compartmentalize and partition the plasma membrane by its interactions with membrane components (Kusumi *et al.*, 2012). These interactions between the cytoskeleton and the membrane can regulate protein and lipid mobility (diffusion), as well as protein interactions to form dimers and multimeric complexes. As a consequence, the spatiotemporal coupling of the membrane and cytoskeleton critically modulates signal transduction that dictates cellular consequences (Jaqaman and Grinstein, 2012).

Organization of the membrane by the cytoskeleton is described to occur through a “picket fence” model, in which “fences” (the cytoskeleton) and “pickets” (the transmembrane proteins) generate barriers that transiently defines compartments, also termed “corrals”, in which proteins can diffuse (Kusumi *et al.*, 2012). These protein pickets can be anchored directly to the cytoskeleton, or indirectly through scaffolding proteins that link the protein to the cytoskeleton (Jaqaman and Grinstein, 2012). Thus, cell surface proteins (namely transmembrane proteins) can diffuse within these compartments, encountering the barriers through bumping of the cytoplasmic tail to actin or bumping of other membrane proteins. The transience of these compartments due to the dynamic remodeling of actin would allow diffusing proteins to undergo “hop diffusion”, during which proteins undergo escape from one corral to another corral through temporary discontinuities in the actin network (Jaqaman and Grinstein, 2012; Kusumi *et al.*, 2012). Thus, the organization of the membrane by actin has implications for directing protein dynamics through modulation of the

motion, transport, and spatial arrangement of proteins. This in turn dictates their ability to respond to and transmit signal.

1.3.1 Actin Modulation of Protein Dynamics Influences Signaling

The propensity of actin compartmentalization of the membrane to influence downstream signaling has been supported and revealed by several key studies of receptors in immune cells. Actin has been shown to both restrict and facilitate receptor dynamics. In studies of the FcεRI receptor, Andrews et al found that actin limits the diffusivity of the receptors by restricting them in microdomains that are released upon actin alterations (Andrews *et al.*, 2008).

This regulation of receptor dynamics by actin was advanced one step further and linked to control of signal transduction in B cell receptors (Treanor *et al.*, 2010). In BCR, actin was found to also restrict BCR mobility by confining receptor mobility in microclusters (Treanor *et al.*, 2010; Mattila *et al.*, 2016). Engagement of the receptor induced remodeling of the cytoskeleton that released the receptor from nanoclusters, allowing increased diffusion and mobility that enables increased likelihood of co-receptor encounters. These increased diffusional dynamics would facilitate collision and interactions with its co-receptor and was reflected in the increased downstream signaling (Treanor *et al.*, 2010).

In studies of the receptor CD36, actin is found to define linear channels radiating from the perinuclear region (Jaqaman *et al.*, 2011). These actin-defined regions facilitated fast diffusion of the receptor, which promoted receptor clustering and interaction that enabled downstream signaling

(Jaqaman *et al.*, 2011). Perturbation of the actin structure impeded this rapid linear diffusion and consequently disrupted activation of downstream effectors.

Both of these studies lend support to the importance of receptor dynamics in activating signaling as hypothesized by the “mobile receptor hypothesis” which postulates that the lateral diffusivity of proteins on the membrane is critical to effecting signal transduction through protein interactions (Jans, 1992).

Apart from compartmentalization, actin dynamics can couple with protein dynamics to influence signaling, as observed with EGFR undergoing retrograde flow with actin upon activation (Lidke *et al.*, 2005a). In addition to being necessary for signal transduction, the diffusivity of EGFR has been shown to reflect the signaling states of the receptor, revealing the ligation and dimerization state (Chung *et al.*, 2010; Low-Nam *et al.*, 2011). Thus protein dynamics can couple with actin in different ways that influence and dictate its transmission of signaling.

1.4 Studying Protein Spatiotemporal Dynamics by Quantum Dots

The following is revised from (with permission from Springer):

Vu, T.Q., Lam, W.Y., Hatch, E.W. et al. Cell Tissue Res (2015) 360: 71.

<https://doi.org/10.1007/s00441-014-2087-2>

Current methodologies for imaging proteins in live cells within the context of protrusions rely on fluorescent proteins or organic dye molecule tagging of molecules of interest. However, the weak fluorescent signal and fast photobleaching rates that arise from tracking single molecules using these techniques limits the length of time acquisition and time resolution for capturing longer biological events (Chang *et al.*, 2008). Quantum dots (QDs) have emerged as a powerful tool for

elucidating complex biological phenomena such as the dynamic behaviors and organization of molecules in living systems. In particular, QD single particle tracking (QD-SPT) represents a powerful method for probing the dynamics of individual proteins of interest in living cells with high spatial and temporal resolution. This capability is afforded by their high photostability and brightness that is superior to conventional fluorophores (fluorescent proteins and organic dyes) (Wu *et al.*, 2003; Michalet *et al.*, 2005). These advantageous properties overcome difficulties in photobleaching that limit fluorophore imaging time allowing for acquisition of biological events over long timescales and contribute to the QD's utility as an ultrasensitive detection probe for SPT. Moreover, QD-SPT makes quantifiable dynamic information regarding diffusional properties, co-localization, and spatial and temporal heterogeneity of molecules inside living cells that conventional fluorescence and biochemical methods cannot capture (Courty *et al.*, 2006; Vermehren-Schmaedick *et al.*, 2014).

The method of QD-SPT proceeds through a series of steps including: (1) targeting QDs to the molecule of interest, (2) validating the specificity of the QD probe, (3) acquiring a sequence of fluorescence images in time lapse to capture the biological event, and (4) extracting biological information from the recorded trajectories through single particle tracking to yield measurements such as diffusion coefficient and velocity that inform dynamic information about the molecule of interest (Bannai *et al.*, 2006). These capabilities afforded by the sensitivity of QD-SPT enable the study of diffusion (Dahan *et al.*, 2003), dimerization (Chung *et al.*, 2010; Low-Nam *et al.*, 2011), as well as receptor trafficking dynamics (Lidke *et al.*, 2005a) to understand biological processes not previously possible.

1.5 Thesis Overview

Membrane protrusions direct chemosensory and motility functions that are essential to fundamental physiological processes. In cancer, dysregulation of this protrusion growth underlies invasive and metastatic properties that ultimately result in disease progression. In breast cancer, cell protrusions have been found to house HER2 receptors, and HER2 signaling has been linked to protrusion growth, though details of how HER2 signaling is conducted in protrusions remains unclear. The focus of this dissertation is to elucidate the spatiotemporal features of HER2 signaling in breast cancer cell protrusions. In Chapter 2, I introduce and characterize a novel monovalent HER2-QD for studying the localization and dynamics of HER2, and I show through studies of pAKT-QD spatial distribution and localization the sensitivity of the QD in detecting protein quantity and location. In Chapter 3, I show through electron microscopy (SEM, FIB-SEM), immunofluorescence, super-resolution, and single-particle tracking the organization of HER2 and downstream pAKT in cells and the HER2 dynamics driving its signaling. I show that HER2 and pAKT are localized primarily to protrusions, HER2 dynamics in filopodia are fast and diffusive, and this rapid motion is facilitated by the linear actin architecture of filopodia that is necessary for HER2 signaling. Finally, in Chapter 4, I will summarize the results from these studies and discuss future directions for the work.

CHAPTER 2: SENSITIVE METHOD FOR DETECTING PROTEIN QUANTITY AND LOCATION WITHIN THE SPATIAL ARCHITECTURE OF SINGLE CELLS

2.1 Introduction

The spatial location and temporal trafficking of signaling molecules in the subcellular environment is a critical means by which cells conduct normal signaling (Kholodenko, 2006). However, technological means to probe the location of proteins quantitatively, precisely, and more importantly within the context of the cellular environment remains a challenge. Currently a standard and routine method for detecting relative protein expression in molecular biology is the western blot. However, due to the nature of how protein is acquired (large quantities of cells are lysed to obtain enough sample for protein detection) and the method of measurement, the structural information of the cellular environment is lost and single cell resolution is inaccessible due to bulk assessment. And though protein immunoblots can be measured, they are not reliably quantitative in measuring protein levels (Gassmann *et al.*, 2009).

It is widely accepted that inherent variability exists in aspects of signaling (i.e. protein expression, phosphorylation state) in both normal and cancer cells within a population (Irish *et al.*, 2006). Thus, generalized measurement techniques such as western blots lacking single-cell resolution are inadequate for studying detailed signaling biology because they overlook key spatial information about individual proteins and their quantity in the cellular environment.

Here I present a method to analyze the quantity, distribution, and localization of proteins within the spatial architecture of cells at single cell resolution using bright, fluorescent quantum dots (QDs). I study the receptor tyrosine kinase HER2 and serine-threonine kinase AKT, two key PI3K pathway components that are dysregulated in cancers such as breast and ovarian (Vivanco and

Sawyers, 2002; Baselga and Swain, 2009). Sensitive quantification of HER2 has been suggested as informative predictor for treatment efficacy, and signaling biology of HER2 and pAKT especially as it relates to subcellular localization are incompletely understood (Bellacosa *et al.*, 2005; Bertelsen and Stang, 2014; Parakh *et al.*, 2017). Thus, improved methods for studying HER2 and AKT signaling biology could reveal better strategies to effectively target their aberrant behavior. I demonstrate through the QD-imaging based assay a sensitive way to quantitate protein levels in single cells and a quantitative method of analyzing the spatial distribution and localization of proteins that reveal new details about HER2 and AKT signaling.

2.2 Materials and Methods

2.2.1 Cell Culture

Human breast cancer epithelial cell line SKBR3 were obtained from ATCC (Manassas, VA). Cell media and antibiotics were obtained from Gibco-Thermo Fisher (Waltham, MA). SKBR3 (HER2 overexpressing) cells were grown in McCoy's 5A containing 10% FBS. Media was supplemented with 100 µg/mL streptomycin and 100 U/mL penicillin. For immunofluorescence labeling experiments, 100,000 cells were plated per 18 mm diameter, No. 1.5 glass coverslips (Electron Microscopy Sciences, Hatfield, PA) and cultured for 72 hours in 12-well plates (Corning Inc., Corning, NY). Cells were maintained at 37°C in a humidified atmosphere of 5% CO₂.

2.2.2 Wide-Field Fluorescence Microscopy

For wide-field epifluorescence imaging, fixed SKBR3 cells were imaged using an inverted epifluorescence microscope (Zeiss Axio Observer.Z1, 40x/1.4 oil objective or 63x/1.4 oil objective) equipped with an EM-CCD camera (Luca R 604, Andor Technology) using Micro-Manager. Cells

were imaged over the total height of the cells by acquiring z-stacks at a z-step of 150 nm. Fluorescence emissions for CellMask™ Green, Alexa488 and NuclearMask™ Deep Red were detected using FITC and Cy5 filter cubes (excitation 480 nm/emission 535 nm and excitation 620 nm/emission 700 nm respectively; Chroma, Bellows Fall, VT), and QD fluorescence was detected using a QD605 or QD655 filter cube (excitation 435nm/emission 605nm and excitation 435 nm/emission 655 nm respectively; Semrock, Rochester, NY). Image stacks were deconvolved using AutoQuant X2 (Media Cybernetics, Rockville, MD). For CellMask™ Green, WGA-Alexa488, and NuclearMask™ Deep Red, the 3D Blind Deconvolution algorithm was used with an adaptive PSF, medium noise value of 20, and 5 total iterations for 60 frames at a stack spacing of 275 nm. For HER2-QD655 and pAKT-QD605, the No/Nearest Neighbor algorithm was used with haze removal factor 0.99 and z-kernel width 2 for 60 frames at a stack spacing of 275 nm.

2.2.3 Characterization of HER2-affiFAP-MG-QD Probe

HER2 was labeled by an affibody that binds the extracellular domain of HER2 ($Z_{\text{HER2:342}}$, (Eigenbrot *et al.*, 2010)) at the junction of domains III and IV. HER2 affibody ($Z_{\text{HER2:342}}$) was fused to a fluorogen activating protein (FAP_{dl5**}) at the N-terminus, C-terminus or both terminus (construct schematic and probe was prepared in the same manner as EGFR affiFAP, which were previously described in (Wang *et al.*, 2015)). Three HER2 affiFAP constructs showed similar binding affinity to the fluorogen *in vitro* and to HER2 on SKBR3 cells. The HER2 affibody-FAP fusion ($Z_{\text{HER2:342}}\text{-FAP}_{\text{dl5**}}$), hereafter termed HER2 affiFAP, was selected for use in subsequent experiments. HER2 affiFAP was monovalently assembled to a quantum dot via selective binding of

the FAP to its cognate fluorogen Malachite Green (MG) as previously detailed (Szent-Gyorgyi *et al.*, 2008; Saurabh *et al.*, 2014; Wang *et al.*, 2015; Wang *et al.*, 2017b).

2.2.4 Immunolabeling of HER2 and pAKT in Fixed Cells

SKBR3 cells were fixed in 2% PFA containing 1 µg/mL of the membrane marker wheat germ agglutinin-Alexa488 (WGA-Alexa488, Life Technologies) for 10 mins at 37°C, then transferred to a fresh solution of 2% PFA for 20 mins at 37°C. For HER2 immunolabeling, cells were permeabilized in 0.1% Triton-X for 10 mins at room temperature, labeled with HER2 affiFAP (500 nM, 30 mins, 37°C) and incubated for 1 hr in blocking solution (8% NHS and 2% BSA at room temperature). MG-QD655 was pre-complexed as described above to a working concentration of 5 nM, incubated with free biotin at 50 nM for 5 mins at room temperature to occupy unbound streptavidin, diluted in blocking solution to 1 nM and added to cells for 1 hr at 37°C. Following, cells were rinsed in 2% blocking solution and mounted in borate buffer for image acquisition. To verify HER2-specific binding of the probe, cells were labeled following the same scheme with FAP alone (no affibody) and MG-QD655 as a negative control to ensure absence of non-specific binding. For pAKT immunolabeling, cells were permeabilized in methanol for 30 mins in three cycles (10 mins at -20°C, 10 mins at room temperature, 10 mins at -20°C), rehydrated in PBS for 20 mins at room temperature, and incubated for 1 hr in a blocking solution of 8% normal goat serum and 2% BSA. Cells were labeled with primary antibody to pAKT (Ser473, Cell Signaling Technology, Danvers, MA) diluted 1:100 in blocking solution (1.5 hr, 37°C), incubated for 1 hr in blocking solution, and then labeled with secondary antibody QD605 (goat anti-rabbit, Life Technologies) diluted 1nM in blocking solution for 1 hr at 37°C. Following, cells were rinsed in 2% blocking

solution, labeled with 1 $\mu\text{g}/\text{mL}$ CellMaskTM Green for 15 mins at 37°C, and mounted in 1X PBS for image acquisition. To verify pAKT-specific binding, cells were labeled following the same scheme with no primary antibody and secondary antibody alone as a negative control to ensure absence of non-specific binding.

2.2.5 Cell Treatment with NRG1- β 1 and Latrunculin B

Cells were serum-starved overnight, then treated using one of the following schemes: (1) with 20 ng/mL neuregulin1-beta1 (396-HB/CF, R&D Systems Minneapolis, MN) for 5 mins, 15 mins, or 1 hr, (2) with 40 ng/mL for 15 mins, or (3) 40 ng/mL for 5 mins and fixed at different times following (t_d). All cells were stimulated at 37°C under a humidified 5% CO₂ atmosphere, and all treatments were diluted with serum-free media for application to cells. Cells were immediately fixed after treatment as described.

2.2.6 HER2-siRNA Transfection

Cells were transfected with HER2-targeting siRNA (Hs_ERBB2_14 FlexiTube siRNA, Qiagen, Hilden, Germany), HER3-targeting siRNA (Hs_ERBB3_7 FlexiTube siRNA, Qiagen) or control non-silencing siRNA (AllStars Negative Control siRNA, Qiagen) using siLentFectTM Lipid Reagent for RNAi (170-3360, Bio-Rad, Hercules, CA). siRNA and transfection reagent were diluted in 100 mM NaCl solution and incubated with cells plated at 50% confluency at 20 nM siRNA for 58 hr. Following siRNA transfection, cells were serum-starved for 6 hr, then treated with 40 ng/mL neuregulin1-beta1 for 15 mins, and fixed and labeled for HER2 as previously described.

2.2.7 HER2-QD Quantification

For siRNA experiments, HER2-QD quantity per cell was measured for siControl or siHER2 treatment by quantifying the number of HER2-QD in the maximum projection of each image and

dividing by the number of cells in the image ($\frac{\#QDs \text{ per image}}{\#cells \text{ per image}}$). The HER2-QD count per image was quantified by custom MATLAB R2014B software (MathWorks), 'QD Counter', which created a maximum projection of a z-stack and located and counted the number of QDs present in the QD channel. The number of cells per image was determined by identifying the number of individual cells visible by WGA staining.

2.2.8 Western Blot

Cells were lysed in a RIPA buffer (Sigma-Aldrich) with Halt Protease and Phosphatase Inhibitor Cocktail (Pierce-Thermo Scientific) and then cleared by centrifugation. Protein concentration was estimated with a BCA assay (Pierce-Thermo Scientific). Proteins present in cell lysates (50 μ g) were resolved by SDS-PAGE and transferred onto Immobilon-FL PVDF membrane (EMD Millipore). Membranes were probed with antibodies specific for HER2 (3B5, Sigma-Aldrich) and Actin (sc-1615, Santa Cruz Biotechnology, Dallas, TX). Immunoreactive proteins were detected and quantified using infrared fluorescent IRDye[®] secondary antibodies and Odyssey[®] imagers (LI-COR Biosciences, Lincoln, NE).

2.2.9 Quantification of Western Blot

Western blots were quantified by capturing the HER2 signal from the largest band within a rectangular region, then propagating the same sized rectangular region across all other HER2 bands as well as over an area with no signal (background). The average intensity value of each rectangle was measured using ODYSSEY infrared imaging system (v3.0, LI-COR, Lincoln NE) with the background intensity subtracted. The same steps were repeated for measuring actin intensity. Each

intensity value was divided by actin within the same lane to normalize HER2 expression per experiment, and the final value divided by the value of siControl to yield relative HER2 expression.

2.2.10 Spatial Localization of pAKT-QD using Whole Cell Marker

For analysis of pAKT-QD using whole cell CellMask™, custom MATLAB software, ‘QDandMembraneViewer’ was used to quantify the distance of each pAKT-QD relative to the membrane, the number of pAKT-QD, and generate the 3D cell render. The program computes the cellular boundary as labeled by the fluorescent whole cell marker using a combination of Gaussian filtering, intensity thresholding, and edge detection. The program localizes QD position by (1) filtering the image with a band pass filter to isolate QDs, (2) locating QDs by finding local maxima in the image, (3) calculating QD location with centroid calculation, and (4) calculating the z-position from its mean z-position.

2.2.11 Spatial Localization of pAKT-QD using Subcellular Markers

For analysis of pAKT-QD in membrane or cytoplasm, custom MATLAB software, ‘CellAnalyzer’ was used to quantify the number of HER2-QD in the two regions as previously described (Vermehren-Schmaedick *et al.*, 2014). The program performs super-resolution detection of fluorescently-labeled membrane location using a combination of phase congruency measurements (Kovesi, 2000) and threshold-based segmentation methods. This program localizes QD position by: (1) identifying candidate QDs in each image plane, (2) localizing the position with a sub-pixel accurate method based on radial symmetry (Parthasarathy, 2012), and (3) linking QDs from each z-plane and using the linking criteria that requires a QD at the same XY pixel to be present in at least 3 planes to account for blinking behavior of QDs, and (4) calculating the z-position from its mean z-

position. The number of pAKT-QD in the membrane and cytoplasm were quantified for the mid-volume optical sections (across a depth of 5-7 μm) of each cell.

2.2.12 Spatial Distribution of pAKT-QD by 1D Probability Density Plots

The spatial distribution of pAKT-QD was plotted in 1D for the shortest distance of the pAKT-QD to the membrane using a kernel density estimate ('ksdensity' in MATLAB, MathWorks). The kernel density estimate generates a probability density estimate (PDE) for the data based on a normal kernel function that fits a Gaussian distribution to each data point. 1D PDE (distributions) were plotted using 1000 equally spaced points at a bandwidth of the kernel-smoothing window that was optimal for estimating normal densities. For the 1D population distribution of pAKT-QD, pAKT-QD distances within a cell and across all cells in a treatment were pooled and plotted as a single 1D distribution.

2.2.13 Spatial Distribution of pAKT-QD by 2D Probability Density Plots

For spatial density maps of pAKT-QD, custom MATLAB software, 'pde2DDriver' that calculates a 2D probability density estimate of the maximum projection of the pAKT-QD stack was utilized. The 2D probability density estimate fits a Gaussian distribution to the x- and y-coordinates of the localized pAKT-QD (Botev 2009). The resulting 2D PDE was plotted as (1) a contour plot over the maximum projection of the membrane, QD, and nuclear image to generate a spatial map of the cell, and (2) as a 3D surface plot of the 2D contour.

2.2.14 Classification of Membrane-Adjacent (Narrow) and Membrane-Distant (Broad) States

For analysis of the spatial states of cells, the 1D spatial distributions of pAKT-QD for each cell was separated as "narrow" (membrane-adjacent) or "broad" (membrane-distant). Distributions

of cells were classified as “narrow” if less than 50% of the pAKT-QD resided less than 2 μm from the membrane (as defined by the edge of the whole cell marker). Distributions of cells were classified as “broad” if more than 50% of the pAKT-QD resided at least 2 μm beyond the membrane. The number of cells classified as “narrow” or “broad” was divided by the total number of cells within each treatment to calculate the percent of cells representing each spatial state.

2.2.15 Statistical Analyses

For the HER2-QD data, the non-parametric Mann-Whitney rank sum test was conducted (‘ranksum’ function in MATLAB) at a $p < 0.05$ significance level to test the null hypothesis that data from two groups come from continuous distributions with equal medians against the alternative that they do not. For western blot data, a two-sample t-test (‘ttest2’ function in MATLAB) at a $p < 0.05$ significance level was conducted to test the null hypothesis that the data from two groups come from a normal distribution with equal means against the alternative that they do not.

2.3 Results

2.3.1 QDs Bind Specifically to Protein Target

I utilized two modalities for targeting QDs to two proteins of interest: HER2 and pAKT. For HER2, I used a monovalent affibody HER2-quantum dot probe (HER2-QD) that employs a new conjugation scheme to produce compact, high affinity live tracking probes (Szent-Gyorgyi *et al.*, 2008; Saurabh *et al.*, 2014; Wang *et al.*, 2015; Wang *et al.*, 2017b). These HER2-QD probes were generated by linking a small recombinant protein consisting of a HER2 affibody (58 amino acid peptide) $Z_{\text{HER2:342}}$ fused to a fluorogen activating protein ($\text{FAP}_{\text{dL5**}}$) to QDs using a malachite green analog (MG-Biotin). For labeling of pAKT, I employed sequential tagging of primary and

secondary antibodies as previously established (Jacob *et al.*, 2016). Due to the novel nature of this HER2-QD probe, I present detailed characterizations of this particular probe in the following section.

HER2 Affibody-FAP-MG-QD probes selectively bind to HER2.

HER2 receptors were quantified and localized by a bifunctional probe consisting of a HER2-specific affibody ($Z_{\text{HER2:342}}$) assembled to a fluorescent quantum dot (QD). Affibodies are a class of small (~7 kDa) affinity proteins that have been developed to bind with high specificity and affinity to a number of targets including HER2 (Eigenbrot *et al.*, 2010; Lyakhov *et al.*, 2010), and QDs are nanoparticles with optical properties of high brightness and photostability that make them advantageous for single particle tracking and imaging (Wu *et al.*, 2003; Michalet *et al.*, 2005). Monovalent association between affibody and QD was enabled by an emerging class of fluoromolecules called fluorogen activating proteins (FAPs), proteins derived from single-chain variable fragment antibodies (scFv), that selectively bind cognate small molecule fluorogens (Szent-Gyorgyi *et al.*, 2008; Saurabh *et al.*, 2014; Wang *et al.*, 2015). FAPs have an established high binding affinity and fast association time with fluorogens such as Malachite Green (MG) (Szent-Gyorgyi *et al.*, 2008; Saurabh *et al.*, 2014; Wang *et al.*, 2015), enabling its robust use in diverse applications from protein trafficking studies to single-particle tracking (Saurabh *et al.*, 2014; Schwartz *et al.*, 2015).

I made use of the FAP-MG system to target streptavidin-QDs using biotinylated MGs that specifically bind to a compact FAP-affibody fusion molecule (affiFAP) for the two-step monovalent detection of HER2 receptors using QDs. The schematic for labeling is shown in Figure 2.1A

(details in **Methods**). I labeled HER2 with affiFAP at high concentrations to tag many HER2 receptors on the cell surface (step 1, **Figure 2.1A**), and targeted low concentrations of MG-QD655, precomplexed at a stoichiometric ratio (1:1) that does not impede protein diffusion or induce protein aggregation (Saurabh *et al.*, 2014), to the affiFAP to obtain single-QD detection of HER2 receptors (step 2, **Figure 2.1A**). HER2 receptors labeled will be a combination of monomers and dimers. Validations of the HER2-QD probe were performed in a manner similar to past characterizations (Fichter *et al.*, 2010; Vermehren-Schmaedick *et al.*, 2014) to confirm HER2 specificity (**Figure 2.1C**) and single QD detection of HER2 by measuring the blinking behavior of the probe (**Figure 2.1B, right**). Representative fluorescent blinking profiles from two HER2-QDs show characteristic on-off behavior typical of single QDs. Additional characterizations confirmed also the specificity of the FAP and MG complex, and the unaltered specificity of the HER2 affibody following FAP fusion and MG conjugation (**Figure 2.2**). Specifically, these characterizations verified the functionality of the HER2 affiFAP to MG (**Figure 2.2A-B**), the unimpeded activation of MG by the FAP following HER2 affibody fusion (**Figure 2.2C-D**), the preserved specificity of the HER2 affiFAP fusion to HER2 (**Figure 2.2E-F**), and the functional labeling of the HER2 affibody-FAP-MG to HER2 in SKBR3 cells (**Figure 2.2G**).

Characterization of HER2 affibody-FAP-MG-QD binding to HER2

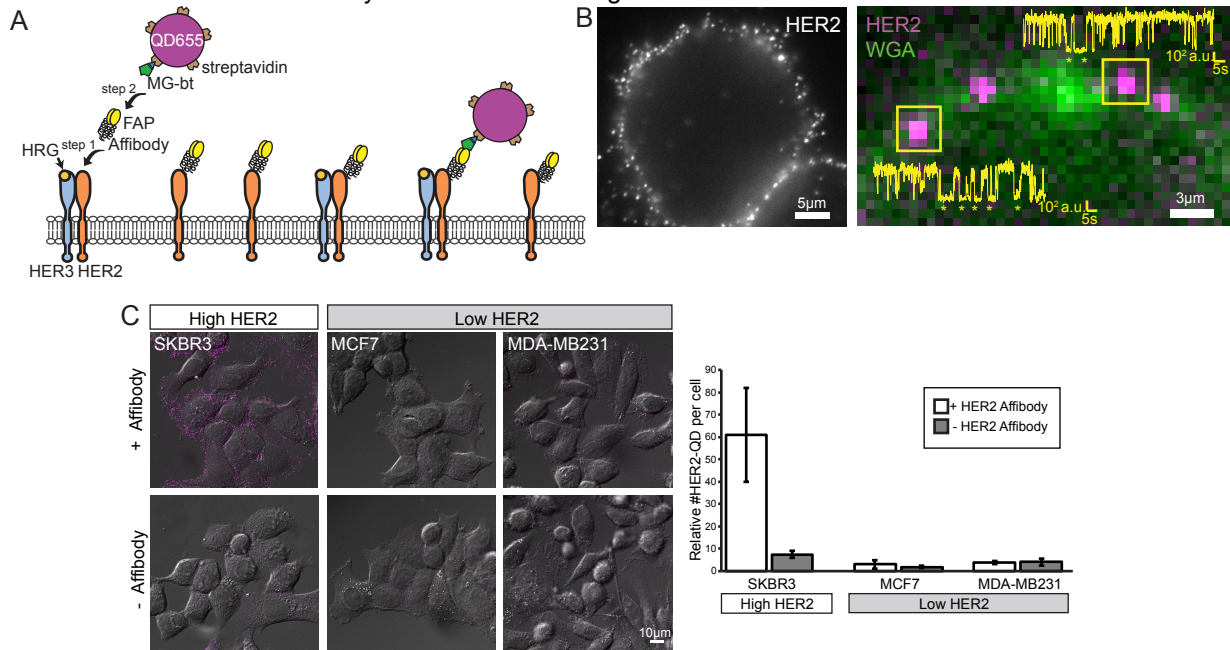
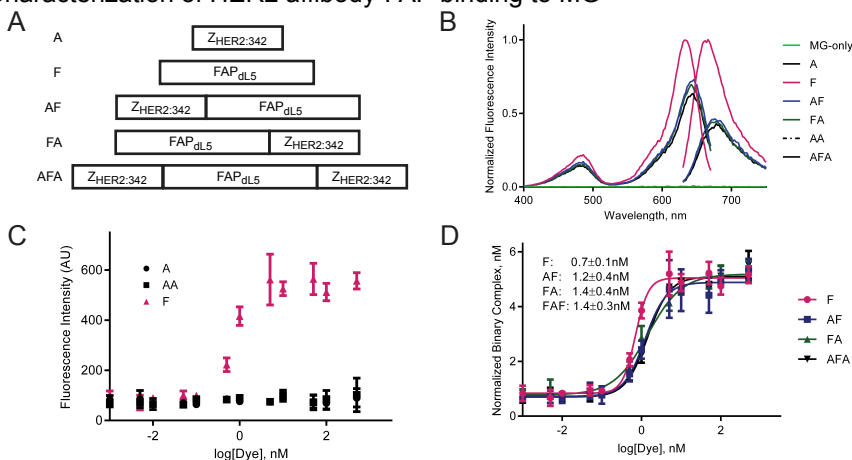


Figure 2.1: Characterization of HER2 affibody-FAP-MG-QD probe for monovalent and specific HER2 label.

(A) Two-step monovalent labeling of HER2 with single QDs in SKBR3. HER2 affibody-FAP fusion, AF ($Z_{HER2.342}$ -FAP $_{DL5^{**}}$), was added to cells (step 1) and detected by streptavidin QD655 and biotinylated MG (step 2) conjugated at 1:1. (B) Discrete HER2-QD fluorescence enables single QD detection of HER2. HER2-QD in fixed SKBR3 imaged at the plane of the coverslip (*left*), and blinking profiles (yellow, on *right*) of two HER2-QDs (magenta) on WGA-Alexa488 membrane (green) show characteristic on-off behavior of single HER2-QD probes. y -axis: intensity, x -axis: time, * are QD at off-state. (C) Validation of HER2-QD specificity. Max projection of HER2-QD on DIC of HER2-positive SKBR3 cells, and HER2-negative MCF7 and MDA-MB231 cells (*left*). HER2-QD quantity per cell plotted as mean \pm SD (*right*, $n=30$ cells)

Characterization of HER2 affibody-FAP binding to MG



Characterization of HER2 affibody-FAP-MG binding to HER2

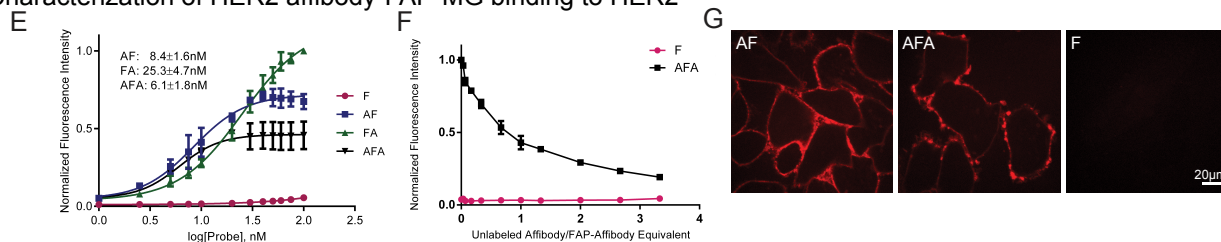


Figure 2.2: Characterization of HER2 affibody-FAP-MG for specific HER2 label.

(A) HER2 affibody-FAP fusion constructs. (B) HER2 affibody-FAP fusion and MG functionality confirmed by fluorescence spectra. MG-Btau (1 μ M), cell-impermeant analog of MG, was pre-complexed to probe constructs (10 μ M). (C) MG binding to FAP yields fluorescence enhancement, while MG binding to affibody alone did not. MG-Btau titrated with 5 nM of affibody ZHER2:342 (A), FAP_{dL5}** (F), or dimeric affibody (AA). Fluorescence measured at 636 nm (excitation) and 664 nm (emission). (D) FAP and MG association is unperturbed by HER2 affibody fusion to FAP as shown by binding equilibrium analysis. Fluorescence intensity corrected for fluorogen-only background, then normalized to FAP-MG fluorescence (1 nM). (E) HER2 affibody-FAP binds with high affinity to HER2 as shown by dissociation constant analysis of HER2 affibody-FAP on SKBR3. Mean fluorescence was corrected with FAP-MG background in cells, then normalized to mean fluorescence of probes (250 nM). (F) FAP conjugation preserves specificity of HER2 affibody to HER2 as shown by competition assay of nonfluorescent HER2 affibody (A) binding to cell surface. Cells labeled with AFA or F (250 nM), followed by serial dilution of A. MG-Btau (100 nM) added prior to measurement. (G) HER2 affibody-FAP fusion probes and MG display HER2 labeling in live SKBR3 cells, while FAP alone did not. HER2 detected by MG in cells labeled with fusion probes (30 nM) and MG-Btau (40 nM). Probe characterizations by Dr. Yi Wang.

pAKT-QD probes selectively bind to pAKT.

For labeling of pAKT, we employed sequential tagging using a primary and secondary antibody scheme. We utilized a primary polyclonal antibody that recognizes AKT1, AKT2, and AKT3 that are phosphorylated at Ser473, and detected this by a secondary antibody conjugated to a QD. Validations of the pAKT-QD were performed similar to past characterizations (Jacob *et al.*, 2016) and confirmed that this pAKT-QD was specific to pAKT (Figure 2.3).

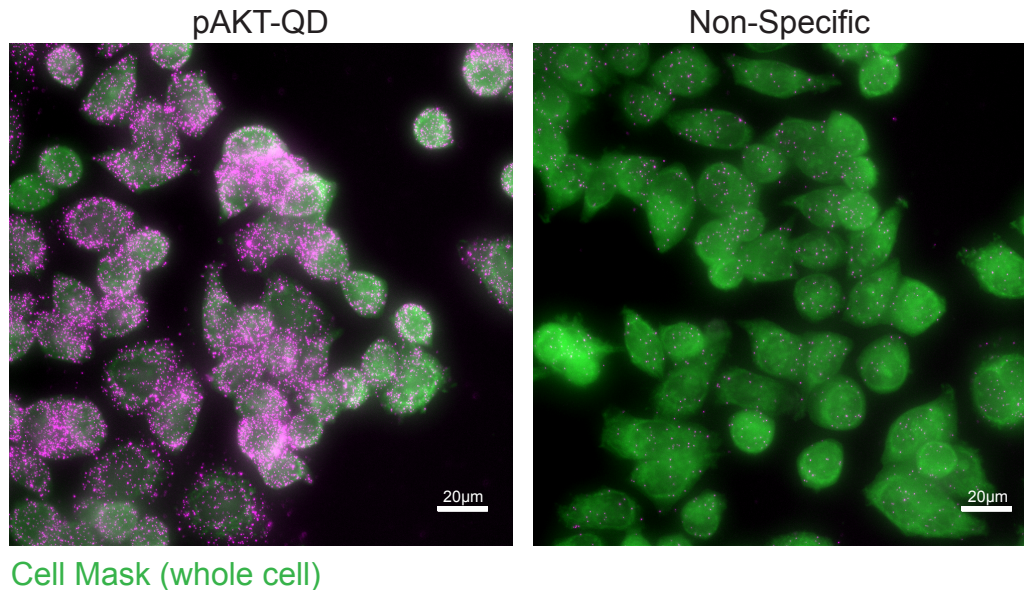


Figure 2.3: pAKT-QD probe shows specific labeling for pAKT.

For pAKT labeling, sequential tagging by a primary antibody against S473 and secondary antibody conjugated to QD was employed. For non-specific binding, only secondary antibody conjugated to QD was utilized. Only cells with both primary and secondary antibody displayed pAKT labeling, verifying the specificity of the pAKT-QD probe.

Altogether, these data show that our characterized HER2-QD and pAKT-QD probes have been validated to bind to their target proteins in a specific manner.

2.3.2 Increased Sensitivity of Protein Quantification by QD for Single Cells

Using the HER2-QD probe, we compared protein quantification by an imaging-based assay of QD tagged proteins compared to a conventional method of protein detection by western blot as a proof of concept of the QD assay's improved sensitivity. The punctate nature of QD fluorescence enables the ability to count individual proteins by the number of discrete QD particles visible. We demonstrated the capability of the QD assay in detecting subtle variations in HER2 quantity present amongst individual cells in experiments of HER2 and HER3 knockdown by siRNA. Application of the imaging-based QD assay, in which images of HER2-QD labeled cells by widefield

epifluorescence microscopy were quantified for discrete HER2-QD count, facilitated analysis of HER2 expression within an intact cellular architecture compared to the western blot technique.

Both the QD assay and western blot methods detected an expected decrease in HER2 expression of SKBR3 cells following siRNA knockdown of HER2 (siHER2), but our QD assay detected differences in the effect of siHER2 amongst individual cells, underscoring the variation in the degree of HER2 knockdown present within the same population of cells (**Figure 2.4A**). This is in contrast to the aggregate quantification obtained by the western blot technique, in which a single readout based on band intensity is produced to reflect HER2 expression for the cell population (**Figure 2.4B**).

This increased sensitivity by QD quantification revealed an interesting observation of HER2 upregulation in cells knocked down for HER3 (siHER3) (**Figure 2.4A**, siControl vs. siHER3) that was not obvious by western blot analysis (**Figure 2.4B**, siControl vs. siHER3). This upregulation is believed to be an increase in the number of HER2 protein rather than an increased availability for affibody binding as demonstrated by studies in the following chapter showing similar levels of HER2 binding regardless of HER2-HER3 activation (**Figure 3.7**). Additionally, the variability in HER2 expression present in siHER3 treated cells observed by QD quantification further demonstrated the heterogeneity in cell response. A subset of cells resembled control cells (in HER2 expression), but most exceeded control cells in HER2 expression. This heterogeneity in HER2 expression likely results in a net intensity of the siHER3 protein immunoblot that appears similar to siControl, and ultimately reflects a loss of critical information. Thus, the QD assay provides increased sensitivity for protein quantification in single cells compared to standard methods of protein detection.

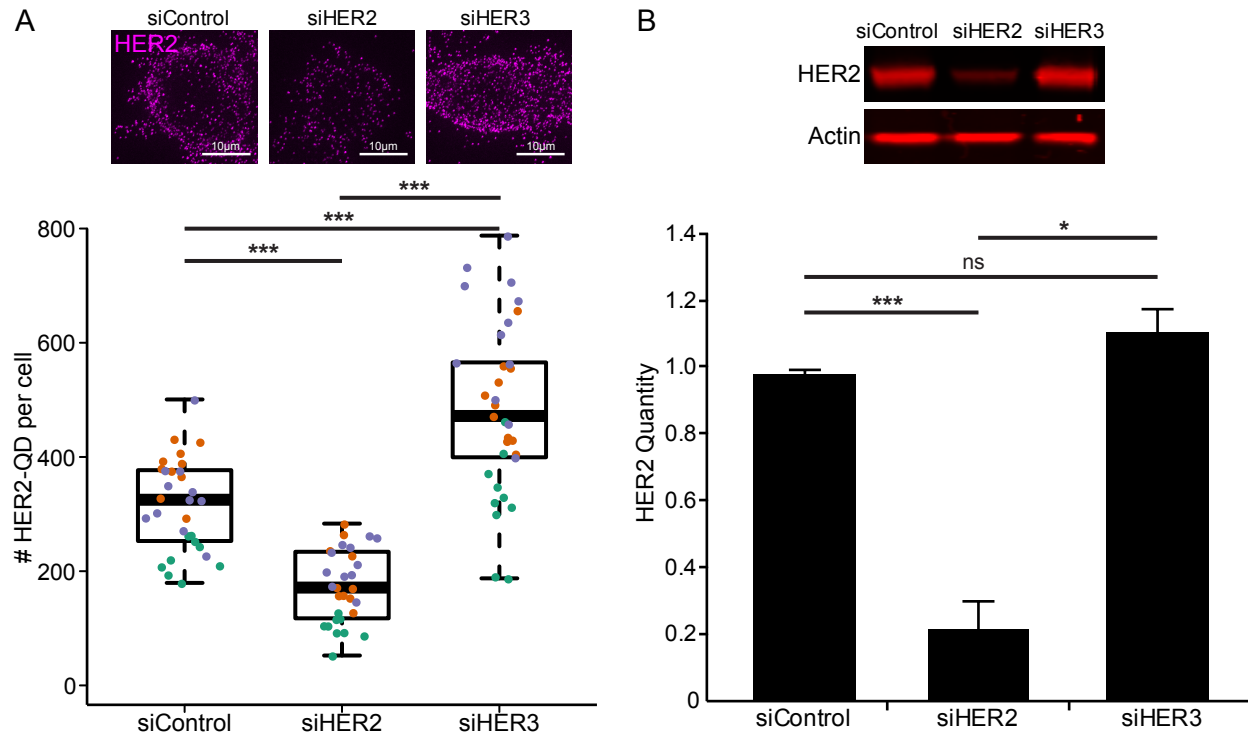


Figure 2.4: Quantification of HER2 by QD labeling demonstrates increased sensitivity for single cells compared to quantification by western blot.

(A) HER2 expression per cell quantified by discrete HER2-QD counts (boxplot, *bottom*) of maximum z-stack projections of HER2-QD channel (micrographs, *top*). HER2-QD quantity is reduced following HER2 knockdown by siRNA. Additionally, HER2-QD quantity is upregulated in a subset of cells following HER3 knockdown by siRNA. For boxplot, orange, green, and purple dots represent three different experiments, n=30 ROIs, 1079 cells. *** p<0.001, Mann-Whitney rank sum test. (B) Total HER2 expression by western blot (top) and quantification of western blots from three different experiments (bottom). The ensemble nature of this quantification overlooks individual differences in HER2 expression amongst cells. Bar plot is mean ± SEM. Cells were stimulated with 15 mins of the HER3-specific growth factor neuregulin1 (NRG1) following siRNA treatment. Note that (A) was labeled by an affibody targeting the extracellular domain of HER2 and (B) was labeled by an antibody binding an intracellular domain on the C-terminus. Western blot and quantification by Dr. Sunjong Kwon.

2.3.3 Discrete QD Enables Quantitative Spatial Localization of Proteins in Single Cells

The intact cellular architecture utilized by this imaging-based approach enables the study of the structural organization of the cell in relation to cellular outputs such as signaling. In addition to the ability to count the punctate fluorescence emitted by individual QD-labeled protein, we can also extract valuable spatial information based on a protein's localized coordinates in the cellular environment. In **Figure 2.5** and **Figure 2.6**, we demonstrated the utility of this QD imaging

approach by analyzing the spatial distribution and localization of the PI3K pathway component AKT.

I demonstrated the capability to extract spatial information of pAKT in relation to its single cell organization using two strategies for illuminating the cellular architecture: (1) a whole cell marker that labels the cytoplasm and nucleus of the entire cell (**Figure 2.5**) and (2) distinct tagging of cellular organelles by fluorescent labeling of membrane and nuclei individually (**Figure 2.6**).

Spatial distribution of pAKT by whole cell marker.

I utilized the first strategy of illuminating the cellular architecture through the whole cell marker “Cell Mask” to study how the spatial distribution of pAKT is altered following increasing durations of stimulation (**Figure 2.5A**). SKBR3 cells were stimulated with the HER3-specific growth factor neuregulin1 (NRG1) which is known to potentiate signaling through HER2-HER3 dimerization (Hynes and Lane). Widefield epifluorescence images (**Figure 2.5A**) were analyzed by detecting the edge of the Cell Mask marker (which I term as “membrane”), and localizing pAKT-QDs relative to this membrane for individual cells.

Single cell reconstructions of the localized pAKT-QDs (**Figure 2.5B, top**), and a measure of pAKT-QD distances relative to the membrane was plotted as a distribution (**Figure 2.5B, bottom**). These individual cellular plots show differences in the width of the distribution (narrow vs broad) that suggest a heterogeneity in the spatial organization of pAKT between cells. I classified and quantified this heterogeneity by distinguishing a “narrow” and “broad” distribution based on whether a majority of pAKT reside within 2 μm near or beyond the membrane (see **Methods**). Cells with pAKT that are primarily membrane-adjacent were labeled as “narrow” and cells with

pAKT that are primarily membrane-distant were labeled as “broad” (**Figure 2.5C**). I quantified the proportion of cells identified by each distribution (**Figure 2.5D**). At a baseline level of serum-starvation, most cells contained pAKT distributed away from the membrane (membrane-distant, broad distribution) (**Figure 2.5D**). Following 5 mins of NRG1 stimulation, there was an increase in the proportion of cells with pAKT distributed near the membrane (membrane-adjacent, narrow), and this proportion decreased with increasing duration (15 min and 1 hr) of NRG1. This suggested that at 5 mins of stimulation, most cells have pAKT distributed near the membrane, and with increasing stimulation time, most cells contain pAKT populations predominantly residing in the cytoplasm.

I next analyzed the spatial distribution of the entire population of pAKT from all cells (**Figure 2.5E**) and quantified the proportion of pAKT residing near the membrane (**Figure 2.5E**). Consistent with the increase in the proportion of cells with membrane-adjacent pAKT, there was an increase in the proportion of pAKT near the membrane at 5 mins of NRG1 stimulation (**Figure 2.5F**). This proportion of membrane-adjacent pAKT decreased with increasing stimulation time, again suggesting that there is an increase in the population of pAKT towards the cytoplasm with time.

Lastly, I determined pAKT quantity per single cell by analyzing the distribution of pAKT quantity (**Figure 2.5G**) and mean pAKT quantity per cell (**Figure 2.5H**) for each stimulation duration. With increasing stimulation time, a greater percentage of cells displayed increased phosphoactivity (**Figure 2.5G-H**). Together, these data suggest that at a cellular level, HRG stimulation induces HER2-HER3 signaling that yields increased phosphorylation of AKT at the

membrane, and with longer stimulation, these pAKT population proportions change such that they reside in the cytoplasm. At the population level, the presence of different pAKT spatial states (membrane-adjacent and membrane-distant) and phosphorylation levels suggests that heterogeneity exists in the signaling state adopted by cells within a population.

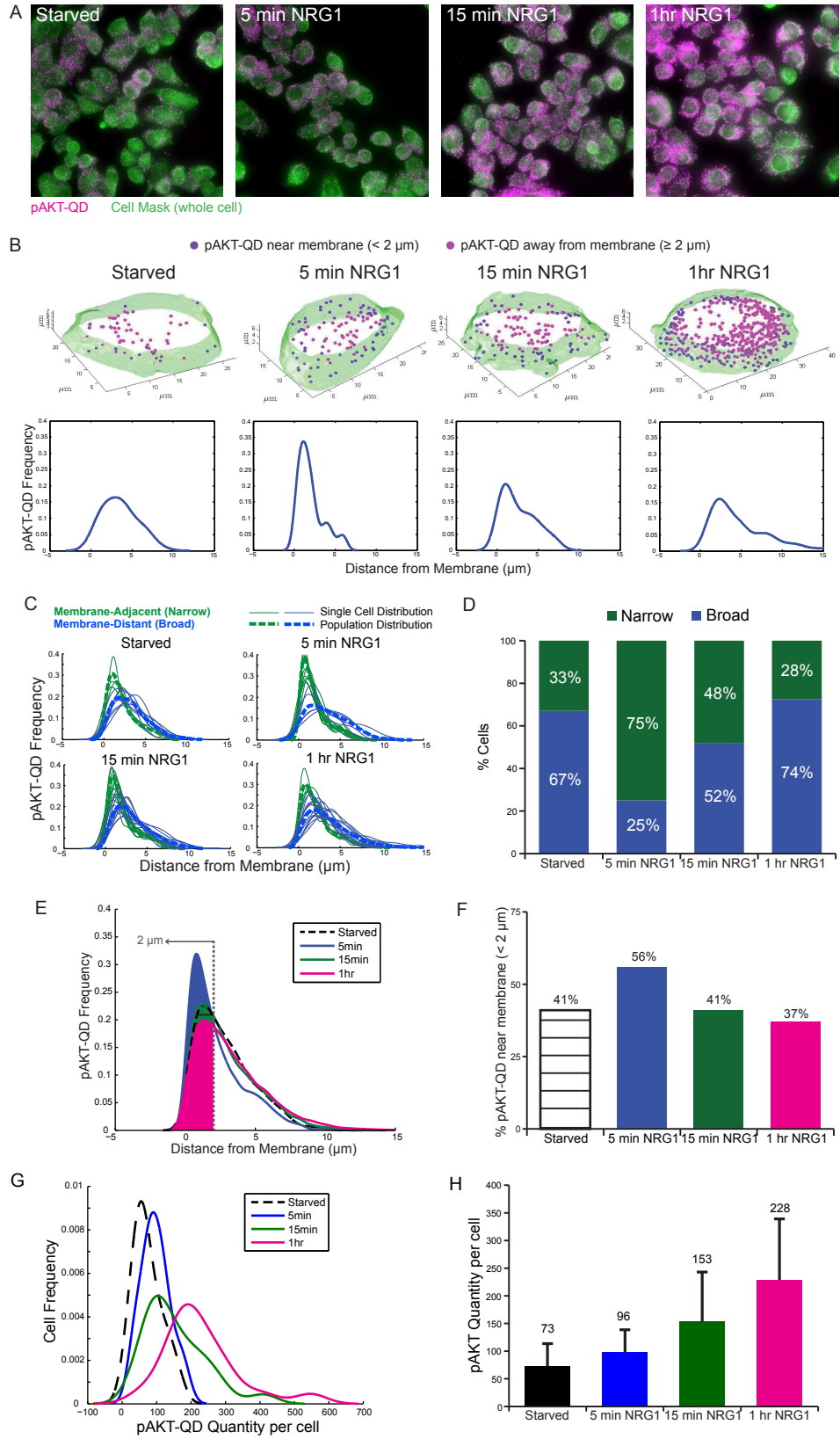


Figure 2.5: Quantitative spatial distribution of pAKT-QD in single cells. (Figure legend on next page)

Figure 2.5 (continued):

(A) SKBR3 cells labeled for pAKT-QD (magenta) and Cell Mask whole cell marker (green), and stimulated with NRG1 for 5 min, 15 min, and 1 hr. (B) Top: 3D visualization of pAKT-QD relative to the Cell Mask edge (“membrane”) of individual cells from (A). Bottom: Distribution of pAKT-QD distance from the membrane for individual cells (top). Purple dots represent pAKT-QD near membrane ($< 2 \mu\text{m}$ from the membrane), and magenta dots represent pAKT-QD away from membrane ($\geq 2 \mu\text{m}$ from the membrane). (C) Distribution of pAKT-QD for single cells from (A) classified as “narrow” or “broad” for cells with membrane-adjacent or membrane-distant pAKT populations respectively. (D) Percent of cells characterized as “narrow” or “broad” as quantified from (E). (E) Total distribution of pAKT-QD distance for all cells analyzed from (A). Shaded region represents population of pAKT-QD near membrane ($< 2 \mu\text{m}$). (F) Percent of pAKT-QD near membrane within each treatment condition as quantified by shaded region in (C). (G) Distribution of pAKT-QD quantity per cell for conditions from (A). (H) pAKT-QD quantity per cell as quantified in (G). Bar plot is mean; error bar is SD. $n=12-23$ cells for each condition. Software written by Dr. Damien Ramunno-Johnson.

Spatial localization of pAKT by subcellular markers

I next utilized a strategy of illuminating the cellular architecture through tagging of subcellular structures of the membrane, nucleus, and cytoplasm. This strategy enabled better discernment of pAKT spatial localization by colocalization of the protein with a cellular structure. To track the time course of pAKT spatial localization during signaling, I stimulated SKBR3 cells with a 5 min pulse of NRG1, removed the stimuli, and monitored pAKT at different times following the pulse stimulation (t_d , **Figure 2.6A**).

I quantified pAKT as count (**Figure 2.6B**) and proportion (**Figure 2.6C**) in the membrane and cytoplasm per cell. Additionally, I determined pAKT quantity per cell (**Figure 2.6D**). Consistent with the previous figure (**Figure 2.5C-H**), immediately following stimulation ($t_d=0$ sec), there was a marked increase in the proportion and quantity of pAKT at the membrane. At the same time, there was a corresponding decrease in pAKT at the cytoplasm, suggesting that a subset of pAKT may move from the cytoplasm to the membrane post-stimulation (Starved vs $t_d=0$ sec, **Figure 2.6B-C**). This balance of pAKT proportion at these subcellular regions was retained for the most part until 5 mins post-stimulation, when there was a substantial increase in quantity and proportion

of pAKT at the membrane, but not a corresponding decrease in quantity at the cytoplasm, suggesting that a subset of AKT was being phosphorylated at the membrane ($t_d=1$ min vs $t_d=5$ min, **Figure 2.6B-D**). By 15 mins post-stimulation, signaling was dampened as confirmed by the decrease in pAKT at both subcellular regions ($t_d=5$ min vs $t_d=15$ min, **Figure 2.6B-D**). Though at 30 mins post-stimulation, I observed an unexpected increase in pAKT amount in the membrane and cytoplasm (but unchanged pAKT proportions) that may represent a delayed signaling response by some cells ($t_d=15$ min vs $t_d=30$ min, **Figure 2.6B-D**). Lastly, spatial density maps plotted as contour and surface plots lend further visual evidence of the degree of pAKT spatial localization relative to the subcellular organization of the cell at the various time points (**Figure 2.6F** and **Figure 2.7**).

Together, these data suggest that following stimulation, there is a steady increase in pAKT quantity at the membrane that reaches a maximum at 5 mins post-stimulation, decreases at 15 mins post-stimulation, but increases again by 30 mins (**Figure 2.6E**). This points to a cycle of signaling that peaks within minutes following stimulation, returns back to a basal state, with a second cycle of delayed signaling following. The precision in which I was able to perform molecular accounting of individual pAKT-QDs reveals that the increase in membrane pAKT at 0 sec post-stimulation was likely due to movement of pAKT from the cytoplasm to the membrane, and at 5 mins post-stimulation was due to phosphorylation of AKT at the membrane. However, further work will need to be done to corroborate that the general trend observed here is also reflected by the conventional method of western blot.

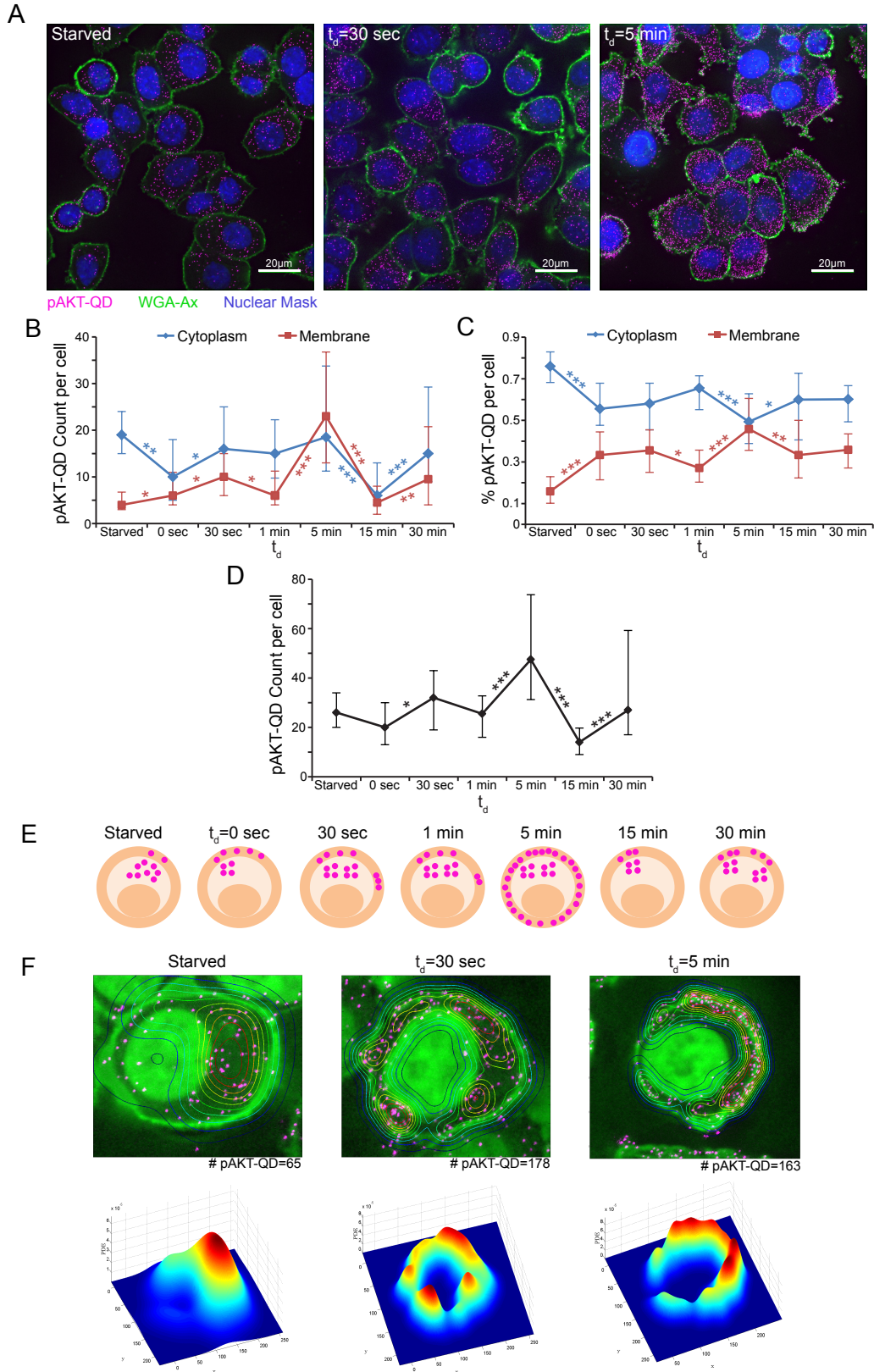


Figure 2.6: Quantitative spatial localization of pAKT-QD in subcellular regions of single cells. (Figure legend on next page)

Figure 2.6 (continued):

(A) SKBR3 cells labeled for pAKT-QD (magenta), WGA-Ax for membrane (green), and nuclei (blue). Cells were stimulated with NRG1 for 5 min, then fixed at times following stimulation (t_d). Images are maximum projection of pAKT-QD channel overlaid on a single mid-optical section of WGA-Ax and nuclei channel image. (B) pAKT quantity in membrane and cytoplasm per cell (for the mid-volume optical sections, depth 5-7 μm). Plot is median count; error bar is SD. (C) Percent of pAKT in membrane and cytoplasm per cell (for the mid-volume optical sections, depth 5-7 μm). Plot is median percent; error bar is SD. (D) pAKT quantity per cell. Plot is median, error bar is SD. (E) Schematic depicting relative change in pAKT localization in membrane and cytoplasm at times following a 5 min HRG pulse (t_d). (F) Top: Spatial density map of pAKT represented as contour lines overlaid on single SKBR3 cells labeled for pAKT-QD (magenta), WGA-Ax for membrane (green), and nuclei (green). Contour line spacing depicts degree of localization (tightly spaced contour lines are highly localized pAKT). Images are maximum projection of mid-optical sections of pAKT-QD, WGA-Ax, and nuclei channel. Bottom: Spatial maps (from top) visualized as 3D surface plots highlighting regions of high pAKT density as peaks in red. Width of peak depicts degree of localization (narrow peaks are highly localized pAKT). All cells were stimulated with HRG for 5 min, then fixed at times following stimulation (t_d). $n=58-70$ cells for each condition. $***p<0.001$, Mann-Whitney rank sum test. Software written by Dr. Damien Ramunno-Johnson. Spatial maps by Alec Bowcock.

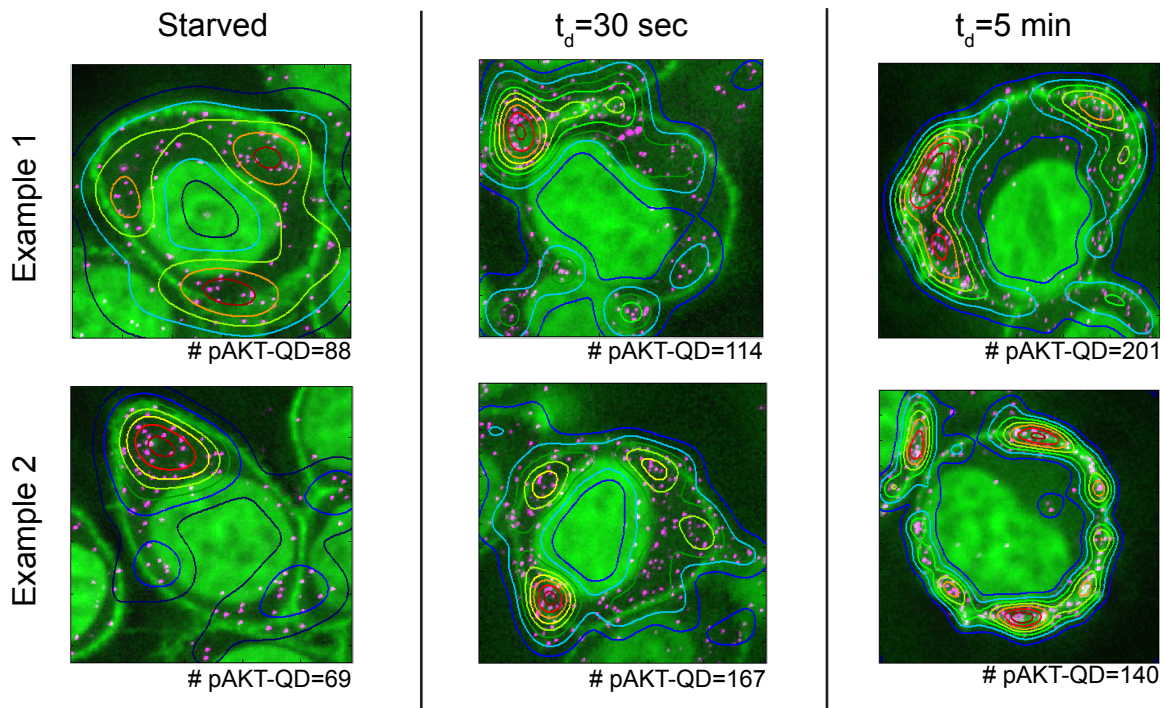


Figure 2.7: Additional spatial maps of SKBR3 cells from Starved conditions, 30 sec and 5 min post-NRG1 stimulation.

Additional examples of spatial density map of pAKT shows high localized pAKT in cells post-NRG1 stimulation. Spatial maps represented as contour lines overlaid on single SKBR3 cells labeled for pAKT-QD (magenta), WGA-Ax for membrane (green), and nuclei (green). Contour line spacing depicts degree of localization (tightly spaced contour lines are highly localized pAKT). Images are maximum projection of mid-optical sections of pAKT-QD, WGA-Ax, and nuclei channel. Spatial maps by Alec Bowcock.

2.4 Discussion

2.4.1 Sensitive Detection of HER2-QD in Single Cells Reveal Increased HER2 with HER3 Knockdown

In this chapter, I presented characterizations of a HER2-QD probe and demonstrated the application of this QD approach for the quantification of protein levels that was advantageous over the current standard of protein detection through western blot. Due to the punctate nature of QD fluorescence and the imaging-based nature of this assay, individual HER2-QD particles can be quantified for individual cells. The increased sensitivity of this approach allows analysis of protein levels at single cell resolution that was not possible from ensemble measurements acquired through protein immunoblots. This improvement in cellular resolution was verified by the finding that variation in cell responses exist amongst different cells of the same population. For instance, I observed through the QD assay that HER2 is expressed at varying quantities in cells, and this heterogeneity resulted in different levels of HER2 knockdown following HER2 siRNA treatment.

Interestingly, this method allowed us to discern an increase in HER2 following HER3 knockdown that was undetectable by western blot (**Figure 2.4**). It is necessary to note here though, that the comparison between the QD assay and western blot is not directly comparable due to the different affinity reagents employed (anti-HER2 affibody against HER2 extracellular domain for QD assay vs anti-HER2 antibody against intracellular domain for western blot). Though it is possible that even with a similar affinity reagent, the western blot technique may not have captured the HER2 expression difference revealed by the single cell variability sensitively captured by the QD-assay.

Regardless, these results suggest interesting HER2 modulation. While it has been established that HER3 expression increases following HER2 knockdown or inhibition (Garrett *et al.*, 2011), upregulation of HER2 following knockdown of HER3 has not been previously detected (Liu *et al.*, 2007; Lee-Hoeflich *et al.*, 2008; Jaiswal *et al.*, 2013). This HER3 knockdown-induced increase in HER2 expression has interesting biological implications for targeting HER2-HER3 signaling. HER2-HER3 is the preferential dimer driving mitogenic signaling in cancer (Hynes and Lane, 2005; Baselga and Swain, 2009). It is possible that knockdown of this dimerization partner drives cells to compensate through upregulation of HER2 to enable HER2 homodimers as a substitute for HER2-HER3. This points to the dependence of cells on HER2-driven signaling, and also to their ability to adapt by developing compensatory effects in the absence of major signaling partners. Thus, maximal effective targeting of HER2 signaling in the future requires synergistic approaches that not only inhibit independent HER2 and HER3 functions and their capacity to dimerize, but also novel strategies that aim at reducing cellular heterogeneity.

2.4.2 Quantitative Analysis of pAKT-QD Spatial Organization Underscore Cell Heterogeneity and Protein Localization Time Course

The ability to image proteins labeled by QDs within their intact cellular environment enabled us to analyze the spatial distribution and localization of pAKT in a subcellular context. I demonstrated the capability to examine the spatial organization of pAKT using two modalities of cell structure illumination: (1) a whole cell marker and (2) labeling of individual cellular organelles, both in conjunction with the QD (Figure 2.5 and Figure 2.6).

Using the first method of whole cell labeling by Cell Mask, I analyzed the spatial distribution of pAKT relative to the membrane (**Figure 2.5**). I found that upon stimulation, pAKT is distributed near the membrane, and with increasing stimulation duration, this population proportion increases within the cytoplasm. Our findings that cells exhibited different spatial states as represented by cells with membrane-adjacent and membrane-distant populations of pAKT demonstrated that there is heterogeneity present between cells of the same population. This heterogeneity is present in both the spatial distribution of pAKT and the level of phosphoactivity present within each cell and raises the interesting notion that these parameters could provide key information about a cell's signaling state. Importantly, it is possible that these cells transition from one spatial state to another, or are resistant to adopting a particular state due to a number of factors: stage of cell cycle or differentiation state (Chaffer and Weinberg, 2011). Of interest would be correlating these spatial states with the quantity of phosphoactivity, as well as their cellular morphology as a method of identifying different cell populations.

One limitation of the previous method is the inability to distinguish the boundaries of adjacent cells due to the lack of a membrane marker, thus restricting analysis to only cells without bordering neighbors. Using a second method in which subcellular organelles were labeled individually, I was able to better discern the spatial localization of pAKT (**Figure 2.6**). Using this technique, I measured with high sensitivity the quantity of pAKT in the membrane and cytoplasm at different times following stimulation and showed that pAKT levels increased steadily to reach a peak at 5 mins post-stimulation, decreased, and rose again 30 mins following. By molecularly accounting for pAKT at different time points, I showed that the increase in pAKT at the membrane

immediately following stimulation was likely attributed to a movement of pAKT from the cytoplasm to the membrane, and that at 5 mins post-stimulation due to phosphorylation of AKT at the membrane. These data demonstrate the strength of the QD assay in precisely measuring the spatial localization of pAKT in different subcellular compartments in a quantitative manner.

Together, these results establish the utility of the QD as a sensitive probe for extracting protein quantity and spatial information within the intact cellular environment at single cell resolution. Further work comparing the results found through the QD assay to the conventional method of western blot analysis to corroborate the trend of AKT observed will strengthen these results. Regardless, the power of this imaging tool opens the door to studying aspects of biology ranging from protein localization and cell heterogeneity to protein dynamics. In the next chapter, I further explore the strength of the QD and apply this tool to study the spatiotemporal dynamics of HER2 to further uncover its signaling biology.

CHAPTER 3: SPATIOTEMPORAL DYNAMICS OF HER2 SIGNALING IN PROTRUSION IS MEDIATED BY ACTIN

A version of the following has been submitted to Molecular Biology of the Cell on August 16, 2017:

3.1 Introduction

Many different types of cells exhibit protrusions, which are fine, nanoscale-sized structures that are extensions of the cell membrane periphery. Protrusions are used to move and navigate, as well as to sense environmental chemicals and communicate with nearby cells, (Insall and Machesky, 2009; Ridley, 2011; Plotnikov and Waterman, 2013; Fairchild and Barna, 2014). Such functions are essential to normal basic biological processes including embryogenesis, wound healing, and inflammatory response (Wood *et al.*, 2002; Redd *et al.*, 2004; Kornberg and Roy, 2014; Prols *et al.*, 2016). Several protrusion types have been defined based on shape, molecular composition and function. These include flat-sheet-like lamellipodia involved in cell migration (Abercrombie *et al.*, 1971; Pollard and Borisy, 2003), and slender, antennae-like filopodia that sense chemical gradients to guide cell movement (Mattila and Lappalainen, 2008).

In cancer, dysregulated protrusion growth is linked to increased cellular invasiveness and disease progression (Machesky, 2008; Mattila and Lappalainen, 2008; Arjonen *et al.*, 2011; Jacquemet *et al.*, 2015). Filopodia and other protrusions express a variety of cytokines, integrins, and other small molecule receptors, as well as signaling and cytoskeletal proteins (Hsiung *et al.*, 2005; Lidke *et al.*, 2005a; Huttenlocher and Horwitz, 2011; Sanders *et al.*, 2013). Several of these proteins are highly aberrant in cancer. For example, elevated expression levels of myosin-X and fascin is associated with poor outcome in several tumor types including cancers of breast, ovarian, and lung (Pelosi *et al.*, 2003; Daponte *et al.*, 2008; Machesky and Li, 2010; Yang *et al.*, 2013; Cao *et al.*, 2014; Huang *et al.*, 2015). Moreover, proteins such as integrins and cytoskeletal filaments such as

actin are found at concentrated levels in protrusions (Mattila and Lappalainen, 2008; Huttenlocher and Horwitz, 2011). Understanding the spatiotemporal and dynamic behavior of these molecules in the cell protrusion environment may yield new insight into cancer and fundamental cell function.

HER2 is a member of the ERBB/HER receptor tyrosine kinase family and is over expressed in several cancers (e.g. breast, ovarian, prostate, pancreatic, and gastric cancers) (Slamon *et al.*, 1989; Menard *et al.*, 2001; Rubin and Yarden, 2001; Yarden and Sliwkowski, 2001; Edwards *et al.*, 2004; Gravalos and Jimeno, 2008). HER2 drives downstream signaling of tumor growth and metastasis by heterodimerizing with HER-family receptors – most notably HER3 – and HER2 pathway activation is linked with protrusion growth (Grothey *et al.*, 2000; Marone *et al.*, 2004; Yokotsuka *et al.*, 2011; Jeong *et al.*, 2017). Localization of HER2 and modulation of HER2 expression has been reported on membrane protrusions in breast cancer cells (Hommelgaard *et al.*, 2004; Lerdrup *et al.*, 2007; Peckys *et al.*, 2015; Chung *et al.*, 2016; Jeong *et al.*, 2017). EGF receptor dimerization is enriched at the cell periphery and undergo retrograde transport and endocytosis in cancer cell protrusions (Lidke *et al.*, 2005a; Chung *et al.*, 2010). While HER2 dimerization and endocytic trafficking dynamics have been described in non-protrusive regions of cells (Lidke *et al.*, 2004; Tada *et al.*, 2007), little or no information exists on the spatiotemporal dynamic behavior of HER2 signaling at protrusions. Finally, a high density of HER2-HER3 heterodimers has been reported to enable transphosphorylation between adjacent HER2-HER3 heterodimers, suggesting a functional role for HER2 signaling in protrusions (Zhang *et al.*, 2012). Such information would help shed light on how the presence of HER2 and other growth factor receptors on protrusions conducts cell functional signaling outcome.

Here, I study the spatiotemporal dynamics of HER2 at protrusions of breast cancer cells, before and after treatment with the HER3 ligand, neuregulin 1 (NRG1). I use super-resolution fluorescence and focused ion beam (FIB) electron microscopy to examine protrusion morphology, and HER2 and actin localization/structure with nanoscale detail (Betzig *et al.*, 2006; Hess *et al.*, 2006; Rust *et al.*, 2006; Huang *et al.*, 2008; Pavani *et al.*, 2009; Patterson *et al.*, 2010; Jorgens *et al.*, 2017). I conduct single particle tracking (Fichter *et al.*, 2010; Vermehren-Schmaedick *et al.*, 2014; Vu *et al.*, 2015; Jacob *et al.*, 2016; Relich *et al.*, 2016) using new monovalent affibody HER2-quantum dot probes (HER2-QDs) that employ a new conjugation scheme to produce compact, high affinity live tracking probes (Szent-Gyorgyi *et al.*, 2008; Saurabh *et al.*, 2014; Wang *et al.*, 2015; Wang *et al.*, 2017b). I report that: 1) breast cancer cell lines and breast tumor tissue possess filopodia and lamellipodia with morphologically similar nanoscale structure; 2) HER2 stimulation of protrusion growth is rapid and spatially localized; 3) HER2 and downstream pAKT (PI3K pathway output) molecules are primarily localized in protrusions; 4) HER2 motion is primarily diffusive in protrusions and characterized by unusually rapid receptor dynamics in filopodia; and 5) disruption of actin that perturbs its linear structure reduces HER2 rapid mobility to that similar to HER2 motion in non-protrusive cellular regions. I propose a mechanism of rapid HER2 signaling that does not require active transport and is supported by the interaction of signaling molecules with the local protrusion environment to mediate efficient growth of cancer cell protrusions.

3.2 Materials and Methods

3.2.1 Cell Culture

Human breast cancer epithelial cell lines SKBR3, MCF-7, and MDA-MB231 were obtained from ATCC (Manassas, VA), and 21MT-1 was kindly provided by Dr. Kornelia Polyak (Dana-Farber Cancer Institute) and developed by the laboratory of Dr. Ruth Sager (Dana Farber Cancer Institute). Cell media and antibiotics were obtained from Gibco-Thermo Fisher (Waltham, MA). SKBR3 (HER2 overexpressing) cells were grown in McCoy's 5A containing 10% FBS. MDA-MB231 (low HER2-expressing, Basal-like) and MCF-7 (low HER2-expressing, Luminal A) were grown in DMEM containing 10% FBS. 21MT-1 (HER2 overexpressing) cells were grown in equal parts DMEM and Ham's F12 containing 10% horse serum, 10 µg/mL insulin (Sigma-Aldrich, St. Louis, MO), 100 ng/mL cholera toxin (Sigma-Aldrich), 20ng/mL EGF (BD Biosciences, San Jose, CA), and 500 ng/mL hydrocortisone (Sigma-Aldrich). All media were supplemented with 100 µg/mL streptomycin and 100 U/mL penicillin. For live cell imaging or immunofluorescence labeling experiments, 100,000 cells were plated per 18 mm diameter, No. 1.5 glass coverslips (Electron Microscopy Sciences, Hatfield, PA) and cultured for 72 hours in 12-well plates (Corning Inc., Corning, NY). Cells were maintained at 37°C in a humidified atmosphere of 5% CO₂.

3.2.2 Live Cell Microscopy

SKBR3 cells were imaged in real-time using either differential interference contrast (DIC) or fluorescence video microscopy on an inverted epifluorescence microscope (Zeiss Axiovert 200 M, 63x/1.4 oil objective, Oberkochen, Germany) equipped with an EM-CCD camera (iXon Ultra 897, Andor Technology, Belfast, Ireland) using Micro-Manager v1.4.17 (Edelstein *et al.*, 2014). Cells on coverslips were situated in a magnetic chamber (CM-B18-1, Quorum Technologies, Ontario,

Canada) maintained at a constant temperature of 37°C using a heating inset (model P S1, PeCon GmbH, Erbach, Germany), a heating ring for the 63x objective, and a temperature control unit (Temp Module S1, PeCon GmbH). For DIC microscopy, cells were imaged in serum-media (McCoy's 5A with 10% FBS), and for HER2-QD imaging, cells were suspended in serum-media until immediately prior to imaging. During HER2-QD imaging, background and toxicity was minimized by imaging cells in FluoroBrite[™] DMEM (Gibco-Life Technologies) buffered with 25 mM HEPES (Gibco-Life Technologies) and supplemented with 50 ng/mL ascorbic acid. DIC video microscopy was performed at a rate of 1 fps and fluorescence video microscopy was performed at rates of either 7 fps or 20 fps at a z-plane near the coverslip over 5000 frames. An Optosplit II dual emission system (Cairn Research, Kent, UK) allowed simultaneous acquisition of two color channels (FITC and QD655) during fluorescence imaging.

3.2.3 Wide-Field Fluorescence Microscopy.

For wide-field epifluorescence imaging, fixed SKBR3 cells were imaged using an inverted epifluorescence microscope (Zeiss Axio Observer.Z1, 63x/1.4 oil objective) equipped with an EM-CCD camera (Luca R 604, Andor Technology) using Micro-Manager. Cells were imaged over the total height of the cells by acquiring z-stacks at a z-step of 150 nm. Fluorescence emissions for Alexa488 and Alexa647 were detected using FITC and Cy5 filter cubes (excitation 480 nm/emission 535 nm and excitation 620 nm/emission 700 nm respectively; Chroma, Bellows Fall, VT), and QD fluorescence was detected using a QD655 filter cube (excitation 435 nm/emission 655 nm, Semrock, Rochester, NY). Image stacks were deconvolved using AutoQuant X2 (Media Cybernetics, Rockville, MD). For WGA-Alexa488, WGA-Alexa647, pAKT-Alexa488, and

phalloidin-Alexa647, the 3D Blind Deconvolution algorithm was used with an adaptive PSF, medium noise value of 20, and 5 total iterations for 87 frames at a stack spacing of 150 nm. For HER2-QD655, the No/Nearest Neighbor algorithm was used with haze removal factor 0.99 and z-kernel width 2 for 87 frames at a stack spacing of 150 nm.

3.2.4 Scanning Electron Microscopy

For structured illumination microscopy (SIM), fixed SKBR3 cells were mounted in ProLong Gold antifade reagent (Life Technologies, Carlsbad, CA) and cured overnight at room temperature. Cells were imaged on a Zeiss Elyra PS.1 microscope with a 63x/1.4 oil objective equipped with an EM-CCD camera (iXon 897, Andor Technology) using ZEN software (Zeiss). Cells were imaged over a height of 3-5 μm from the coverslip by acquiring z-stacks at a z-step of 110 nm with 3 grating rotations. Fluorescence for WGA-Alexa488 was excited with a 488 nm laser, and emission was captured by a band-pass (BP) filter (495-575 nm) and long-pass (LP) filter (750 nm). Fluorescence for phalloidin-Alexa647 was excited with a 635 nm laser and emission was captured by an LP filter (655 nm). Images were reconstructed using ZEN to generate the final super-resolution SIM image.

3.2.5 Structured Illumination Microscopy

For structured illumination microscopy (SIM), fixed SKBR3 cells were mounted in ProLong Gold antifade reagent (Life Technologies, Carlsbad, CA) and cured overnight at room temperature. Cells were imaged on a Zeiss Elyra PS.1 microscope with a 63x/1.4 oil objective equipped with an EM-CCD camera (iXon 897, Andor Technology) using ZEN software (Zeiss). Cells were imaged over a height of 3-5 μm from the coverslip by acquiring z-stacks at a z-step of 110 nm with 3 grating rotations. Fluorescence for WGA-Alexa488 was excited with a 488 nm laser, and emission was captured by a band-pass (BP) filter (495-575 nm) and long-pass (LP) filter (750 nm). Fluorescence

for phalloidin-Alexa647 was excited with a 635 nm laser and emission was captured by an LP filter (655 nm). Images were reconstructed using ZEN to generate the final super-resolution SIM image.

3.2.6 2D STORM Imaging

2D STORM imaging was performed on a custom PALM/STORM setup constructed on a Nikon Ti-U inverted microscope frame as described previously (Creech *et al.*, 2017). Fresh imaging buffer containing an oxygen scavenging system and mercaptoethylamine (MEA) (Sigma-Aldrich, St. Louis, MO) was added 15 min before imaging. For 2D STORM imaging of Alexa647, both the 647 nm laser (1-2 kW/cm²) and the 405 nm laser (0-10 W/cm²) were applied to the sample simultaneously. The intensity of the 405 nm laser was increased gradually as the imaging progressed to ensure appropriate switching rates of the Alexa647 fluorophores. At these power densities, the EM-CCD was operated in frame transfer mode at 10 ms exposure time with an EM gain setting of 300, and each data set typically contained 50,000 frames. In all 2D STORM experiments, 100 nm gold nanoparticles were used as fiduciary markers. A custom-built focus stabilization system was used to maintain the image focus within ± 25 nm. All image acquisition was done with Micro-Manager (Edelstein *et al.*, 2014). Raw SMLM movies were processed using a custom-written MATLAB package (Nickerson *et al.*, 2014).

3.2.7 Double-Helix 3D Super-Resolution Imaging

3D super-resolution imaging was performed on a Nikon N-STORM microscope with 100X 1.49 NA objective and the Double-Helix (DH) SPINDLE™ (Jain *et al.*, 2016; Wang *et al.*, 2017a) module with a Double-Helix phase mask (Pavani *et al.*, 2009; Grover *et al.*, 2012) optimized for far-red dyes. Images were captured using a Hamamatsu Orca Flash 4.0 sCMOS camera (2x2 binned) using a 30 ms exposure. The molecules were imaged using a 647 nm laser and the density of active

molecules was maintained throughout the acquisition using a 405 nm laser to reactivate Alexa647 dye molecules. For each image 200,000 frames were acquired, resulting in more than 4 million localizations per reconstruction. Samples were imaged in freshly prepared buffer containing 1% beta-mercaptoethanol (\textbeta ME), 100 mM Tris, pH 8.0, 10 mM NaCl and an oxygen scavenging system (Dempsey *et al.*, 2011). Individual fluorophores were localized in 3D using Double-Helix's TRAX™ software. The data were drift corrected using the cross-correlation function and rendered using the normalized Gaussian method with the ImageJ plugin, ThunderSTORM (Ovesny *et al.*, 2014). The z-depth was color coded using the ImageJ look up table (LUT) "Spectrum" (Schneider *et al.*, 2012). The 3D super-resolution renderings of actin were created from tiff stacks of Control and Latrunculin B treated cells with 50 nm axial steps and 10 nm lateral steps that were imported into Imaris (Imaris X64 v 8.0.1, Bitplane Inc, Zurich, Switzerland). The video rotations (**Movie 17** and **Movie 18**) were created using the 3D view and animation functions in Imaris.

3.2.8 Volume Electron Microscopy Sample Preparation

De-identified human breast tissue from a biopsy of a metastatic bone lesion was chemically fixed with EM-grade 2% paraformaldehyde and 1% glutaraldehyde in phosphate buffered saline (PBS). Separately, the bone lesion was characterized as HER2 positive by a pathologist based on hematoxylin and eosin stained slides of a parallel specimen 10% buffered formalin fixed and paraffin embedded. The specimen was processed for electron microscopy using a Pelco Biowave microwave (Ted Pella, Inc., Redding, CA) to assist with each step; all steps, unless indicated, were conducted at 150 watts, sometimes under vacuum. The specimen was first rinsed in buffer and then submerged

in reduced 2% osmium tetroxide with 1.5% potassium ferricyanide at 100 watts for 3 min power ON, 2 min OFF, 3 min power ON, 2 min OFF, 3 min power ON. Specimen was rinsed 3 times in ddH₂O and then submerged in aqueous 1% thiocarbohydrazide at 100 watts for 1 min power ON, 40 sec OFF, 1 min power ON. Following water rinses, the specimen was submerged in 2% osmium tetroxide at 100 watts for 1 min power ON, 40 sec OFF, 1 min power ON. Following rinses in ddH₂O, the sample was submerged in 5% aq. uranyl acetate at 100 watts for 2 min power ON, 2 min OFF, 2 min power ON. The sample was then dehydrated through an ascending acetone gradient (50%, 75%, 95%, 100%, 100%) for 40 sec power ON at each step. The specimen was infiltrated with a 100% acetone and 100% Epon resin mixture (1:1) for 3 min power ON and then with 100% resin four times for 3 min power ON before being polymerized in the oven at 60°C for 24 hours. Epon resin was made from Embed Kit (14120, Electron Microscopy Sciences, Hatfield, PA) mixture included: 73.5 g Embed 812, 45.5 g DDSA, 38.5 g NMA, and substituted 4.2 mL BDMA instead of DMP-30. 650 nm sections were cut, on a Leica Ultracut 7 (Leica Microsystems, Germany), and stained with toluidine blue to assess tissue architecture.

3.2.9 Volume Electron Microscopy Imaging

For FIB-SEM, resin-embedded samples were polished with a dry diamond knife tool to expose the area of interest on both the top and one side of the block and then mounted to a 45° pre-tilt SEM stub using colloidal silver paint. Blocks were sputter coated with 10 nm palladium with a Hummer. Milling and imaging of the block was performed on a FEI Helios Nanolab 660 Dual Beam FIB with AutoSlice and View software (FEI Inc., Hillsboro, OR). 6144 by 4096 pixel images were collected with the Elstar in-lens TLD detector in BSE mode at 2 kV with horizontal field width

of 30 μm at a working distance of 3 mm; FIB milling was performed at 77 pA to generate a z-dimension step size of 5 nm – 1240 total slices for a complete depth of 6.2 μm . Volume representations, manual segmentations, measurements, and movie creations were performed using Amira software (FEI Inc., Hillsboro, OR).

3.2.10 HER2 Labeling using affiFAP-MG-QD for Live Single QD Imaging

Biotinylated MG was pre-complexed with streptavidin-QD655 (Life Technologies) at a 1:1 stoichiometric ratio to a working concentration of 1 nM MG-QD655 for 15 mins at room temperature. HER2 affiFAP was added to live cells at 500 nM in 1% BSA and incubated for 10 mins in 37°C, 5% CO₂. Following the HER2 affiFAP, pre-complexed MG-QD655 was diluted to 500 pM and labeled to cells for 5 mins at 37°C, 5% CO₂. Immediately following labeling, cells were rinsed in PBS and mounted in imaging media of FluoroBrite™ DMEM (Gibco-Life Technologies) buffered with 25 mM HEPES (Gibco-Life Technologies) and supplemented with 50 ng/mL ascorbic acid to minimize photobleaching. A membrane marker (CellMask™ Plasma Membrane Green, Life Technologies) was added dropwise into the chamber containing cells at 0.03X prior to the start of live acquisition. Cells were maintained at a constant temperature of 37°C for the duration of imaging.

3.2.11 Immunolabeling of HER2, pAKT, and Actin in Fixed Cells

SKBR3 cells were fixed in 2% PFA containing 1 $\mu\text{g}/\text{mL}$ of the membrane marker wheat germ agglutinin-Alexa488 (WGA-Alexa488, Life Technologies) or -Alexa647 (WGA-Alexa647, Life Technologies) for 10 mins at 37°C, then transferred to a fresh solution of 2% PFA for 20 mins at 37°C. For HER2 immunolabeling, cells were permeabilized in 0.1% Triton-X for 10 mins at room temperature, labeled with HER2 affiFAP (500 nM, 30 mins, 37°C) and incubated for 1 hr in

blocking solution (8% NHS and 2% BSA at room temperature). MG-QD655 was pre-complexed as described above to a working concentration of 5 nM, incubated with free biotin at 50 nM for 5 mins at room temperature to occupy unbound streptavidin, diluted in blocking solution to 1 nM and added to cells for 1 hr at 37°C. Following, cells were rinsed in 2% blocking solution and mounted in borate buffer for image acquisition. To verify HER2-specific binding of the probe, cells were labeled following the same scheme with FAP alone (no affibody) and MG-QD655 as a negative control to ensure absence of non-specific binding. For pAKT immunolabeling, cells were permeabilized in methanol for 30 mins in three cycles (10 mins at -20°C, 10 mins at room temperature, 10 mins at -20°C), rehydrated in PBS for 20 mins at room temperature, and incubated for 1 hr in a blocking solution of 8% normal goat serum and 2% BSA. Cells were labeled with primary antibody to pAKT (Ser473, Cell Signaling Technology, Danvers, MA) diluted 1:100 in blocking solution (1.5 hr, 37°C), incubated for 1 hr in blocking solution, and then labeled with secondary antibody Alexa488 (goat anti-rabbit, Life Technologies) diluted 1:250 in blocking solution for 1 hr at 37°C. Following, cells were rinsed in 2% blocking solution and mounted in 1X PBS for image acquisition. To verify pAKT-specific binding, cells were labeled following the same scheme with no primary antibody and secondary antibody alone as a negative control to ensure absence of non-specific binding. For actin immunolabeling, cells were labeled with 500 nM phalloidin-Alexa647 (A22287, Life Technologies) overnight at 4°C and gently rinsed in PBS prior to mounting in PBS for image acquisition.

3.2.12 Immunolabeling of HER2 in Membrane or Cytoplasm

To observe whether HER2 undergoes internalization following receptor stimulation, a protocol to label live cells with HER2 affiFAP prior to stimulation and to tag MG-QD only after fixation and permeabilization was used to (1) avoid labeling-induced internalization that may result following long stimulation durations, and (2) to identify HER2 receptors that remained membrane bound or HER2 receptors that internalized. SKBR3 cells were serum-starved overnight, labeled with HER2 affiFAP (500 nM for 10 mins at 37°C), then stimulated with HRG for 5 mins, 15 mins, or 1 hr. Following, cells were fixed and permeabilized, then labeled with MG-QD (as described for fixed cells). HER2 receptor location was confirmed by a secondary method using the fluorescence of the affiFAP-MG complex without the QD. SKBR3 cells were labeled with HER2 affiFAP, then placed in serum-containing conditions for 1 hr. Following, cells were fixed and permeabilized, then labeled with a membrane impermeant MG (MG-Btau, 100nM) in a similar manner to MG-QD.

3.2.13 HER2 staining for 2D STORM

SKBR3 cells were cultured in 8-well μ -Slide chambers (ibidi, Fitchburg, WI) situated on No. 1.5 glass-bottom coverslips for 24-48 hrs at 37°C in a humidified atmosphere of 5% CO₂ in McCoy's 5A media supplemented with 10% FBS. Prior to plating, chambers were washed in 1 M NaOH for 2 hr at room temperature, rinsed with PBS five times, and incubated with PBS overnight. Cells were fixed in 3.7% PFA in 1X PHEM buffer for 20 mins, then rinsed with PBS. For HER2 immunolabeling, cells were blocked in 5% BSA for 30 mins, then labeled with 16 μ g/ml Herceptin, a clinical monoclonal antibody that labels the extracellular domain of HER2, for 45 mins at room temperature. Following, cells were washed three times in PBS for 5 mins, then labeled with secondary antibody Alexa647 (goat anti-human, Life Technologies) diluted at 1:1000 (1 μ g/ml) for

30 mins with protection from light. Cells were washed three times in PBS for 5 mins, and post-fixed with 3.7% PFA in 1X PHEM buffer for 10 mins. Following post-fixation, cells were washed with PBS and stored in the dark until imaging.

3.2.14 Actin staining for 3D Super-Resolution

SKBR3 cells were cultured in MatTek dishes (MatTek, Ashland, MA) situated on No.1.5 glass-bottomed coverslips for 72 hrs at 37°C in a humidified atmosphere of 5% CO₂ in McCoy's 5A media supplemented with 10% FBS. Cells were prepared using a method developed by Xu et al. 2012. Briefly, cells were washed in cytoskeleton preserving buffer (CB buffer), then fixed and extracted in 2% glutaraldehyde and 0.25% Triton-X in CB buffer for 10 mins at 37°C. Cells were washed in CB buffer in 37°C, suspended in 0.1% NaBH₄ in PBS for 15 mins to quench free glutaraldehyde, and washed in PBS two times. TetraspeckTM Microspheres (0.1 μm, Invitrogen) were added to cells at a 1:200 dilution for 15 mins at 37°C to serve as fiducial markers, then cells were washed three times in PBS. F-Actin was labeled overnight at 4°C with Alexa647 conjugated Phalloidin (Invitrogen) at a concentration of 0.5 μM. Immediately before imaging, samples were rinsed once in PBS, then placed in imaging buffer (Xu *et al.*, 2012).

3.2.15 Cell Treatment with NRG1-β1 and Latrunculin B

Cells were serum-starved overnight, then treated with 40 ng/mL neuregulin1-beta1 (396-HB/CF, R&D Systems Minneapolis, MN), 100 nM Latrunculin B (428020-1MG, Calbiochem-EMD Millipore, Billerica, MA), or a combination of 40 ng/mL neuregulin1-beta1 (NRG1) and 100 nM Latrunculin B (LatB) for 15 mins at 37°C under a humidified 5% CO₂ atmosphere. All treatments were diluted with serum-free media for application to cells. Cells were immediately fixed after treatment as described. For localized NRG1 application in live cell imaging, SKBR3 cells were

serum-starved for 4 hr prior to NRG1 injection. Micropipettes were heat-pulled (PC-10 Dual-Stage Puller, Narishige, East Meadow, NY) from glass capillaries (outer diameter = 3 μm , 1B100F-4, World Precision Instruments, Sarasota, FL), gently positioned near cells (MHW-3 Manual Hydraulic Manipulator, Narishige) and vacuum injected (5 one-sec pulses at 5 kPa over 10 sec duration, IM-31 Microinjector, Narishige). Glass micropipettes were back-filled with 2.5 ng/ μL NRG1 solution or 1X PBS and locally applied to a subcellular site of a cell during live acquisition. Control experiments using micropipettes filled with CellMaskTM Plasma Membrane Green confirmed a localization of approximately 5-6 μm from the tip of the pipette immediately following vacuum injection (**Movie 4**). For Latrunculin B application during live cell imaging, cells were treated with 100 nM LatB during the affiFAP and MG-QD labeling steps (15 mins), then suspended in imaging solution containing 100 nM LatB in an imaging chamber for live acquisition. Cells were maintained at a constant temperature of 37°C for the duration of imaging.

3.2.16 HER2-siRNA Transfection

Cells were transfected with HER2-targeting siRNA (Hs_ERBB2_14 FlexiTube siRNA, Qiagen, Hilden, Germany) or control non-silencing siRNA (AllStars Negative Control siRNA, Qiagen, Hilden, Germany) using siLentFectTM Lipid Reagent for RNAi (170-3360, Bio-Rad, Hercules, CA). siRNA and transfection reagent were diluted in 100 mM NaCl solution and incubated with cells plated at 50% confluency at 20 nM siRNA for 58 hr. Following siRNA transfection, cells were serum-starved for 6 hr, then treated with 40 ng/mL neuregulin1-beta1 for 15 mins, and fixed and labeled for HER2 as previously described.

3.2.17 Assessment of Filopodia from Cell Images

Filenames of images of siControl and siHER2 treated cells were scrambled, de-identified of their treatment conditions, and provided to a blind observer for assessment for the presence of filopodia in cells. Individual cells were graded at planes near or at the coverslip for the presence (Y) or absence (N) of 5 or more filopodia. Following, the percentage of cells containing 5 or more filopodia ($\% = \frac{Y_{ROI}}{Y_{ROI} + N_{ROI}}$) was measured for each ROI (n=60 ROI's from 3 different experiments), linked back to its corresponding siControl or siHER2 group, and recorded for the prevalence of filopodia-rich cells in each condition.

3.2.18 HER2-QD Quantification

For siRNA experiments, HER2-QD quantity per cell was measured for siControl or siHER2 treatment by quantifying the number of HER2-QD in the maximum projection of each image and dividing by the number of cells in the image ($\frac{\#QDs \text{ per image}}{\#cells \text{ per image}}$). The HER2-QD count per image was quantified by custom MATLAB R2014B software (MathWorks), 'QD Counter', which created a maximum projection of a z-stack and located and counted the number of QDs present in the QD channel. The number of cells per image was determined by identifying the number of individual cells visible by WGA staining. For HER2-QD quantification in protrusions, images of WGA staining from cells on the plane of the coverslip were annotated in Fiji (Fiji is Just ImageJ) using the freehand selection tool to demarcate areas of protrusions (P) or the entire cell (EC). Protrusions were identified on the basis of (1) their ruffled and discontinuous staining as evidence of cell membrane that contain extensive folds and elaborations, and (2) a greater than 1 μm distance between the extracellular edge of WGA stain and the cytoplasmic edge of the membrane label (in

comparison to the approximately 1 μm distance observed in the continuous and “smooth” staining of membranes relatively low in protrusions). The entire cell was annotated by tracing the extracellular edge of WGA staining of each cell (entire cell denotes all membrane regions including protrusions and cytoplasmic regions). HER2-QDs were manually counted in the annotated regions using PointPicker in Fiji, where QDs displaying at least a 2x2 pixel size residing within the border and in contact with the annotated border was counted. HER2-QD surface density in protrusions and entire cell was calculated by dividing the sum number of QDs present in each annotated region and dividing by the area of the region ($\frac{\text{Total \#QDs in annotated area region}}{\text{Total area of annotated region } (\mu\text{m}^2)}$). For analysis of HER2-QD in membrane or cytoplasm, custom MATLAB software, ‘CellAnalyzer’ was used to quantify the number of HER2-QD in the two regions as previously described (Vermehren-Schmaedick *et al.*, 2014). The number of HER2-QD in the membrane and cytoplasm were quantified for the mid-volume optical sections (across a depth of 5-7 μm) of each cell.

3.2.19 pAKT-Alexa Quantification in Protrusions

For pAKT-Alexa quantification in protrusions, images of WGA staining from cells on the plane of the coverslip were annotated as previously described. pAKT-Alexa density in protrusions and entire cell was calculated by dividing the sum intensity of Alexa present in each annotated region and dividing by the area of the region ($\frac{\text{Total intensity in annotated region}}{\text{Total area of annotated region } (\mu\text{m}^2)}$).

3.2.20 Protrusion to Entire Cell Ratio Measurement

To compare the density of HER2 or pAKT in protrusions versus the entire cell, the density measurements from the two cellular locations were compared by a protrusion to entire cell ratio.

The protrusion-to-entire cell ratio was calculated by dividing the density of HER2 in the protrusion

by the density of HER2 in the entire cell for each individual cell.

(*protrusion to entire cell ratio* = $\frac{\text{Density of HER2 in Protrusion}}{\text{Density of HER2 in Entire Cell}}$) The protrusion-to-entire cell

ratio for pAKT was calculated identically.

3.2.21 Western Blot

Cells were lysed in a RIPA buffer (Sigma-Aldrich) with Halt Protease and Phosphatase Inhibitor Cocktail (Pierce-Thermo Scientific) and then cleared by centrifugation. Protein concentration was estimated with a BCA assay (Pierce-Thermo Scientific). Proteins present in cell lysates (50 μg) were resolved by SDS-PAGE and transferred onto Immobilon-FL PVDF membrane (EMD Millipore). Membranes were probed with antibodies specific for HER2 (3B5, Sigma-Aldrich) and Actin (sc-1615, Santa Cruz Biotechnology, Dallas, TX). Immunoreactive proteins were detected and quantified using infrared fluorescent IRDye[®] secondary antibodies and Odyssey[®] imagers (LI-COR Biosciences, Lincoln, NE).

3.2.22 Single QD Tracking

Single particle tracking of quantum dot-tagged HER2 receptor complexes was performed as previously described (Vermehren-Schmaedick *et al.*, 2014; Valley *et al.*, 2015). Briefly, I applied custom-written MATLAB algorithms to subtracting the camera offset and dividing by a gain factor to convert image data from raw output to Poisson distributed ‘counts’ as previously described (Lidke *et al.*, 2005b; Smith *et al.*, 2010). Areas in each image were identified as possible candidates for single particle fitting using a difference of Gaussian filtering step as described in (Huang *et al.*, 2011) and each candidate area was fit using the maximum likelihood method described in (Smith *et al.*, 2010). Fits that were above a threshold intensity and matched the expected point spread function

shape (log-likelihood ratio test described in (Huang *et al.*, 2011)) were connected into trajectories. Trajectory connection was performed using a modification of the cost matrix approach (Jaqaman *et al.*, 2008). Trajectories were visually inspected to verify absence of connection errors before further analyses. HER2 trajectories were assigned to filopodia, lamellipodia, and cell body based upon the location of the receptor track relative to the membrane label. Maximum intensity time projections of the HER2-QD channel was used to identify filopodia that were difficult to resolve by membrane label alone. Trajectories corresponding to slender filaments less than 900 nm in diameter and more than 2 μm in length (as visualized by HER2-QD time projection) from the edge of the membrane label were classified as filopodia. Trajectories along characteristically broad membrane sheets that extended at least 3 μm from the cell body were classified as lamellipodia, and trajectories along regions of the membrane appose to the bulk cytoplasm were classified as cell body. HER2-QD was also found in motion in cell regions that could be mistakenly interpreted as cytoplasmic but were on the ‘underside’ of cells at the plane of the cover slip. This was confirmed by: 1) real-time focusing of dynamic HER2-QDs showing that they are in the same plane of focus as single blinking QDs adherent to the coverslip and 2) 3D deconvolution of cells fixed following conditions similar to real-time tracking that showed the presence of HER2-QDs at the plasma membrane at the plane of the coverslip and absence of HER-QDs in the cell cytosol. To avoid potential artifacts introduced by interference of the motion of HER2-QDs with the coverslip, these trajectories were not included in our analysis.

3.2.23 Dynamic Analysis of HER2-QD Trajectories

All analyses were performed using custom-written MATLAB algorithms. The diffusion constant of each trajectory was determined using a maximum likelihood estimation (D_{MLE}) that takes into account the experimental effects of finite exposure time of the camera, varying localization precision and intermittent trajectories (Relich *et al.*, 2016). For 1D analysis, the 2D trajectories were first rotated to give a minimum root-mean-square displacement in the y-direction. The x-coordinate was then used with a 1D diffusion constant estimation. Cumulative probability distributions of square displacements were calculated from all single-frame jumps over all trajectories for each condition. Simulations of a 1D random walk were performed by drawing jumps from a normal distribution with $\mu = 0$ and $\sigma^2 = 2Dt$, where D is the diffusion constant and t is the time step. The particle is confined in a region $L = 4 \mu\text{m}$ to reflect the representative average length of a filopodia. If the position of the particle after a jump was beyond the boundary, the particle was reflected back into the confined region. The instantaneous speeds of trajectories were computed as the mean single-jump velocity within a sliding window containing six localizations. MSD Analysis: Mean square displacements versus time intervals were calculated over all jumps and all trajectories for each condition.

3.2.24 Statistical Analyses

Data in each experiment was evaluated by 'qqplot' function in MATLAB R2014b to test for the normality of data. For data in which the normality assumption was not met, the non-parametric Mann-Whitney rank sum test was conducted ('ranksum' function in MATLAB) to test the null hypothesis that data from two groups come from continuous distributions with equal medians against the alternative that they do not. For multiple comparisons, the Mann-Whitney rank sum

test was conducted between relevant groups with a Bonferroni adjustment of α based on the number of comparisons at a $p < 0.05$ significance cut off. The Bonferroni adjusted p-value was determined by dividing 0.05 by the number of comparisons. For comparing the equality of cumulative probability distributions of HER2 dynamics in different regions, distributions of diffusion constant, and instantaneous velocity, the non-parametric Kolmogorov-Smirnov test was conducted ('kstest2' in MATLAB) to test the null hypothesis that data from two groups come from the same continuous distribution at a $p < 0.05$ significance level. For comparing the linear correlation between HER2 expression and percent of filopodia positive cells, Pearson's correlation test was conducted ('corr' in MATLAB) to test the null hypothesis of no correlation between the two variables at a $p < 0.05$ significance level and for computing the Pearson's correlation coefficient.

3.3 Results

3.3.1 Breast Cancer Cell Protrusion Exhibit Similar Nanoscale Morphology *In Vitro* and *In Vivo*

I explored the form and function of a variety of protrusion structures present in breast cancer tissues and cultured cell lines using DIC microscopy, and 2D and 3D EM. The DIC image in **Figure 3.1A** shows that cultured SKBR3 breast cancer epithelial cells extend protrusions at polarized ends of the cell body. These protrusions at the substrate surface are both sheet-like lamellipodia and finger-like filopodia. Time lapse DIC microscopy shows dynamic changes in lamellipodia and filopodial protrusion, including filopodial extension and retraction from lamellipodia, that take place over time durations of >10-15 minutes in a motile cell (**Movie 1**). Example video stills show a lamellipodium from which slender filopodia extend (t=0 sec and 4 min 38 sec, **Figure 3.1B**). At

times, the entire protrusive structure, composed of both filopodia and a lamellipodium, appeared as isolated units with filopodial sites positioned at far-reaching distances from the cell body (t=12 min 16 sec and 16 min 49 sec, **Figure 3.1B**, **Movie 2**). We used SEM to provide higher resolution information about filopodia and lamellipodia. **Figure 3.1C** shows images of HER2+ SKBR3 cells and **Figure 3.2** shows images of 21MT-1 and MCF7 cells. These images show 2-5 μm long, 80-130 nm diameter filopodia that extend from lamellipodial edges.

We used focused ion beam scanning electron microscopy (FIB-SEM) with 5 nm resolution to explore the three dimensional shapes of protrusions in biopsies taken from a HER2+ metastatic breast tumor (resin section of tissue biopsy in **Figure 3.3**). **Figure 3.1D** (*left*) shows that protrusions were at the polarized apical surfaces of cells. Complete reconstruction of a protrusion showed the *in vivo* architecture of a filopodium extending from the body of a lamellipodium (**Figure 3.1D**, *right* and **Movie 3**). The lamellipodium was widest, 1.3 μm , at the base where it joined the cell and tapered in width to 690 nm where the filopodia began their extension. The average diameter of filopodium extending from the lamellipodium was 140 nm. However, the width of each filopodium varied along its length. The length of the complete structure, from where the lamellipodium joined the cell to the tip of the longest filopodia was 3 μm . Together, the lamellipodium and filopodia extended into an intercellular space and had sites of membrane to membrane contact with filopodia from neighboring breast cancer cells. No junctional complexes were observed at these contact sites. The lamellipodia contained mitochondria, vesicles, and ribosome. In contrast, filopodia contained some ribosomes but had very few large organelles (mitochondria, vesicles). It is remarkable that lamellipodia and filopodia are similarly organized in

nanoscale-restricted spatial morphology *in vitro* and *in vivo*. This is important since it encourages the use of *in vitro* models to study lamellipodia and filopodia functions.

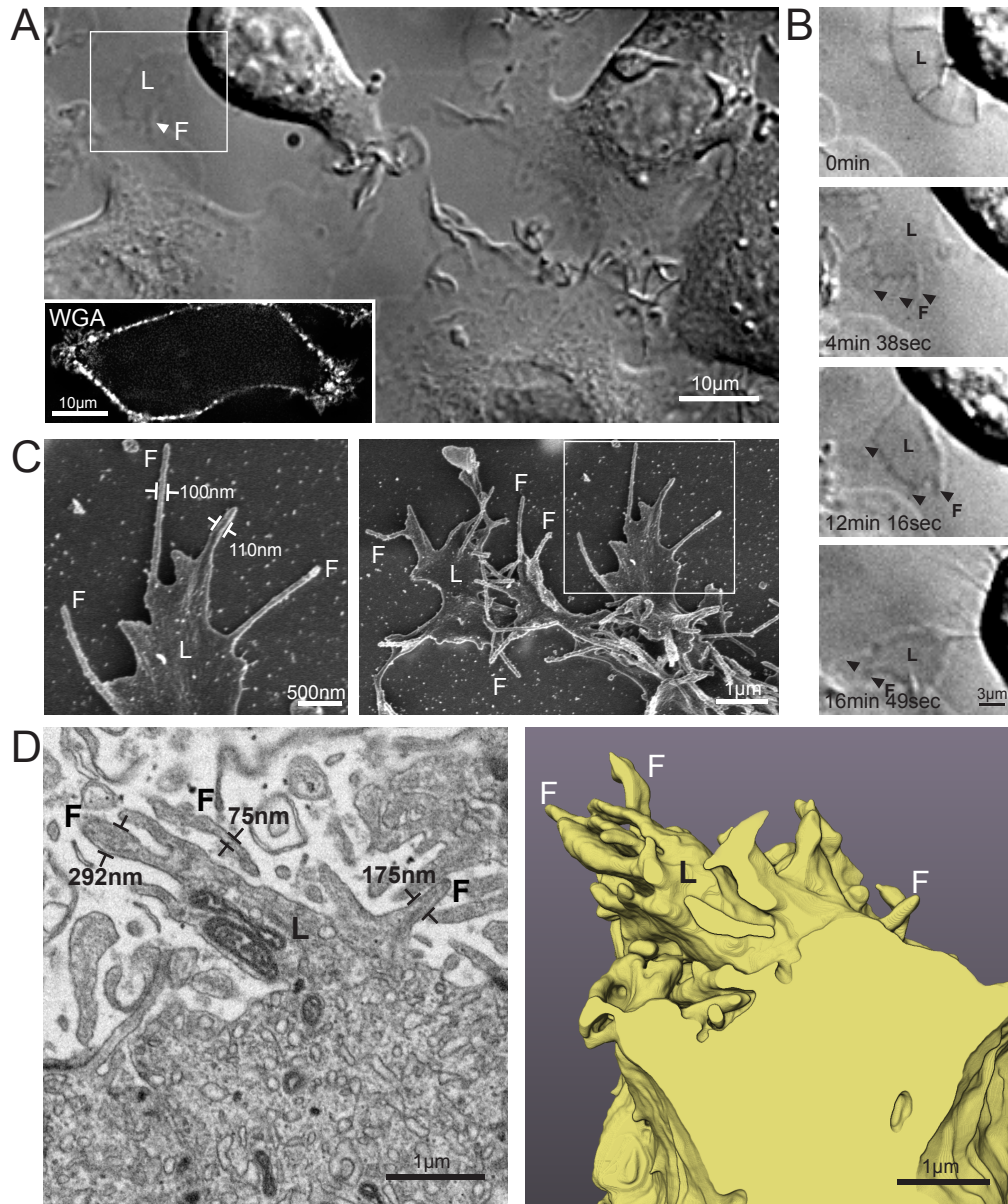


Figure 3.1: Morphology of filopodial and lamellipodial protrusions in *in vitro* and *in vivo* breast cancer epithelial cells.

(A) Single frame from a DIC movie (see **Movie 1**) shows SKBR3 breast cancer cells in serum-media extending protrusions. White box: example lamellipodium (L) and filopodium (F) in a motile cell. Inset: wheat germ agglutinin (WGA)-Alexa488-labeled membrane of SKBR3 cell with protrusions at polarized ends of its cell body. (B) Frame stills from **Movie 1** (also **Figure 3.1A**, white box) showing lamellipodia and filopodia morphology over duration of several minutes. A lamellipodium (L, 0 sec) extends numerous filopodia (arrowheads, 4 min 38 sec) and migrates peripherally from the main cell body (see **Movie 2**). (C) SEM shows the slender architecture of filopodia (F) that extend from lamellipodia (L) in *in vitro* cultured SKBR3 cells. **Figure 3.2** shows similar morphology in additional breast cancer epithelial cells, and **Figure 3.4** shows heterogeneity present in the extent of protrusion elaboration amongst SKBR3 cells. (D) Left: *in vivo* HER2-positive breast tumor cell from a biopsy of a metastatic bone lesion imaged by volume EM (single 5 nm slice). Right: segmented, 3D, rendered volume (yellow) of the lamellipodium (L) and filopodia (F) display similar morphological features and size scale as *in vitro* (C). See **Movie 3** for volumetric stack overlay. See **Figure 3.3** for wide-field view of stained resin section of the tumor biopsy. SEM images taken with help from Darcie Babcock and Claudia Lopez. FIB-SEM images acquired by Dr. Danielle Jorgens.

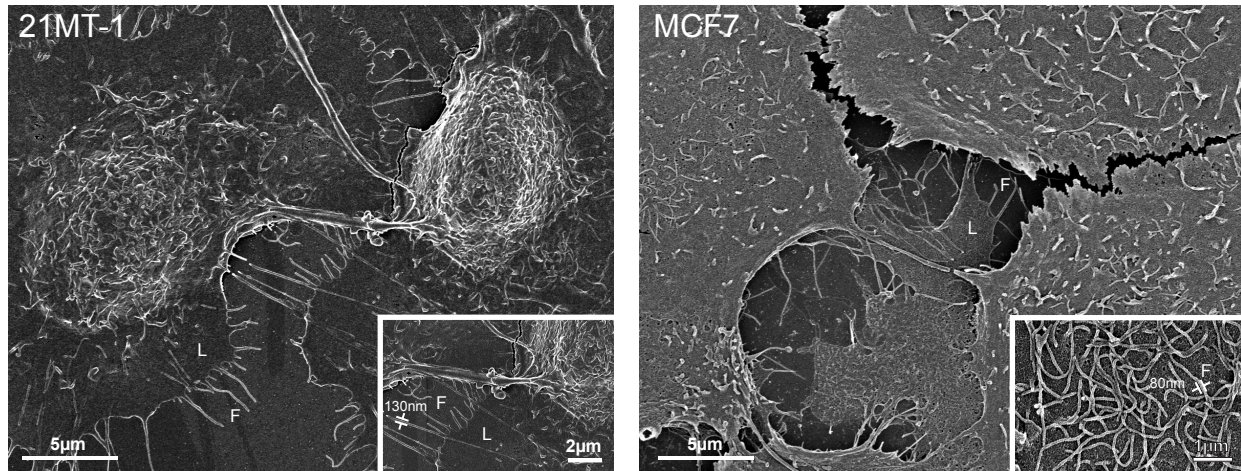


Figure 3.2: SEM of filopodia and lamellipodia in additional breast cancer epithelial cell types.

Additional SEM of slender filopodia (F) extending laterally from the thin sheet of lamellipodial sheets (L) in additional types of breast cancer epithelial cells, 21MT-1 (*left*) and MCF7 (*right*). Inset shows dimensions of filopodia ranging from 80 nm to 130 nm that are similar in other high and low HER2 expressing (21MT-1 and MCF7, respectively) breast cancer epithelial cells. Images acquired by Dr. Koei Chin.

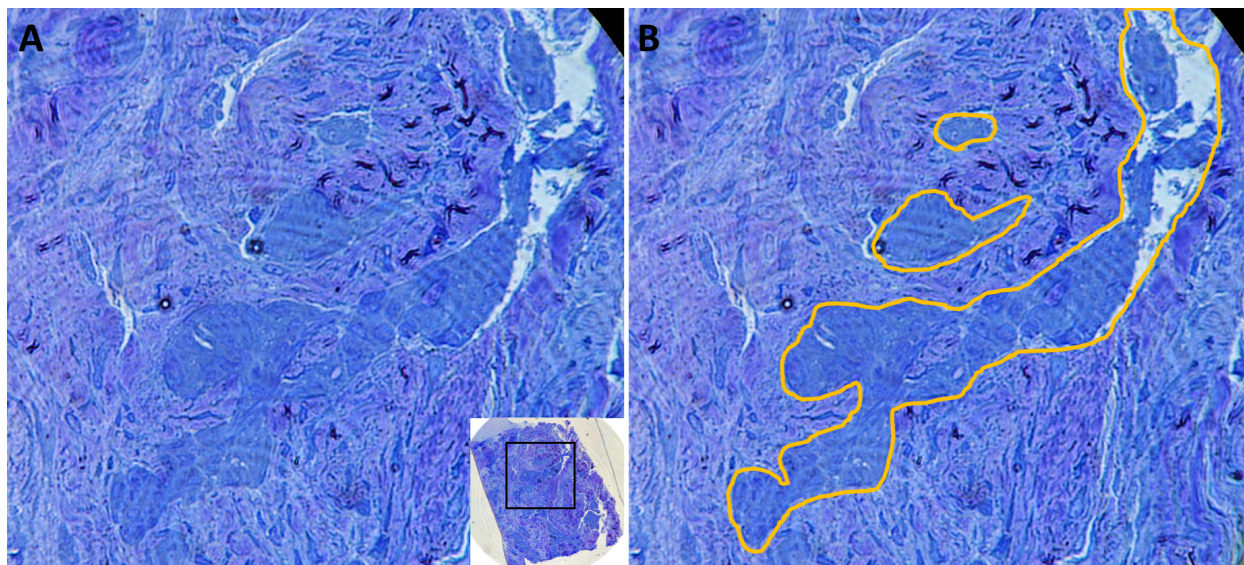


Figure 3.3: Toluidine-blue stained 600 nm thick resin section of the in vivo HER2-positive breast tumor cell obtained from a biopsy of a metastatic bone lesion that was prepared for Volume EM.

(A) The mass of breast cancer cells is observed infiltrating old bone. Inset is low magnification of whole section. (B) The breast cancer infiltrate is outlined in orange. Resin section acquired by Dr. Danielle Jorgens.

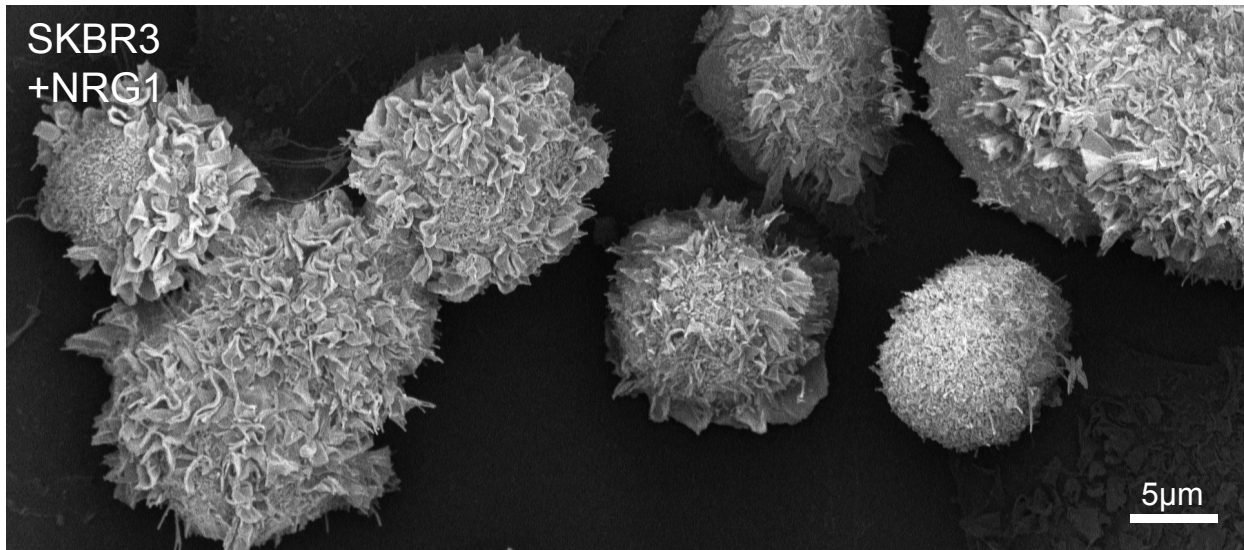


Figure 3.4: SEM of filopodia and lamellipodia in NRG1-stimulated SKBR3 breast cancer cells.

NRG1-stimulation induces global membrane ruffling and extension of lamellipodial and filopodial protrusions in SKBR3 cells. Heterogeneity in the extent of protrusion elaboration amongst cells is apparent at this nanometer scale of resolution. SEM image acquired with help from Darcie Babcock.

3.3.2 HER2 Signaling of Protrusion Growth is Rapid and Spatially Localized

I explored the linkage between HER2 signaling propagation and protrusion formation (Grothey *et al.*, 2000; Marone *et al.*, 2004; Yokotsuka *et al.*, 2011; Jeong *et al.*, 2017) by examining the effect of localized stimulation of HER2 in live cells, in real time. We treated HER2+ cells with NRG1, a growth factor known to influence cell-cell signaling by binding to HER3 in HER2-HER3 heterodimers (Hynes and Lane, 2005).

Figure 3.5A shows that NRG1 produces global membrane ruffling over SKBR3 cells, and elaboration of surface-associated filopodia and lamellipodia in SKBR3 cells within 15 minutes. SEM images show these structures at higher resolution and illustrate the variability between cells in the degree of protrusion elaboration (**Figure 3.4**). We used a fine-tipped glass micropipette to deliver the growth factor to subcellular sites of SKBR3 cells (**Movie 4** shows degree of injection precision by

dye). Localized delivery of NRG1 to serum-starved cells induced protrusion extension at the site of NRG1 delivery; protrusion extension was absent from other portions of the cell (**Figure 3.5B**, *first row* and **Movie 5**, **Figure 3.5B**, *second row* and **Movie 6**). These changes occurred within 3 minutes following NRG1 stimulation. Protrusions did not form in control cells that were treated with phosphate buffered saline (PBS) (**Figure 3.5C**). I confirmed NRG1 mediated protrusion growth was dependent on HER2 by showing that siRNA mediated silencing of HER2 expression reduced protrusion growth. I confirmed that siRNA reduced HER2 expression by measuring binding of HER2-QDs; these HER2-QD probes were generated by linking a small recombinant protein consisting of a HER2 affibody (58 amino acid peptide) $Z_{\text{HER2:342}}$ fused to a fluorogen activating protein (FAP_{dL5**}) to QDs using a malachite green analog (MG-Biotin) (**Methods**, see characterization and validation, **Figure 2.1** and **Figure 2.2**). This analysis along with additional western blots probed for HER2, confirmed that HER2 expression was reduced significantly and linked directly with HER2-mediated signaling (**Figure 3.5D**). siRNA treatment also decreased filopodial protrusion growth (**Figure 3.5E**; **Methods**) and HER2-QD quantity significantly correlated with filopodial growth (**Figure 3.5F**). Together, these data show that NRG1-activated HER2 signaling is rapidly responsive, evoking protrusion growth that is not widespread and is highly localized at the site of NRG1 signaling stimulation.

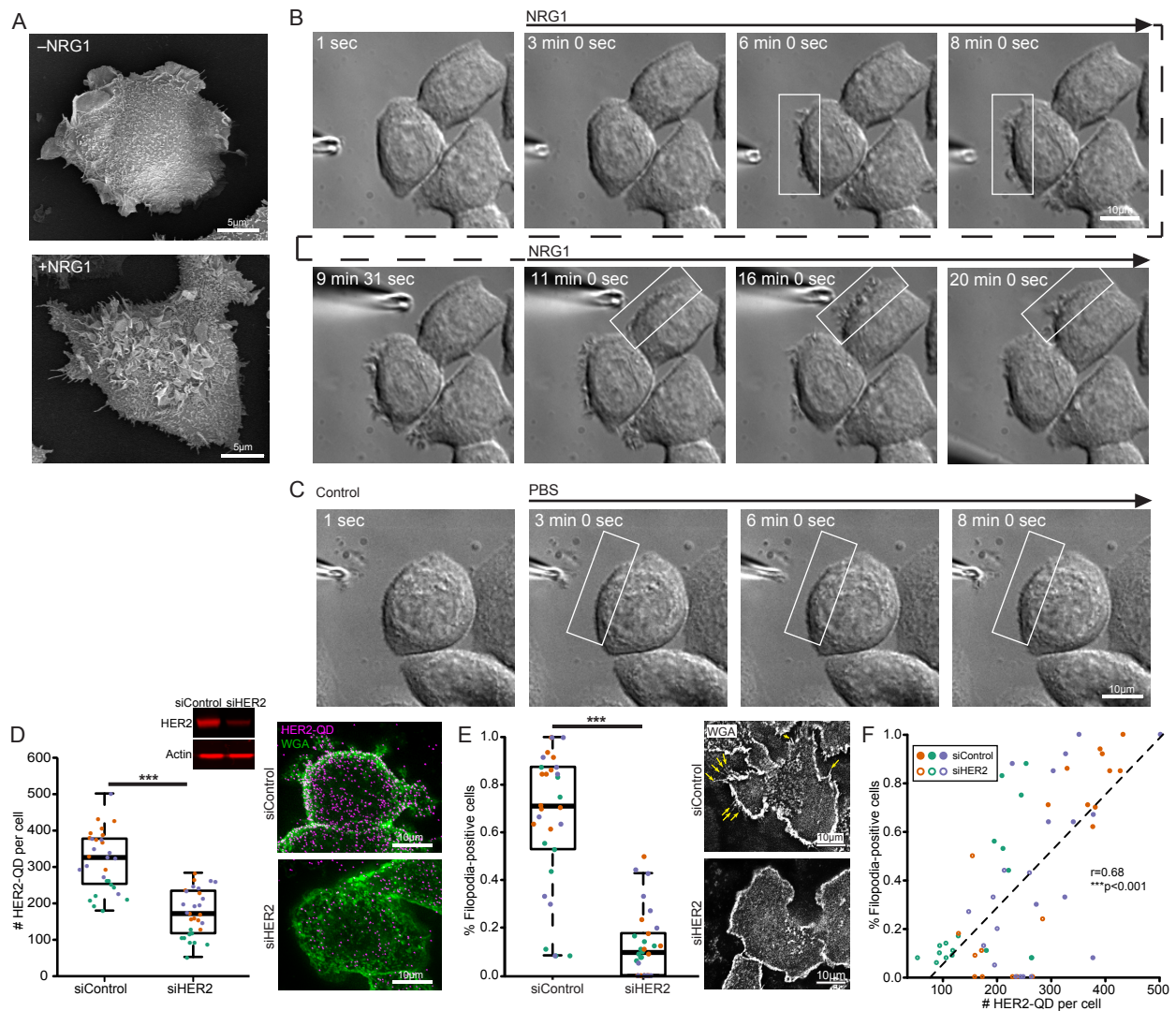


Figure 3.5: Rapid, spatially localized nature of HER2-evoked protrusion growth.

(A) SEM micrographs show NRG1-stimulated SKBR3 cells (15 minutes, +NRG1) provokes increased surface-attached filopodia and lamellipodia and global membrane ruffling compared to cells in serum-free media (-NRG1). (B) Localized delivery of NRG1 via micropipette at subcellular sites (Movie 5 and 6) of two different SKBR3 cells evokes HER2-HER3 signal activation and protrusion extension at rapid timescale (< 3 mins). (C) Control microinjection of NRG1-free PBS buffer does not evoke similar protrusion growth. (D) HER2 expression is reduced in HER2 siRNA vs. control siRNA treated cells. HER2 expression per cell quantified by discrete HER2-QD counts (boxplot, left) of maximum z-stack projections (micrographs, right), and by western blot (inset). Cells stimulated with 15 mins of NRG1 for both HER2 siRNA and control siRNA conditions. See Figure 2.1 and Figure 2.2 for HER2-QD probe characterization. (E) Filopodial protrusion growth is reduced in HER2 siRNA treated cells vs. control HER2 siRNA. % filopodia-positive cells quantified (boxplot, left) from the WGA-membrane labeled fluorescence channel of experiments in (D) (right, yellow arrows point to example filopodia). *** p < 0.001, Mann-Whitney rank sum test for (D) and (E). (F) Percent of filopodia-positive cells plotted as a function of HER2 expression. Significant positive correlation shown between levels of HER2 expression and filopodia-positive cells ($r=0.68$). Solid dots, control siRNA; open dots, HER2 siRNA. *** p < 0.001, Pearson's correlation test. For (D), (E), and (F): orange, green, and purple dots represent three different experiments, n=30 ROIs, 721 cells. See Table 3.2, statistics. Western blot produced by Dr. Sunjong Kwon.

3.3.3 Protrusions are the Primary Site of HER2 and pAKT Signaling

I tested the hypothesis that protrusion growth that is highly localized at sites of NRG1 activation is the outcome of signaling activation and downstream signaling molecules that remain confined at protrusions. I explored this by measuring the effect of NRG1-stimulation on the density of HER2 on protrusions and on formation of pAKT as an indication of active, membrane associated HER2-PI3K pathway signaling.

I used several imaging approaches to measure the presence of HER2 on the protrusions. In one, I used super-resolution Stochastic Optical Reconstruction Microscopy (STORM) to visualize populations of Herceptin-Ax647 labeled HER2 signaling complexes in SKBR3 cells. STORM images show that HER2-Ax647 resides at the peripheral edges of SKBR3 cells (**Figure 3.6A, left**), appearing as clusters of HER2 in both filopodia and lamellipodia (**Figure 3.6A, right**). I further assessed the extent of HER2 localization at protrusions by measuring the binding of HER2-QD (see **Methods**) to HER2 complexes. Similar to STORM imaging, HER2-QD labeling showed protrusion-rich localization of HER2 in lamellipodia and filopodia (**Figure 3.6B**). These studies showed that NRG1 stimulation induced protrusion growth and that HER2-QD was localized at the plasma membrane and on protrusions. I saw little evidence of HER2-QD complexes in the cytoplasm even after 60 minutes following NRG1 stimulation (**Figure 3.7**) suggesting that they were protected from down regulation by endocytosis (Bertelsen and Stang, 2014). I annotated protrusion-rich regions within individual cells (**Figure 3.6B**) by staining with fluorescently labeled WGA, a lectin that binds to sialic acid and *N*-acetylglucosaminyl residues on the cell membrane. This enabled visualization of membrane folds and elaborations and facilitated discrimination

between HER2-QD on protrusion-rich regions of the membrane and the cytosol. I annotated WGA-stained cells as shown in **Figure 3.6B** (*P*, solid line; *EC*, dotted line) to define protrusion-rich regions of the membrane (*P*, solid line) and the entire cell (*EC*, dotted line), which represented membrane, cytoplasm and nucleus. Quantification of HER2-QD density in these regions showed that HER2-QD is predominantly localized at protrusion-rich regions of cells and that this HER2-QD density is retained on the cell surface following NRG1 stimulation (**Figure 3.6C**, *left*). I defined a protrusion-to-entire cell ratio that compares HER2-QD density in the protrusion and entire cell regions for each individual cell analyzed. Plots of the protrusion-to-entire cell ratio in **Figure 3.6C** (*right*) confirmed that HER2-QD is preferentially located on protrusions (protrusion-to-entire cell ratio > 1) prior to stimulation and that this distribution is maintained following NRG1 stimulation.

I explored the possibility that NRG1-HER2-HER3 complexes on protrusions activates downstream signaling primarily in protrusions by assessing the association between immunostained pAKT and HER2 in untreated and NRG1-treated SKBR3 cells. **Figure 3.6E**, *left* shows that pAKT-Ax in serum-starved (-NRG1) cells was present at similar density in protrusions and entire cell regions. However, **Figure 3.6E**, *right* shows that pAKT-Ax at the protrusions increased compared to the entire cell following NRG1 activation of HER2-HER3 signaling (protrusion-to-entire cell ratio > 1). These data show that the protrusions of breast cancer cells are the primary site of NRG1-HER2-pAKT activation and downstream signaling of protrusion growth.

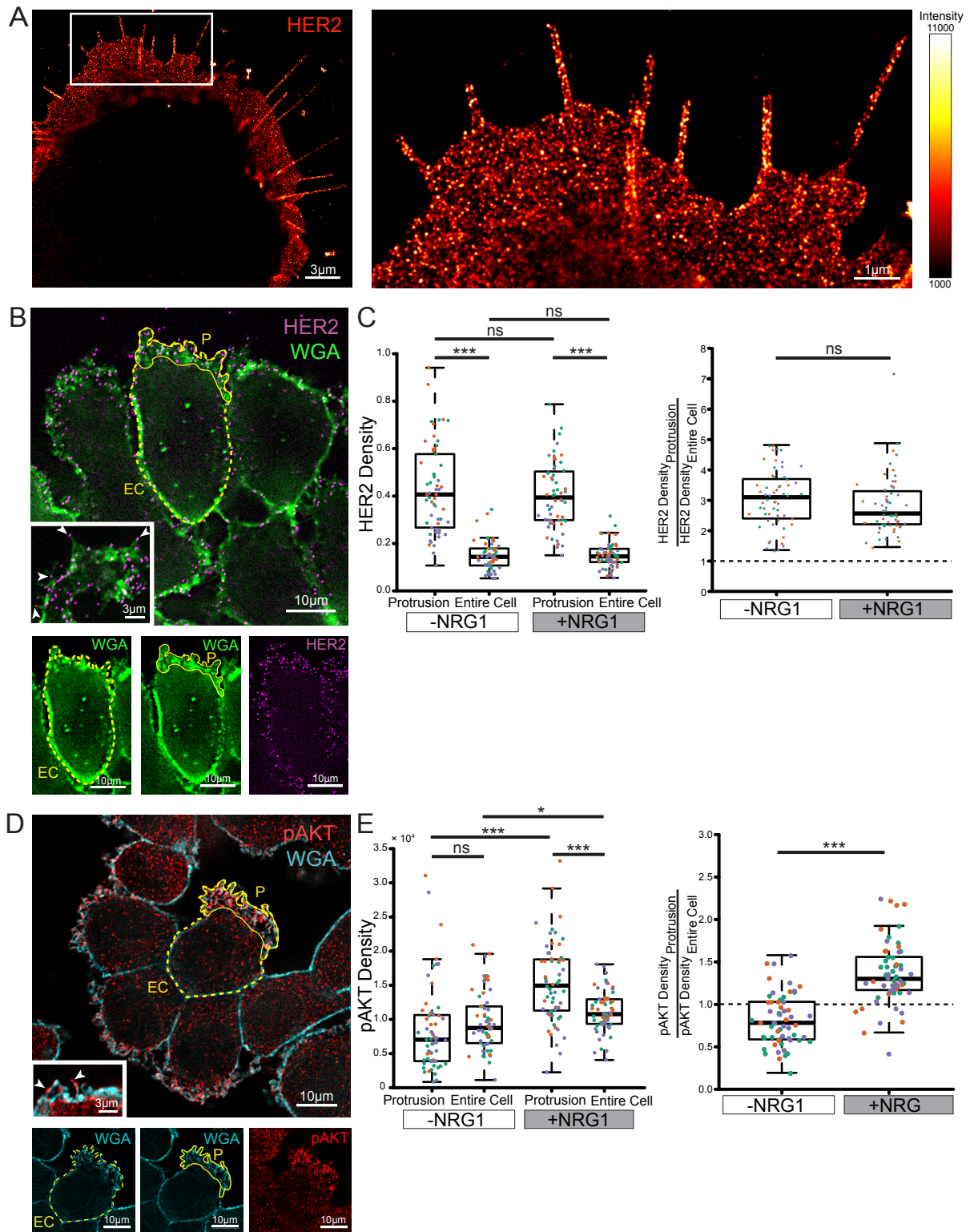


Figure 3.6: Protrusions are the primary site of HER2-HER3 pathway activation and downstream pAKT signaling of protrusion growth. (Figure legend on next page)

Figure 3.6 (*Figure legend continued*):

(A) Left: Super-resolution (STORM) imaging showing HER2-Alexa647 localization in protrusions of serum-cultured SKBR3 cells. Right: Magnified image (white box, *left*) detailing HER2 in lamellipodia and filopodia at substrate surface. (B) Left: Discrete HER2-QD imaging showing localization in protrusions. HER2-QDs (magenta) and WGA-Alexa488 membrane (cyan) in NRG1 stimulated SKBR3 cells. Inset: close up detailing HER2-QDs in lamellipodia and filopodia (*arrowheads*). Example annotations of protrusion (P, *solid line*) and entire cell (EC, *dotted line*) regions; lower images show individual color channels. (C) Quantitative comparison showing predominance of HER2-QD at protrusion sites. Relative HER2-QD density in protrusion vs. entire cell regions (*left*) and ratio of HER2-QDs in protrusion:entire cell (*right*) for individual +NRG1 and -NRG1 SKBR3 cells. (D) Wide-field fluorescence imaging of pAKT-Alexa showing predominant localization in protrusions. pAKT-Alexa488 (red) and WGA-Alexa647 membrane (cyan) in +NRG1 SKBR3 cells. Inset: close up of pAKT-Alexa in filopodia (*arrowheads*). (E) Predominance of pAKT-Alexa at protrusion sites as quantified by pAKT-Alexa488 relative density (*left*) and ratio of pAKT-Alexa fluorescence density at protrusions:entire cell (*right*) for individual +NRG1 and -NRG1 SKBR3 cells. +NRG1: 15 mins stimulation in serum-free media, -NRG1: serum-free alone. *** $p < 0.001$, * $p < 0.05$, ns= non-significant, Mann-Whitney rank sum test. In (C) and (E), orange, green, and purple dots represent three different experiments, n=118-119 cells. See **Figure 3.7**, additional HER2 localization. See **Table 3.2**, statistics. STORM images acquired by Dr. Jing Wang.

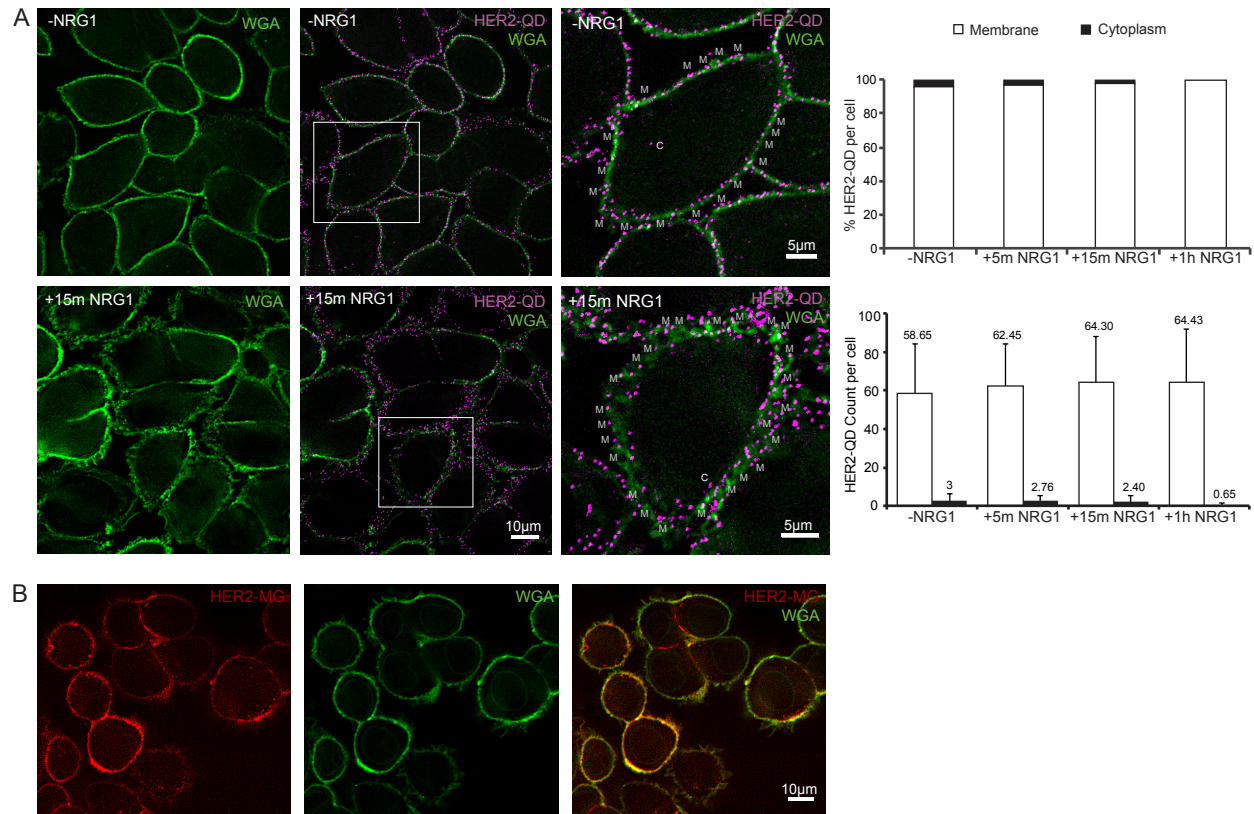


Figure 3.7: Activated HER2 receptors localize to membrane protrusions and remain primarily membrane bound.

(A) HER2 receptors localize to the membrane and undergo little internalization. HER2-QD (magenta) and WGA-Alexa488 membrane (green) of untreated (-NRG1, *top row*) and 15 mins NRG1 stimulated (+15m NRG1, *bottom row*) SKBR3 cells at the mid-section of cells. Magnified view of cells from -NRG1 and +15 min NRG1 (third column) show that most HER2-QDs align on membrane label (M) and few receptors reside in the cytoplasm (C). HER2 quantity in membrane and cytoplasm for the mid-volume optical sections (across a depth of 5-7 μm) of each cell is plotted as mean percentage of HER2 per cell in each region (bar plot on *top right*) or as mean count of HER2 per cell in each region (bar plot on lower right). Error bars: SD, n=68-70 cells for each condition. (B) HER2 residence on membrane is additionally confirmed by HER2-MG fluorescence. HER2-MG (red) and WGA-Alexa488 membrane (green) in SKBR3 cells in serum-containing media for 1 hr. Similar to results from QD-detection of HER2, MG-detection confirmed HER2 receptors reside in large part on the membrane, and that there is little internalization of the receptor. Our studies show that recycling and degradation of HER2 in the cytoplasm is a rare event. Software written by Dr. Damien Ramunno-Johnson.

3.3.4 Enhanced Mobility of HER2-QDs in Filopodia

Single particle tracking has revealed that activated EGF receptors undergo retrograde transport along filopodia and subsequent endocytosis at the cell center (Lidke *et al.*, 2005a). I examined the dynamic behavior of HER2 on protrusions which is currently unknown. I measured the movement of discrete HER2-QDs in HER2+ SKBR3 breast cancer cells. **Figure 3.8A** shows time-collapsed projections of successive frames of HER2-QD locations on filopodial and lamellipodial protrusions and on peripheral membranes of the cell body that do not show protrusions. In general, the HER2-QD movements I captured were more rapid than filopodial and lamellipodial extensions and retractions that take place over several minutes (*HER2 and DIC*, **Movie 7**; *HER2 and WGA*, **Movie 8**). I observed HER2-QD movement with and without NRG1 stimulation and found that NRG1 produced an increase in the HER2-QD mobility and instantaneous velocity (**Figure 3.9**). Moreover, I found that the nature of HER2-QD movement varied depending on cellular region. HER2-QDs on filopodia displayed back-and-forth motion along the lengths of filopodia (**Figure 3.8B**, *top panel*, **Movie 9** and **Movie 10**) with instantaneous velocities reaching $2 \mu\text{m/s}$ (*scale bar*, **Figure 3.8B**), a value concomitant with rapid cytoskeletal-assisted active transport (Lippincott-Schwartz, 2004; Nan *et al.*, 2005; Courty *et al.*, 2006; Rajan *et al.*, 2008). HER2-QD motion on lamellipodia and cell body regions appeared non-directional and instantaneous velocities were lower (**Figure 3.8B**, *center and bottom panel*; **Movie 11** and **Movie 12**, *Lamellipodia* and **Movie 13** and **Movie 14**, *Cell Body*).

Cumulative probability distributions of squared displacement per unit time for HER2-QDs showed that they were most mobile in filopodial regions, followed by lamellipodial and cell body regions (**Figure 3.8C**). Diffusion constants calculated for each HER2-QD using maximum

likelihood estimation (Relich *et al.*, 2016), reflected this ordering (**Figure 3.8D**). The rapid speeds of HER2-QDs (up to 2-3 $\mu\text{m}/\text{sec}$) over long distances along the length of filopodia (5 μm) contrasted with the motion along the width of filopodia (x - y - t and x - t plots, **Figure 3.8B**, top) and led us to examine the mobility of HER2-QDs along the length of filopodia. **Figure 3.8D** shows that the mobility of HER2-QD along the length of the filopodial is remarkably fast compared to HER2-QD mobilities in the lamellipodial and cell body regions (Filopodia 1D_long, **Figure 3.8D**) as well as the mobilities measured for other receptor proteins (**Figure 3.8E**, **Table 3.1**). Notably, the mobilities measured for other receptor proteins which were measured on the cell surface and in non-protrusive structures possess similar value to HER2-QD mobilities measured in the cell body.

I quantified aspects of the movement of HER2-QDs along filopodia in an effort to elucidate the mechanisms by which movement occur. I first analyzed the distribution of step sizes taken by HER2 towards the tip or base along the longitudinal axis of a filopodia (Filopodia 1D_long). The distribution of step sizes was symmetric as expected of a protein undergoing simple Brownian motion in 1D (**Figure 3.8F**, **Figure 3.10** for additional examples). I modeled the process by simulating a 1D random walk along a one-dimensional confined region of 4 μm length (typical length of a filopodium) (**Figure 3.8G**). The resulting simulations (**Figure 3.8G**, *right*) yielded trajectories that were similar to and indistinguishable from HER2-QD trajectories along the filopodia longitudinal axis (**Figure 3.8G**, *left*), suggesting that the back-and-forth motion that I observed along the filopodia 1D could arise from Brownian motion along one dimension (additional examples, **Figure 3.10**).

These data show that the primary form of HER2 motion in protrusions is passive Brownian diffusion. This form of HER2 diffusion is strikingly rapid and in filopodial protrusions possesses one of the fastest mobilities in filopodia compared to the motion HER2 in non-protrusive cellular regions, as well as that reported for other types of receptors.

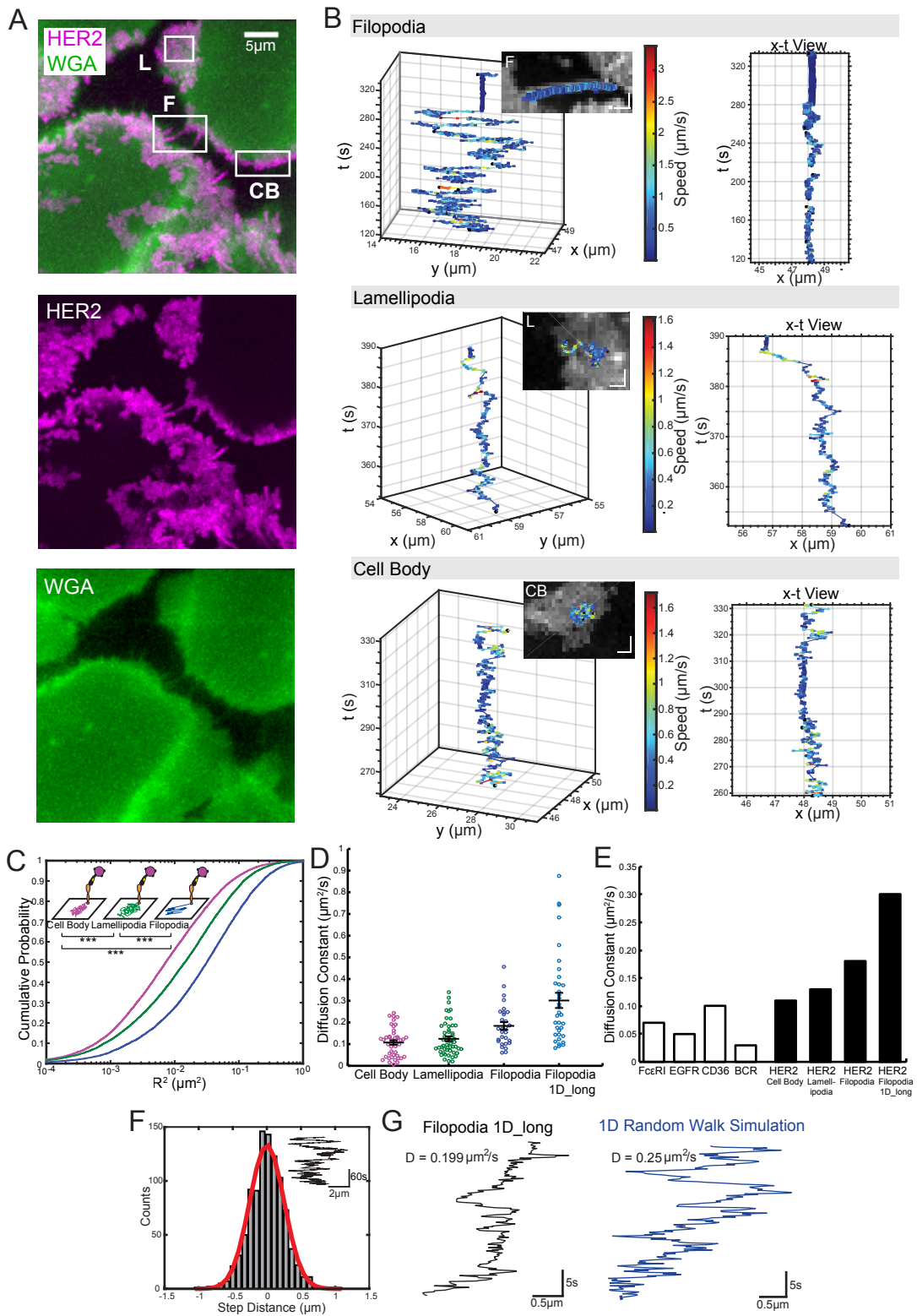


Figure 3.8: Rapid dynamics of HER2-QDs along filopodia compared to other cellular regions. (Figure legend on next page)

Figure 3.8 (*Figure legend continued*):

(A) Example max intensity projection of HER2-QD over time in SKBR3 cultured in serum-media. Regions: filopodia (F), lamellipodia (L), cell body (CB). **(B)** HER2 motion is distinct in filopodia, lamellipodia, and peripheral membrane regions of cells that do not show protrusions (cell body). HER2 trajectories ($x-y-t$, position over time) and ($x-t$). Inset: HER2 trajectory overlay on max intensity projection of HER2-QD over time. Inset scale bars, 1 μm in x, y . Colored bar, HER2 speed. See **Movie 9-14**. **(C)** Cumulative probability distribution of HER2-QD squared displacement comparing HER2-QD mobility that is fast in filopodia versus lamellopodia and cell body regions. *** $p < 0.001$, KS test. $n = 125$ receptors, 40 cells. **(D)** Diffusion constants computed for HER2-QDs in different cell regions shows rapid mobility in filopodia, particularly for motion along the length of filopodia (1D, longitudinal component of filopodial motion). Diffusion constants computed by maximum likelihood estimation. Horizontal bar, mean. Error bars, SEM. $n = 125$ receptors, 40 cells. **(E)** HER2 mobility on filopodia and in particular mobility along the length of filopodia, is faster than that observed for other membrane receptors in non-protrusive cell regions. See **Table 3.1**. **(F)** HER2 step distances towards tip and base of filopodia 1D is symmetric in distribution, a feature consistent with simple Brownian motion. Inset: HER2 trajectory on filopodia 1D from which distances were drawn. See **Figure 3.10A**, additional examples. **(G)** Example showing that the 1D longitudinal component (parallel to length of the filopodium) of a HER2-QD trajectory measured in a filopodia is indistinguishable from a trajectory drawn from simulations of a confined 1D random walk along a 4 μm length with diffusion constant 0.25 $\mu\text{m}^2/\text{s}$. See **Figure 3.10B**, additional simulations. See **Figure 3.9**, HER2 dynamic analysis with NRG1. See **Table 3.2**, statistics. Analysis and simulations conducted with help by Dr. Keith Lidke.

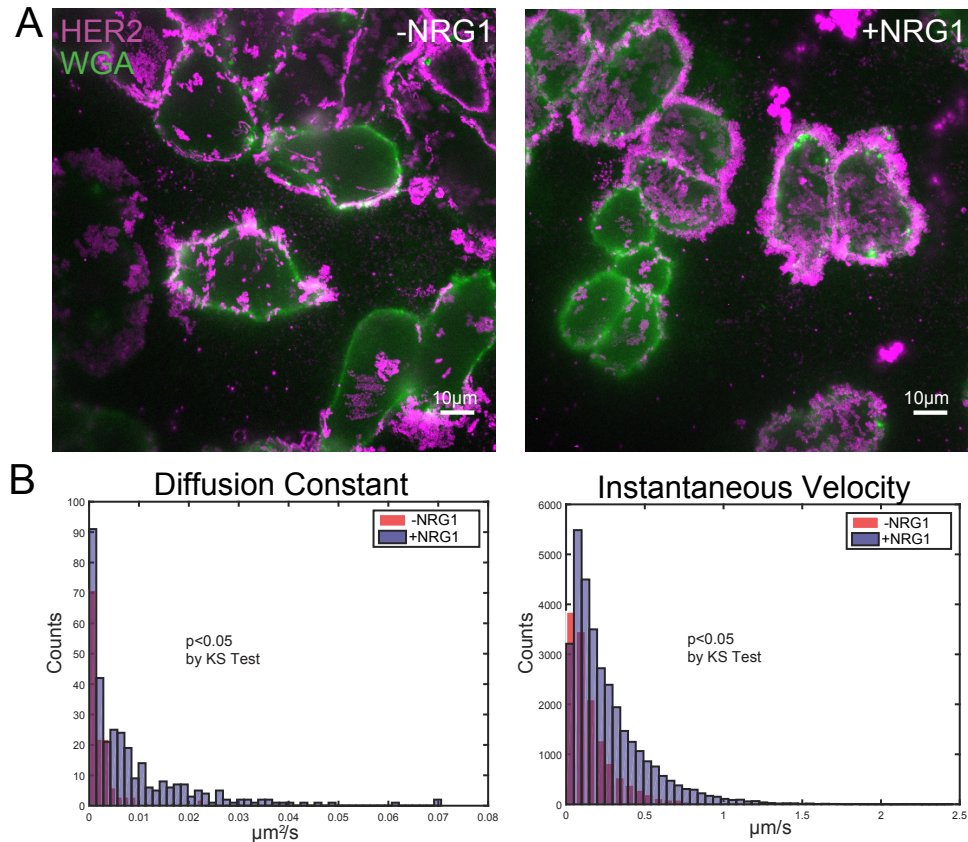


Figure 3.9: HER2 dynamics increase in mobility and instantaneous velocity upon NRG1 stimulation.

(A) Untreated (-NRG1) and NRG1 stimulated SKBR3 cells (+NRG1) demonstrate qualitative differences in dynamics. Maximum projection of HER2-QD (magenta) fluorescence over time overlaid on still-image of membrane (green, acquired at start of acquisition). (B) Histogram of diffusion constant and instantaneous velocity for HER2 receptors in -NRG1 and +NRG1 stimulated cells. HER2 receptors in +NRG1 stimulated cells exhibit higher diffusion constants and faster instantaneous velocity. Counts are values of the diffusion constant and velocities computed from trajectories tracked in protrusion and non-protrusion regions of cells.

Table 3.1: Comparison of diffusion constants of HER2 amongst different cellular regions as well as compared to other membrane receptor proteins.

Receptor	Cells	D ($\mu\text{m}^2/\text{s}$)	Reference
Fc ϵ RI	RBL-2H3 (rat basophilic leukaemia cells)	0.07	Andrew et al. (2008)
EGFR	A431 (human epithelial carcinoma cells)	0.05	Low-Nam et al. (2011)
CD36	human blood cells	0.10	Jaqaman et al. (2011)
BCR*	murine and chicken B cells	0.03	Treanor et al. (2010)
HER2 _{Cell Body}	SKBR3 (human breast carcinoma epithelial cells)	0.11	--
HER2 _{Lamellipodia}	SKBR3	0.13	--
HER2 _{Filopodia}	SKBR3	0.18	--
HER2 _{Filopodia 1D}	SKBR3	0.30	--

HER2 motion is faster than what has been observed for Fc ϵ RI (Andrews *et al.*, 2008), EGFR (Low-Nam *et al.*, 2011), CD36 (Jaqaman *et al.*, 2011), and BCR (Treanor *et al.*, 2010). * Studies cited used single molecule tracking of protein with QDs, with the exception of the BCR study which used single molecule tracking of protein with Cy3.

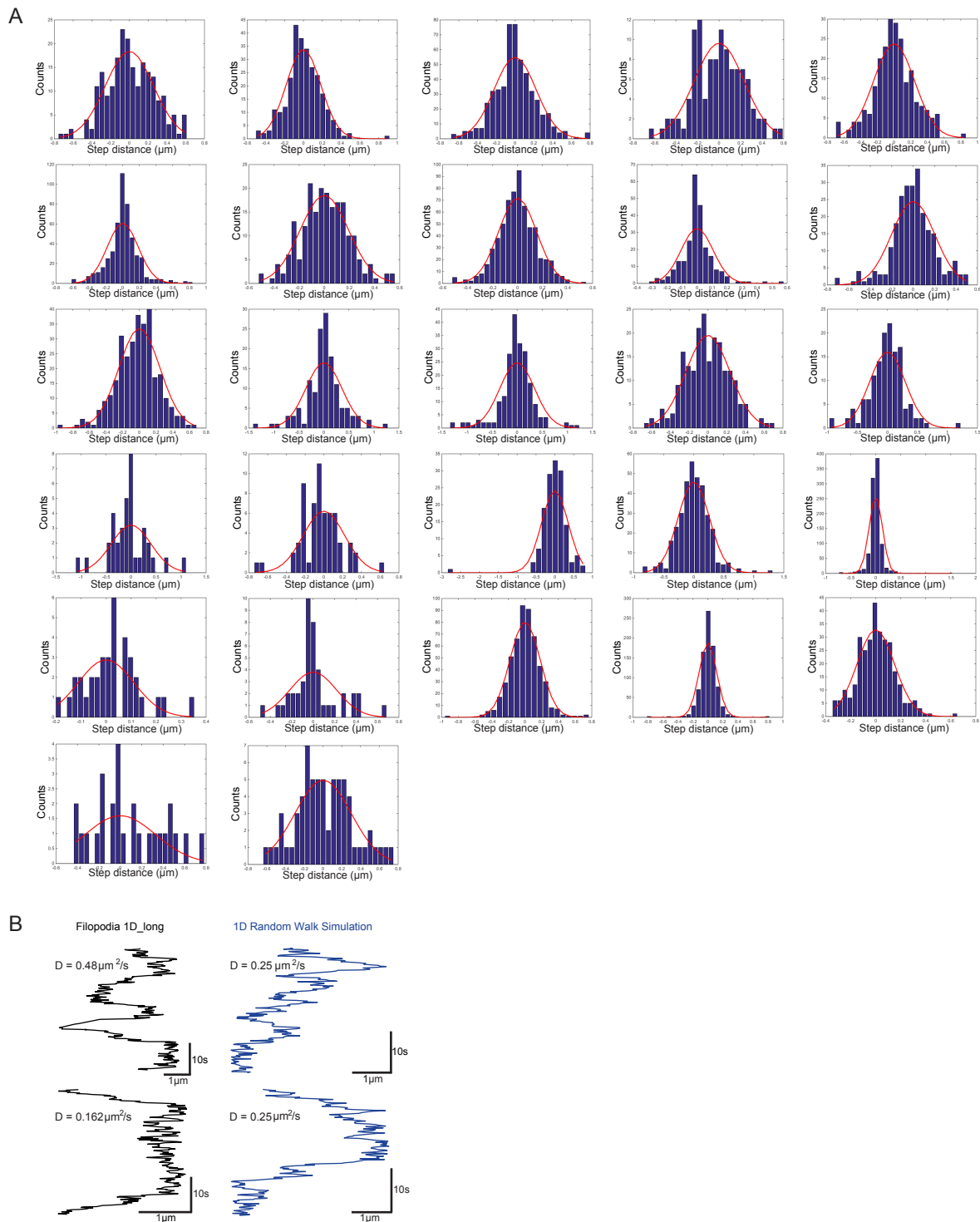


Figure 3.10: HER2 motion along longitudinal axis of filopodia is diffusive Brownian motion.

(A) Additional examples of randomly selected HER2-QD trajectories showing distributions of step distances towards the tip or base of the longitudinal filopodial axis (1D) are generally symmetric, a feature consistent with simple Brownian motion. (B) Additional examples showing that the 1D longitudinal component of HER2-QD live cell trajectories (component parallel to the length of the filopodia) is indistinguishable from trajectories drawn from simulations of a confined 1D random walk along a 4 μm length with diffusion constant $0.25 \mu\text{m}^2/\text{s}$. Simulations conducted by Dr. Keith Lidke.

3.3.5 Disruption of Actin Linear Geometry Reduces HER2 Mobility and Inhibits Signaling

I explored the role of actin in mediating the enhanced HER2-QD mobility observed in filopodia. I first used super-resolution structured illumination microscopy to examine filopodial actin structure using the same conditions of HER2 stimulation as that used in dynamic studies (**Figure 3.11A, left**). Cells grown in serum-containing media exhibited filopodia emerging from lamellipodia. Actin populated the base of filopodia as thick, linear actin bundles embedded in lamellipodia and converged along the base to the tips of the filopodia. Details of actin structure in protrusions was even clearer using 3D super-resolution imaging (**Figure 3.11B, left**, and 3D rendering of cell in **Movie 17**). These images highlight the abundance of actin-rich filopodial protrusions extending several microns from the cell body as seen by SEM (**Figure 3.5A, +NRG1**) and showed the network of linear actin present in thin lamellipodia and filopodia along the edge of the cell at the substrate surface.

Next, I tested the role of actin polymerization on protrusion formation by treating with latrunculin B (LatB), a toxin that blocks actin polymerization (Spector *et al.*, 1983; Wakatsuki *et al.*, 2001; Peng *et al.*, 2011). I observed a retraction of protrusions in cells treated for 15 mins (**Figure 3.11A, right** and **Movie 15**). In some cells, filopodia, visible by WGA staining, remained as short membranous “stubs” protruding from the cell body that were present even if devoid of actin filaments (**Figure 3.11A, arrowheads on right**). The effect of LatB on the underlying actin structure at the substrate surface was even clearer in 3D super-resolution images (**Figure 3.11B, right** and 3D rendering of cell in **Movie 18**). LatB-treated cells showed a substantial reduction in the number of actin-rich filopodia all along the membrane surface and the cells lacked large actin stress fibers along

the substrate-attached membrane, though smaller filaments were present. Notably, the actin remaining at the cell periphery following LatB treatment was non-linear in structure. LatB-induced actin depolymerization was reversible, as cells extended protrusions upon removal of LatB, though protrusions did not regain their full length (**Movie 16**)

I tested the effect of LatB on HER2-QD movement. HER2-QDs on post-LatB protrusion stubs showed a reduction in the range of distance that they traversed compared to HER2-QDs on filopodia in control cells (**Figure 3.11C** and **Movie 19-22**). These reduced HER2-QD movements measured in post-LatB membrane stubs manifest as a left-shift in the cumulative probability distribution of the squared displacement of HER2-QDs (**Figure 3.11D**) and by a decreased diffusion constant in comparison to HER2-QDs on filopodia (**Figure 3.11E**). These slower HER2-QD diffusion constants following LatB treatment were most similar to HER2-QD mobility measured in peripheral membrane regions absent of protrusions (**Figure 3.11E**). The mean squared displacement (MSD) of HER2-QDs under LatB treatment displayed a linear trend with slope similar to HER2-QD motion measured in peripheral membrane regions absent of protrusions (LatB vs Cell Body, **Figure 3.11F**). This similarity in diffusion constant and linear slope of the MSD is consistent with the notion that the linear actin that is present in filopodia facilitates the rapid diffusive motion of HER2-QD in filopodia.

I also explored the impact of LatB on downstream HER2 signaling and found that disruption of the cytoskeleton can influence downstream signaling. Specifically, LatB disrupted actin in the presence of NRG1 stimulation and produced a pronounced decrease in pAKT intensity

(Figure 3.11I). These results suggest that actin facilitates HER2 diffusion in filopodia that is necessary for modulating signaling outcome.

Together, these data demonstrate a key role of actin in mediating rapid HER2 diffusion and its downstream signaling in filopodia. Latrunculin disruption of actin polymerization produced shortened protrusion 'stubs' which contained no actin or actin whose linear structure was perturbed. These protrusion stubs still displayed HER-QD diffusion but the motion resembled HER2-QD dynamics measured in 'normal' physiological conditions in lamellipodia and the cell body, indicating the importance of normal linear actin structure in regulating rapid HER2 filopodial dynamics. The functional consequence of actin in mediating signaling is demonstrated by a marked reduction of pAKT in LatB-treated protrusions. Actin facilitates the rapid diffusion of HER2-QDs along the length of filopodia to enable localized HER2-pAKT downstream signaling. This mechanism of actin-enabled information transport is characterized by rapid diffusion and not by active cytoskeletal transport.

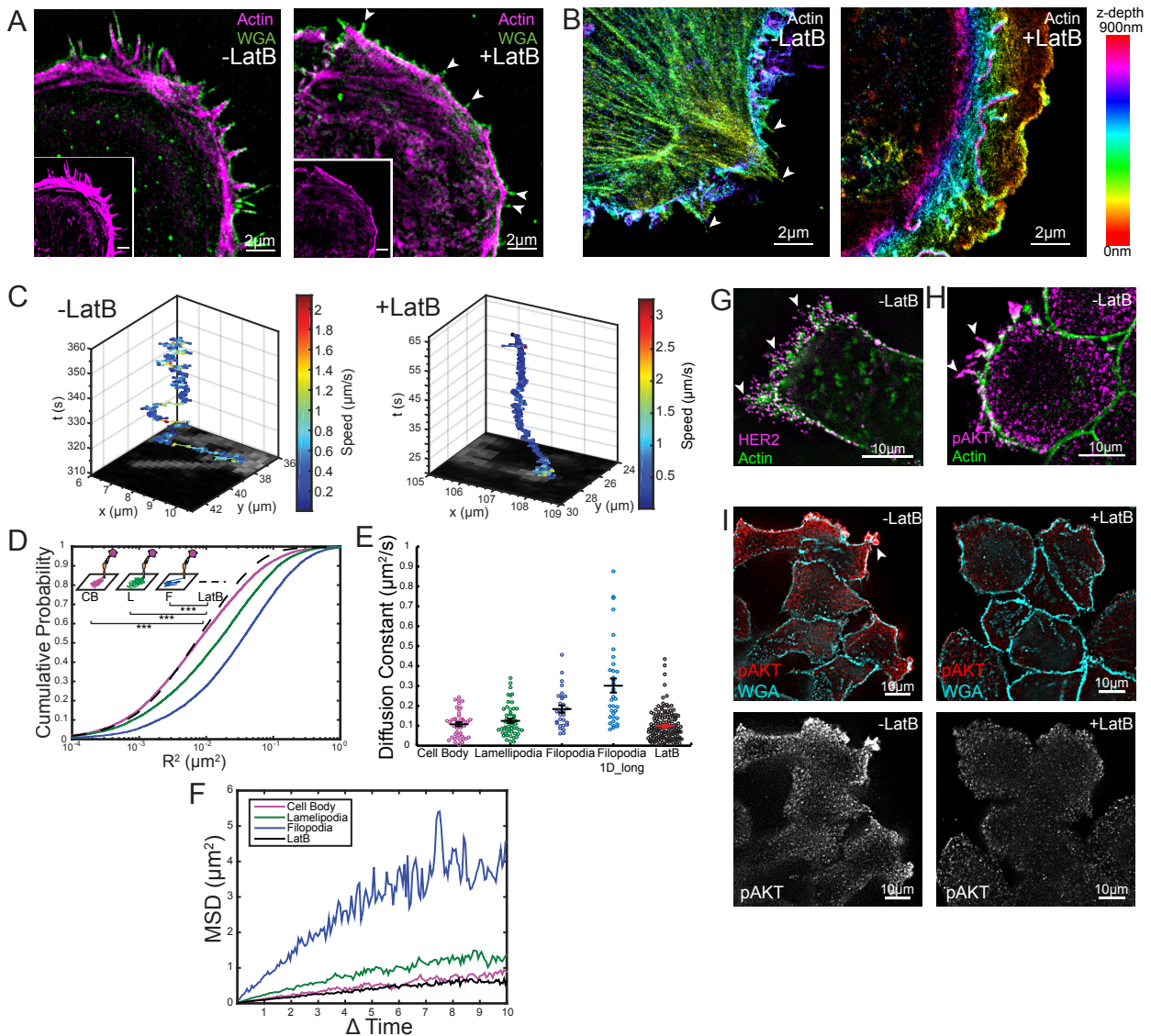


Figure 3.11: Actin Modulates HER2 Mobility and Downstream Protrusion Signaling.

(A) Actin is present in lamellipodia and filopodial protrusions. Latrunculin B (LatB) block of actin polymerization induces protrusion retraction, leaving peripheral membrane ‘stubs’ containing retracted actin or no actin (*arrowheads*). Super-resolution SIM of phalloidin-Alexa647 labeled actin (magenta) and WGA-Alexa488 membrane (green) for control (-LatB) and latrunculin B treated (+LatB) SKBR3 cells cultured in serum-media. Inset is actin; note actin inset intensity of +LatB is slightly saturated to show intracellular actin that is present at lower density than in protrusions. Inset scale bar, 2 μm . (B) Filopodial protrusions contain actin with linear structure (*arrowheads*, -LatB) that is perturbed following LatB treatment (+LatB). 3D super-resolution of actin in SKBR3 cells cultured in serum-media. Colored bar, axial depth. See 3D rendering in **Movie 17** and **18**. (C) HER2-QD trajectories show reduction in range of distance traversed in +LatB cells. HER2-QD trajectory on filopodium of -LatB and on altered protrusion stubs of +LatB of SKBR3. Colored bar, HER2 speed. See **Movie 19-22**. (D) HER2-QDs on +LatB altered protrusions show slower mobility that resembles HER2-QD motion on cell body. Cumulative probability distribution of HER2 squared displacement. *** $p < 0.001$, KS test. (E) HER2-QD mobility on altered protrusion stubs of +LatB cells as measured by diffusion constant is similar to cell body. (F) Mean squared displacement (MSD) of HER2-QDs under LatB treatment show linear trend with slope similar to HER2-QD motion measured in peripheral membrane regions absent of protrusions (LatB vs Cell Body). (Figure legend continued on next page)

Figure 3.11 (*Figure legend continued*):

(G) HER2-QD (magenta) is localized on actin-rich filopodial protrusions (*arrowhead*) in SKBR3 cells in serum-media. (H) pAKT-Alexa488 (magenta) is also localized on actin-rich filopodial protrusions (*arrowhead*) in SKBR3 cells stimulated with NRG1. (I) pAKT, concentrated in protrusion-rich regions (*arrowhead*) after NRG1 stimulation (-LatB), is reduced after latrunculin B (+LatB). pAKT-Alexa488 (red) and WGA-Alexa647 membrane (cyan). +LatB: 15 mins NRG1 and LatB in serum-free media; -LatB: 15 mins NRG1 alone in serum-free media. Values in (D), (E) from cellular regions: CB, L, and F are replotted from **Figure 3.6C, 3.6D** for comparison to +LatB data. n=276 receptors, 95 cells. See **Table 3.2**, statistics. 3D super-resolution images acquired by Katie Heiser. Analysis conducted with help by Dr. Keith Lidke.

Table 3.2: Test of significance for HER2 expression and filopodial growth; HER2 and pAKT density in cellular regions; HER2 dynamics in subcellular regions.

Figure 3.5:

Figure 3.5D: HER2 expression per cell Mann-Whitney rank sum test, $p < 0.05$			
Condition	Condition	p-value	Summary
siControl	siHER2	3.64×10^{-8}	***
Figure 3.5E: Filopodia-positive cells Mann-Whitney rank sum test, $p < 0.05$			
siControl	siHER2	3.12×10^{-8}	***
Figure 3.5F: Filopodia-positive cells vs. HER2 expression Pearson's correlation test, $p < 0.05$			
%Filopodia-positive cells	# HER2-QD per cell	2.37×10^{-9}	***

Figure 3.6:

Figure 3.6C: HER2 relative density (left) Mann-Whitney rank sum test, Bonferroni correction for 4 comparisons, $p < 0.05$ (Bonferroni corrected $p < 0.0125$)					
Cell Region		Cell Region		p-value	Summary
	HRG		HRG		
P	-HRG	WC	-HRG	1.71×10^{-17}	***
P	+HRG	WC	+HRG	3.04×10^{-19}	***
P	-HRG	P	+HRG	0.68	ns
WC	-HRG	WC	+HRG	0.70	ns
Figure 3.6C: HER2 protrusion-to-entire cell density ratio (right) Mann-Whitney rank sum test, $p < 0.05$					
Condition		Condition		p-value	Summary
-HRG		+HRG		0.06	ns
Figure 3.6E: pAKT relative density (left) Mann-Whitney rank sum test, Bonferroni correction for 4 comparisons, $p < 0.05$ (Bonferroni corrected $p < 0.0125$)					
Cell Region		Cell Region		p-value	Summary
	HRG		HRG		
P	-HRG	WC	-HRG	0.0184	ns
P	+HRG	WC	+HRG	1.37×10^{-5}	***
P	-HRG	P	+HRG	1.39×10^{-9}	***
WC	-HRG	WC	+HRG	0.0048	*
Figure 3.6E: pAKT protrusion-to-entire cell density ratio (right) Mann-Whitney rank sum test, $p < 0.05$					
Condition		Condition		p-value	Summary
-HRG		+HRG		5.83×10^{-13}	***

Figure 3.8:

Figure 3.8C: Cumulative probability distribution of HER2 squared displacement Kolmogorov-Smirnov test, $p < 0.05$			
Subcellular Region	Subcellular Region	p-value	Summary
F	L	4.78×10^{-100}	***
F	CB	0	***
L	CB	9.31×10^{-81}	***

Figure 3.11:

Figure 3.11D: Cumulative probability distribution of HER2 squared displacement Kolmogorov-Smirnov test, $p < 0.05$			
Subcellular Region	Subcellular Region	p-value	Summary
F	LatB (protrusion)	0	***
L	LatB (protrusion)	7.14×10^{-136}	***
CB	LatB (protrusion)	7.96×10^{-14}	***

3.4 Discussion

3.4.1 Cellular Protrusions are the Primary Site of Protrusion Growth Regulation

HER2-pAKT chemical signaling that evokes protrusion growth is located chiefly at protrusion structures in breast cancer cells. Filopodial and lamellipodial protrusions not only contain HER2, but contain HER2 at significantly higher abundance in protrusion regions compared to the rest of the cell. HER2 is localized to protrusions and this preferential localization to protrusions is present regardless of activation state. Accordingly, pAKT signaling is localized in higher proportion at protrusions following HER2 stimulation compared to the rest of the cell.

Important implications for cancer-directed therapies arise from the new view that cellular protrusion structures house the molecular signaling apparatus that both initiates and also executes downstream signaling of protrusion growth. HER2 targeted therapies have successfully delayed the progression of HER2+ breast cancers (Baselga and Swain, 2009; Tebbutt *et al.*, 2013), but improved therapies that produce enduring responses have yet to be found. Therapies that target sites specific to protrusions may offer a more effective means of controlling the overactive protrusion growth that underlies metastasis and tumor progression in cancer (Pelosi *et al.*, 2003; Daponte *et al.*, 2008; Machesky and Li, 2010; Yang *et al.*, 2013; Cao *et al.*, 2014; Huang *et al.*, 2015). Indeed, mutations in proteins specific to filopodia have been recently identified and such proteins may serve potential effective targets (Yamaguchi and Condeelis, 2007; Machesky, 2008; Arjonen *et al.*, 2011; Jacquemet *et al.*, 2015). Also, compounds that not only directly regulate signaling molecules (e.g. kinase inhibitors) but rather modulate the integrity of the filopodial environment components such as cytoskeletal actin (see below) may produce new means of potent control. Our studies beg questions as to how current HER2 therapeutics such as lapatinib, trastuzumab, and pertuzumab may modulate

protrusion morphology and signaling in protrusions. As well, our studies emphasize the importance of studying compounds, such as fascin inhibitors, that specifically target filopodial actin assembly in actin-rich protrusions to reduce invasion (Machesky and Li, 2010; Yang *et al.*, 2013; Huang *et al.*, 2015).

Our super-resolution and QD images showing HER2 presence on protrusion structures are consistent with studies showing HER2 in ‘finger-like structures’, ‘ruffles’, and ‘protrusive structures’ (Hommelgaard *et al.*, 2004; Lerdrup *et al.*, 2007; Peckys *et al.*, 2015; Chung *et al.*, 2016; Jeong *et al.*, 2017). Chung *et al.* and Jeong *et al.* have proposed intriguing, important mechanisms by which high HER2 density may induce the morphological formation of protrusions and by which calcium-mediated mechanisms may retain HER2 at the plasma membrane (Chung *et al.*, 2016; Jeong *et al.*, 2016; Jeong *et al.*, 2017). It is yet to be clarified whether the varied morphological classifications of these structures describe distinct protrusive structures or morphological variations of the same dynamic structure. The similarity in the morphology of protrusions that we observe between *in vitro* and *in vivo* suggest that these observations have functional relevance *in vivo*. Our results pointing to pAKT/PI3K pathway align with Jeong *et al.*'s finding of pAKT in protrusions (Jeong *et al.*, 2017), and prompt further questions as to whether other signaling pathways (e.g. MAPK) may also be locally-retained in protrusions to mediate protrusion growth.

3.4.2 Rapid HER2 Transport along Protrusions Enabled by Actin

Cells produce new protrusion growth within minutes following HER2 activation (**Figure 3.5B, Movie 5** and **Movie 6**). This contrasts rates of protein synthesis and turnover that are typically slower in cells (hours). The remarkably fast speed and mobility of HER2 in filopodia,

compared to that of HER2 and other receptors measured in non-protrusive cellular regions (**Figure 3.8C-E**) are concomitant with the rates of actin polymerization: 0.01-1 $\mu\text{m}/\text{sec}$ (Purich and Allison, 1999; Boal, 2012). It is plausible that the rapid HER2 mobility engenders, in part, rapid protrusion growth. Motorized cytoskeletal transport is associated with live neurons (Courty *et al.*, 2006; Sundara Rajan and Vu, 2006), lung cancer cells (Nan *et al.*, 2005), and EGF receptors in HeLa cells (Lidke *et al.*, 2005a). We find, surprisingly, that rapid HER2 transport along filopodia is enabled by passive diffusion. Two recent studies have reported a new role of actin in modulating receptor mobility and consequent downstream signaling (Treanor *et al.*, 2010; Jaqaman *et al.*, 2011). In B cells, the actin network mediates B cell receptor diffusion through actin-delineated boundaries, and in macrophages, 'linear channels' or 'microdomains' defined by actin and microtubule may dictate receptor mobility to enhance the probability of CD36 receptor dimerization (Treanor *et al.*, 2010; Jaqaman *et al.*, 2011; Mattila *et al.*, 2016). Our results showing actin's role in mediating remarkably fast receptor transport in filopodia are in agreement with this new view of the cytoskeleton in directly impacting signaling. Importantly, through our use of both molecular-resolution imaging and live tracking approaches, we show that actin-mediated signaling function arises from the actin structure. When perturbed, the linear arrangement of filamentous actin characteristic of slender filopodia disassembles and the rapid HER2 mobility observed along the length of filopodia slows to mobilities typical of non-protrusive cellular regions. LatB inhibition disrupts the linear actin structure and reduces pAKT signaling, pointing to the functional consequences of reduced HER2 mobility.

CHAPTER 4: SUMMARY, CONCLUSIONS, AND FUTURE DIRECTIONS

4.1 Discrete Quantification and Spatial Localization of HER2 and pAKT by QD

In Chapter 2, I characterized HER2-QD and pAKT-QD probes that enabled the sensitive quantitation and analysis of the spatial localization of these PI3K pathway components. I demonstrated the ability to quantify HER2-QDs in a single cell manner that illuminated the cellular variability within the population. This sensitivity through molecular counting of HER2-QDs led us to discern an upregulation of HER2 in HER3 knockdown cells. Though HER3 upregulation has been found to occur following HER2 knockdown and/or inhibition (Garrett *et al.*, 2011), HER2 upregulation following HER3 is not known (Liu *et al.*, 2007; Lee-Hoeflich *et al.*, 2008; Jaiswal *et al.*, 2013). This upregulation of HER2 is not believed to be a result of a difference in the availability of HER2 for affibody binding. I observed similar levels of HER2 binding regardless of NRG1 activation (**Figure 3.7A**, -NRG1 vs +NRG1 'HER2-QD count per cell'), suggesting that our HER2-QD binds HER2 monomers and dimerized HER2 with similar affinity. These findings raise implications about the dependence of cells on HER2-driven signaling and their ability to adapt and compensate in the absence of major signaling partners.

The imaging-based nature of our QD assay within the intact cellular architecture enabled us to study the spatial distribution and localization of pAKT-QD. I found that cells within a population exhibited different pAKT spatial states that can be characterized by their distribution relative to the membrane. The existence of these different states as well as variations in phosphoactivity of the cell suggested cellular heterogeneity in the signaling states between cells of the same population that could be robustly quantified. Additionally, analysis discerning pAKT-QD

localization in the membrane or cytoplasm allowed us to track the time course of pAKT localization following stimulation.

Together, these results established the strength of the QD for sensitive and quantitative analysis of proteins in the spatial environment of the cell; I applied this tool for the study of HER2 spatiotemporal dynamics in Chapter 3.

4.2 HER2 Signaling is Localized to Protrusions and Mediated by Actin

In Chapter 3, I applied this QD tool to study the spatial organization and temporal dynamics of HER2. Using various imaging modalities: electron microscopy, immunofluorescence, single particle tracking, and super-resolution microscopy, I showed the localized signaling activated at protrusions, and the spatial environment and spatiotemporal dynamics regulating HER2 signaling. I used high resolution SEM and FIB-SEM to identify protrusions in the form of filopodia and lamellipodia in cultured breast cancer epithelial cells that are morphologically similar to breast carcinoma obtained *in vivo*. I found that these filopodial protrusions demonstrate dimensions within 150nm in diameter that are conserved from breast tumor to culture. Given the differences in intercellular environment between the two systems, these similarities lend confidence that our model reflects similar functional and signaling biology to protrusions *in vivo*.

I found that HRG stimulation of HER2-HER3 signaling output manifests in protrusion extension that occurs in a localized and rapid manner at the site of signal initiation. These filopodial protrusions appear to be HER2-mediated, as knockdown of HER2 reduced the quantity of filopodial-positive cells; though HER2 likely facilitates just one aspect of the filopodial protrusion

machinery. This dependence of protrusion formation upon HER2 likely reflects an interdependence between HER2 signaling and protrusion outgrowth. Protrusions are dependent upon HER2 signaling, and conversely, HER2 is dependent upon protrusions as a platform to promote signaling.

Using quantitative immunofluorescence, I found spatial confinement of HER2 signaling pathway molecules at the site of protrusion extension. HER2 was localized to filopodia and this preferential localization to protrusions is present regardless of activation state. Downstream of the HER2 pathway, pAKT was enriched in protrusions following stimulation, suggesting activation of AKT occurs at the membrane or pAKT is distributed to the membrane.

Single particle tracking (SPT) of HER2 using QDs in live breast cancer cells revealed that this localized and rapid signaling may be informed by HER2 spatiotemporal dynamics in protrusions. I found that HER2 motion in filopodia was strikingly fast compared to the lamellipodia and cell body, and that this mobility is much faster than what has been previously observed in other membrane proteins (Lidke *et al.*, 2005a; Andrews *et al.*, 2008; Treanor *et al.*, 2010; Jaqaman *et al.*, 2011). Interestingly, I found that this fast motion was not contributed by directed or active transport as has been observed for other membrane receptors (Lidke *et al.*, 2005a; Sundara Rajan and Vu, 2006), but was instead rapid diffusion. Furthermore, this rapid diffusion of HER2 in filopodia was facilitated by the linear geometry of actin which was necessary for HER2 downstream signaling.

4.3 HER2 Signaling is Spatially Regulated in Protrusions

The spatial confinement of HER2 suggested that protrusions may serve as a platform for signaling. Previous studies have employed EM, confocal, and TIRFM to study the prevalence of HER2 in membrane protrusions, membrane ruffles, or “finger-like” structures that extend from the cell surface (Hommelgaard *et al.*, 2004; Peckys *et al.*, 2015; Chung *et al.*, 2016; Jeong *et al.*, 2017). Our findings are consistent with these past studies, but also provide a quantitative element confirming high density residence of HER2 as well as its downstream effector pAKT in membrane protrusion that is evident on an individual cellular basis, and that is detectable above the intercellular heterogeneity.

Unlike EGFR which is known to endocytose following receptor activation (Sorkin *et al.*, 1993; Baulida *et al.*, 1996), I find, in agreement with other findings (Hommelgaard *et al.*, 2004; Lerdrup *et al.*, 2007), that HER2 remains membrane associated following stimulation (see **Figure 3.7**). This internalization resistance has been attributed to HER2 preferential localization to protrusions (Hommelgaard *et al.*, 2004; Lerdrup *et al.*, 2007) which inhibits downregulation of the receptor at the membrane. This role for protrusions in preventing HER2 signal downregulation may be complemented by their role in serving as a platform for initiation and continued propagation of signaling. Recently, Chung *et al.* found that the high density of HER2 in specific membrane regions induces morphological deformation of these regions to yield “finger-like” structures (Chung *et al.*, 2016). Our finding that knockdown of HER2 correlates with reduction of protrusions supports the fact that protrusion extension is dependent on HER2. Additionally, our data showing that activation of HER2 signaling promotes protrusion growth at the site of stimulation, and

downstream effector pAKT is localized at these sites, provide further evidence that HER2 signaling and protrusions are inextricably linked. Our study is distinct from others in identifying HER2 localization on filopodial protrusions, and our EM studies find that HER2-overexpressing cells are decorated with hair-like filopodia that exhibit a distinct compartmented geometry. These data suggest HER2 signaling and protrusion extension constitute a positive feedback loop such that protrusions serve as a platform for signaling that supports filopodial and membrane elaboration, and these protrusions, in effect, spatially propagates HER2 signaling.

4.4 Linear Actin Structure Facilitates Rapid Signaling of HER2 through Diffusion

The simplified view of the plasma membrane as a homogenous surface has given way to an updated understanding of the membrane as a dynamic and integrated structure organized and partitioned by lipids, membrane proteins and the underlying cytoskeleton (Kusumi *et al.*, 2005; Kusumi *et al.*, 2012). And more recently, the actin cytoskeleton has emerged as a critical spatiotemporal regulator of signaling.

In this study, I distinguish for the first time HER2 dynamics in different subcellular regions of the cell. I observe differences in HER2 mobility in different cellular regions that reflect the distinct geometry of the filopodia, lamellipodia, and cell body, and their underlying membrane skeleton. Our findings show that in filopodia, HER2 receptors traveled almost exclusively in a one-dimensional manner and traversed along the length of the filopodium from base to end, reflecting the slender and elongated geometry of filopodial membrane. In comparison, the non-directionality of HER2 motion observed in the lamellipodia and cell body reflected the different membrane

topology upon which HER2 traveled. A key finding here is that HER2 motion along filopodia was fast, driven by simple diffusion in one-dimension along the filopodial length, while HER2 motion was altogether slower along lamellipodia and cell body, unaccountable by simple diffusion alone. These differences in dynamics are a result of the spatial organization of the cytoskeleton in each subcellular region: the high-level organization of linear parallel actin filament bundles in filopodia compared to the meshwork of actin filaments supporting lamellipodia and the cell body (Le Clainche and Carlier, 2008; Mattila and Lappalainen, 2008). It is interesting that this rapid HER2 motion is diffusive, as EGFR, a receptor from the same ERBB family was found to traffic by directed retrograde transport along filopodia towards the cell body (Lidke *et al.*, 2005a); though this dissimilarity may be attributed to fundamental differences in how these receptors are endocytically regulated.

Our super-resolution microscopy of filopodial protrusions reveal the rich packing of actin filaments and their highly linear geometry, indicating actin as the major molecular component in filopodia influencing HER2 mobility. This was confirmed to be the case by global disruption of actin using latrunculin B, which induced the collapse of the linear actin architecture in filopodia and consequently reduced HER2 mobility as well as functional downstream signaling in actin-altered protrusions. Previous work by Jaqaman *et al* found confinement and increased diffusivity of CD36 receptors in linear membrane regions of actin-defined channels along the cell body (Jaqaman *et al.*, 2011). Additional studies have also made the case for actin in modulating receptor mobility and signaling (Treanor *et al.*, 2010). Our findings suggest that the high-level organization of linear filamentous actin in filopodia may define a similar elongated geometry that is critical for facilitating

fast HER2 diffusion. This is in contrast to the transient membrane corrals defined in the lamellipodia and cell body (Kusumi *et al.*, 2012) which is likely to influence HER2 motion in a more heterogeneous manner (i.e. hop diffusion of receptors between corrals).

Such confinement of proteins in one-dimension may serve as another mechanism by which cells facilitate rapid signaling. The increased diffusivity enabled by the uni-dimensionality of linear actin in filopodia can increase receptor encounters that promote signal transduction (Jans, 1992). Furthermore, confinement can increase receptor concentration by limiting the dimensionality of movement to raise the potential for interaction (Jaqaman *et al.*, 2011; Zimmerberg and Hess, 2011; Jaqaman and Grinstein, 2012).

The fast signaling demonstrated by protrusion outgrowth within minutes following stimulation points to the functionality of rapid and localized signaling in maintaining this process. HER2 motion was observed to occur at speeds of $0.5 - 3 \mu\text{m/s}$, rates that are comparable to typical rates of actin polymerization in cells ($0.1 - 1 \mu\text{m/s}$). Thus, fast receptor dynamics within a localized environment of filopodial protrusions is likely necessary to accommodate this fast protrusion growth by enabling rapid signaling. Together, our findings demonstrate the influence of the nanoscale membrane and cytoskeletal environment in shaping rapid localized signaling, but also the interchangeable influence of receptor dynamics and cellular response. As receptor dynamics and signaling trigger reorganization of actin and membrane, so too does membrane and actin organization influence dynamics, thus underscoring the biological importance of the protrusions nanoscale environment in modulating signaling.

4.5 Future Directions

4.5.1 Filopodial-specific Cytoskeletal Targeting of HER2 Signaling by Fascin Inhibitors

Filopodia serve critical roles in guiding cells and directing cell motility, but when dysregulated, increased numbers of filopodia have been associated with increased invasiveness and metastatic potential, as well as lower survival rates in cancer (Arjonen *et al.*, 2011; Khurana and George, 2011). Recently, the actin bundling protein fascin has been of major interest as a cytoskeletal target due to findings correlating its upregulation with increased metastasis and mortality in patients (Machesky and Li, 2010; Tan *et al.*, 2013). Of interest is the fact that fascin is not expressed in filopodia of normal epithelial cells, and is upregulated as a course of increased invasive potential and motility, suggesting its potential as a pharmaceutical target (Machesky and Li, 2010; Khurana and George, 2011; Huang *et al.*, 2015). Future HER2 dynamics experiments using fascin inhibitors to more precisely disrupt the filopodia architecture would help to elucidate the molecular mechanism by which HER2 interacts with actin to conduct signaling. Given that the actin interfilament spacing bundled by fascin is similar to the dimension of a typical protein (on the order of 10 – 12 nm for interfilament spacing vs 10 nm for a protein), one speculation is that HER2 is gliding along interfilament channels (Reth, 2013; Yang *et al.*, 2013).

Additionally, fascin has been observed to exist in a specialized class of actin-based protrusions termed invadopodia that promote invasion and metastatic aggression in cancer (Murphy and Courtneidge, 2011; Paz *et al.*, 2014). It remains to be investigated how the filopodial protrusions in this study relate to invadopodia which are known to house proteases capable of degrading the extracellular environment. Futures studies that reveal whether the filopodial protrusions I studied

are of similar molecular composition to invadopodia could offer additional ways of targeting their invasive potential.

4.5.2 HER2 Directionality and Influence of Protrusion Geometry on Mobility

The influence of actin on HER2 mobility was reflected in the results of our study. But the mechanism by which actin facilitates fast HER2 motion along filopodia remains unclear. In particular, questions about whether HER2 is directly in contact with actin through a scaffolding protein or transiently interacting with actin filaments that serve as a barrier or channel are future directions to explore. Further work to solidify our understanding of this aspect of HER2 mobility would include analyzing the trajectories of HER2 in protrusions with longer geometries to reveal if an underlying directionality in HER2 movement that was not visible on “shorter” filopodial protrusions (of lengths under 5 μm) exists. Additional analysis of the auto-correlation of HER2 position along the 1D filopodia over time might also reveal whether additional forces apart from what is expected of Brownian diffusion are present. Finally, to confirm if the motion observed from HER2 1D filopodial trajectories are similar to the 1D random walk simulations and thus conclusively diffusional, a quantitative test comparing the correlation of the two trajectories should be conducted. As a preliminary step, this test could take the form of testing whether the distributions of the step distances from the raw 1D trajectory and simulation are derived from similar Gaussian distributions by a Kolmogorov-Smirnov Test.

4.5.3 HER2-HER3 Dimer Dynamics in Protrusions

HER family receptor trafficking remains a topic of interest that is poorly understood. Of the four receptors, EGFR is the best studied, and is understood to be downregulated through endocytosis-mediated degradation (Sorkin *et al.*, 1993). But the regulation of HER2 and HER3 especially in regards to their dimerization dynamics remains a mystery. Our study of HER2 localization to the membrane is consistent with other studies finding that HER2 is internalization resistant in part due to protrusion association (Hommelgaard *et al.*, 2004; Lerdrup *et al.*, 2007). In contrast, its preferential dimer partner, HER3, has been shown to undergo neuregulin-induced downregulation through ubiquitin-mediated as well as lysosomal degradation (Qiu and Goldberg, 2002; Cao *et al.*, 2007). Thus, evidence pointing to the differential regulation of these two partners raises interesting questions about how HER2-HER3 dynamically function following dimerization. Future studies looking at how these two receptors traffic, as well as studies extending our analysis of HER2 dynamics to HER2-HER3 dimer dynamics in protrusions would further illuminate this HER2-HER3 biology. Additionally, understanding how current HER2 therapeutics such as trastuzumab, pertuzumab, and lapatinib modulates HER2-HER3 signaling specifically in protrusions may reveal strategies for improving drug efficacy.

4.5.4 Spatial Targeting of HER2 in Filopodial Protrusions

The high density with which HER2 resides in protrusions and their rapid dynamics on these membrane structures highlight their integrated function in driving cancer progression. Filopodial protrusions serve a critical role for HER2 signaling, but independently also enable increased invasive motility. And as our understanding of the spatiotemporal aspects of HER2 signaling continues to

grow, one avenue of improved therapeutic precision may arise through spatial targeting. These include dual targeting of HER2 signaling function and filopodial-specific cytoskeletal proteins (i.e. fascin), but also delivery of filopodial-targeted HER2 therapeutics as potential strategies for the future. Thus, continued work aimed at an integrated spatiotemporal understanding of cellular signaling will guide a spatial systems approach to precision medicine of the future.

REFERENCES

- Abercrombie, M., Heaysman, J.E.M., and Pegrum, S.M. (1971). The locomotion of fibroblasts in culture. *Experimental Cell Research* 67, 359-367.
- Adams, J.C. (2001). Cell-matrix contact structures. *Cellular and Molecular Life Sciences CMLS* 58, 371-392.
- Ahmed, S., Goh, W.I., and Bu, W. (2010). I-BAR domains, IRSp53 and filopodium formation. *Seminars in cell & developmental biology* 21, 350-356.
- Albertson, D.G. (2006). Gene amplification in cancer. *Trends in Genetics* 22, 447-455.
- Andrews, N.L., Lidke, K.A., Pfeiffer, J.R., Burns, A.R., Wilson, B.S., Oliver, J.M., and Lidke, D.S. (2008). Actin restricts Fc[epsilon]RI diffusion and facilitates antigen-induced receptor immobilization. *Nature cell biology* 10, 955-963.
- Applewhite, D.A., Barzik, M., Kojima, S.-i., Svitkina, T.M., Gertler, F.B., and Borisy, G.G. (2007). Ena/VASP Proteins Have an Anti-Capping Independent Function in Filopodia Formation. *Molecular biology of the cell* 18, 2579-2591.
- Arjonen, A., Kaukonen, R., and Ivaska, J. (2011). Filopodia and adhesion in cancer cell motility. *Cell Adh Migr* 5, 421-430.
- Arteaga, C.L., Sliwkowski, M.X., Osborne, C.K., Perez, E.A., Puglisi, F., and Gianni, L. (2011). Treatment of HER2-positive breast cancer: current status and future perspectives. *Nature reviews. Clinical oncology* 9, 16-32.
- Austin, C.D., De Maziere, A.M., Pisacane, P.I., van Dijk, S.M., Eigenbrot, C., Sliwkowski, M.X., Klumperman, J., and Scheller, R.H. (2004). Endocytosis and sorting of ErbB2 and the site of action of cancer therapeutics trastuzumab and geldanamycin. *Molecular biology of the cell* 15, 5268-5282.

- Bannai, H., Levi, S., Schweizer, C., Dahan, M., and Triller, A. (2006). Imaging the lateral diffusion of membrane molecules with quantum dots. *Nature protocols* *1*, 2628-2634.
- Barzik, M., Kotova, T.I., Higgs, H.N., Hazelwood, L., Hanein, D., Gertler, F.B., and Schafer, D.A. (2005). Ena/VASP proteins enhance actin polymerization in the presence of barbed end capping proteins. *J Biol Chem* *280*, 28653-28662.
- Baselga, J., and Swain, S.M. (2009). Novel anticancer targets: revisiting ERBB2 and discovering ERBB3. *Nat Rev Cancer* *9*, 463-475.
- Baulida, J., Kraus, M.H., Alimandi, M., Di Fiore, P.P., and Carpenter, G. (1996). All ErbB receptors other than the epidermal growth factor receptor are endocytosis impaired. *J Biol Chem* *271*, 5251-5257.
- Bear, J.E., and Gertler, F.B. (2009). Ena/VASP: towards resolving a pointed controversy at the barbed end. *Journal of Cell Science* *122*, 1947.
- Bellacosa, A., Kumar, C.C., Cristofano, A.D., and Testa, J.R. (2005). Activation of AKT Kinases in Cancer: Implications for Therapeutic Targeting. *Advances in Cancer Research* *94*, 29-86.
- Bertelsen, V., and Stang, E. (2014). The Mysterious Ways of ErbB2/HER2 Trafficking. *Membranes (Basel)* *4*, 424-446.
- Betzig, E., Patterson, G.H., Sougrat, R., Lindwasser, O.W., Olenych, S., Bonifacino, J.S., Davidson, M.W., Lippincott-Schwartz, J., and Hess, H.F. (2006). Imaging intracellular fluorescent proteins at nanometer resolution. *Science* *313*, 1642-1645.
- Bisi, S., Disanza, A., Malinverno, C., Frittoli, E., Palamidessi, A., and Scita, G. (2013). Membrane and actin dynamics interplay at lamellipodia leading edge. *Curr Opin Cell Biol* *25*, 565-573.
- Blanchoin, L., Boujemaa-Paterski, R., Sykes, C., and Plastino, J. (2014). Actin dynamics, architecture, and mechanics in cell motility. *Physiol Rev* *94*, 235-263.

- Boal, D. (2012). *Mechanics of the Cell*. Cambridge University Press.
- Bohil, A.B., Robertson, B.W., and Cheney, R.E. (2006). Myosin-X is a molecular motor that functions in filopodia formation. *Proc Natl Acad Sci U S A* *103*, 12411-12416.
- Calderwood, D.A., Shattil, S.J., and Ginsberg, M.H. (2000). Integrins and actin filaments: reciprocal regulation of cell adhesion and signaling. *J Biol Chem* *275*, 22607-22610.
- Calleja, V., Laguerre, M., Parker, P.J., and Larijani, B. (2009). Role of a Novel PH-Kinase Domain Interface in PKB/Akt Regulation: Structural Mechanism for Allosteric Inhibition. *PLoS Biology* *7*, e1000017.
- Campellone, K.G., and Welch, M.D. (2010). A nucleator arms race: cellular control of actin assembly. *Nat Rev Mol Cell Biol* *11*, 237-251.
- Cao, R., Chen, J., Zhang, X., Zhai, Y., Qing, X., Xing, W., Zhang, L., Malik, Y.S., Yu, H., and Zhu, X. (2014). Elevated expression of myosin X in tumours contributes to breast cancer aggressiveness and metastasis. *British journal of cancer* *111*, 539-550.
- Cao, Z., Wu, X., Yen, L., Sweeney, C., and Carraway, K.L., 3rd. (2007). Neuregulin-induced ErbB3 downregulation is mediated by a protein stability cascade involving the E3 ubiquitin ligase Nrdp1. *Molecular and cellular biology* *27*, 2180-2188.
- Carlier, M.F., and Pantaloni, D. (1997). Control of actin dynamics in cell motility. *Journal of molecular biology* *269*, 459-467.
- Chaffer, C.L., and Weinberg, R.A. (2011). A perspective on cancer cell metastasis. *Science* *331*, 1559-1564.
- Chan, A., Delaloge, S., Holmes, F.A., Moy, B., Iwata, H., Harvey, V.J., Robert, N.J., Silovski, T., Gokmen, E., von Minckwitz, G., Ejlertsen, B., Chia, S.K., Mansi, J., Barrios, C.H., Gnant, M., Buyse, M., Gore, I., Smith, J., 2nd, Harker, G., Masuda, N., Petrakova, K., Zotano,

- A.G., Iannotti, N., Rodriguez, G., Tassone, P., Wong, A., Bryce, R., Ye, Y., Yao, B., and Martin, M. (2016). Neratinib after trastuzumab-based adjuvant therapy in patients with HER2-positive breast cancer (ExteNET): a multicentre, randomised, double-blind, placebo-controlled, phase 3 trial. *The Lancet. Oncology* *17*, 367-377.
- Chang, Y.-P., Pinaud, F., Antelman, J., and Weiss, S. (2008). Tracking bio-molecules in live cells using quantum dots. *Journal of biophotonics* *1*, 287-298.
- Chen, Xing J., Squarr, Anna J., Stephan, R., Chen, B., Higgins, Theresa E., Barry, David J., Martin, Morag C., Rosen, Michael K., Bogdan, S., and Way, M. (2014). Ena/VASP Proteins Cooperate with the WAVE Complex to Regulate the Actin Cytoskeleton. *Developmental cell* *30*, 569-584.
- Chesarone, M.A., and Goode, B.L. (2009). Actin nucleation and elongation factors: mechanisms and interplay. *Curr Opin Cell Biol* *21*, 28-37.
- Chung, I., Akita, R., Vandlen, R., Toomre, D., Schlessinger, J., and Mellman, I. (2010). Spatial control of EGF receptor activation by reversible dimerization on living cells. *Nature* *464*, 783-787.
- Chung, I., Reichelt, M., Shao, L., Akita, R.W., Koeppen, H., Rangell, L., Schaefer, G., Mellman, I., and Sliwkowski, M.X. (2016). High cell-surface density of HER2 deforms cell membranes. *Nature Communications* *7*, 12742.
- Clarke, M., Schatten, G., Mazia, D., and Spudich, J.A. (1975). Visualization of actin fibers associated with the cell membrane in amoebae of *Dictyostelium discoideum*. *Proc Natl Acad Sci U S A* *72*, 1758-1762.
- Courty, S., Luccardini, C., Bellaiche, Y., Cappello, G., and Dahan, M. (2006). Tracking individual kinesin motors in living cells using single quantum-dot imaging. *Nano Lett* *6*, 1491-1495.

- Creech, M.K., Wang, J., Nan, X., and Gibbs, S.L. (2017). Superresolution Imaging of Clinical Formalin Fixed Paraffin Embedded Breast Cancer with Single Molecule Localization Microscopy. *Scientific Reports* 7, 40766.
- Dahan, M., Lévi, S., Luccardini, C., Rostaing, P., Riveau, B., and Triller, A. (2003). Diffusion Dynamics of Glycine Receptors Revealed by Single-Quantum Dot Tracking. *Science* 302, 442.
- Daponte, A., Kostopoulou, E., Papandreou, C.N., Daliani, D.D., Minas, M., Koukoulis, G., and Messinis, I.E. (2008). Prognostic significance of fascin expression in advanced poorly differentiated serous ovarian cancer. *Anticancer research* 28, 1905-1910.
- Dempsey, G.T., Vaughan, J.C., Chen, K.H., Bates, M., and Zhuang, X. (2011). Evaluation of fluorophores for optimal performance in localization-based super-resolution imaging. *Nat Meth* 8, 1027-1036.
- Dent, E.W., Gupton, S.L., and Gertler, F.B. (2011). The Growth Cone Cytoskeleton in Axon Outgrowth and Guidance. *Cold Spring Harbor perspectives in biology* 3, a001800.
- Edelstein, A.D., Tsuchida, M.A., Amodaj, N., Pinkard, H., Vale, R.D., and Stuurman, N. (2014). Advanced methods of microscope control using μ Manager software. *Journal of biological methods* 1, e10.
- Edwards, J., Mukherjee, R., Munro, A.F., Wells, A.C., Almushatat, A., and Bartlett, J.M. (2004). HER2 and COX2 expression in human prostate cancer. *European journal of cancer* (Oxford, England : 1990) 40, 50-55.
- Eigenbrot, C., Ultsch, M., Dubnovitsky, A., Abrahmsén, L., and Härd, T. (2010). Structural basis for high-affinity HER2 receptor binding by an engineered protein. *Proceedings of the National Academy of Sciences* 107, 15039-15044.

- Fairchild, C.L., and Barna, M. (2014). Specialized filopodia: at the 'tip' of morphogen transport and vertebrate tissue patterning. *Curr Opin Genet Dev* 27, 67-73.
- Faix, J., and Rottner, K. (2006). The making of filopodia. *Current Opinion in Cell Biology* 18, 18-25.
- Fichter, K.M., Flajolet, M., Greengard, P., and Vu, T.Q. (2010). Kinetics of G-protein-coupled receptor endosomal trafficking pathways revealed by single quantum dots. *Proceedings of the National Academy of Sciences* 107, 18658-18663.
- Fowler, W.E., and Aebi, U. (1983). A consistent picture of the actin filament related to the orientation of the actin molecule. *J Cell Biol* 97, 264-269.
- Franke, T.F. (2008a). Intracellular Signaling by Akt: Bound to Be Specific. *Science Signaling* 1, pe29.
- Franke, T.F. (2008b). PI3K/Akt: getting it right matters. *Oncogene* 27, 6473-6488.
- Franke, T.F., Kaplan, D.R., Cantley, L.C., and Toker, A. (1997). Direct Regulation of the Akt Proto-Oncogene Product by Phosphatidylinositol-3,4-bisphosphate. *Science* 275, 665.
- Franklin, M.C., Carey, K.D., Vajdos, F.F., Leahy, D.J., de Vos, A.M., and Sliwkowski, M.X. (2004). Insights into ErbB signaling from the structure of the ErbB2-pertuzumab complex. *Cancer cell* 5, 317-328.
- Gardel, M.L., Schneider, I.C., Aratyn-Schaus, Y., and Waterman, C.M. (2010). Mechanical Integration of Actin and Adhesion Dynamics in Cell Migration. *Annual review of cell and developmental biology* 26, 315-333.
- Garrett, J.T., Olivares, M.G., Rinehart, C., Granja-Ingram, N.D., Sanchez, V., Chakrabarty, A., Dave, B., Cook, R.S., Pao, W., McKinely, E., Manning, H.C., Chang, J., and Arteaga, C.L.

- (2011). Transcriptional and posttranslational up-regulation of HER3 (ErbB3) compensates for inhibition of the HER2 tyrosine kinase. *Proc Natl Acad Sci U S A* *108*, 5021-5026.
- Gassmann, M., Grenacher, B., Rohde, B., and Vogel, J. (2009). Quantifying Western blots: pitfalls of densitometry. *Electrophoresis* *30*, 1845-1855.
- Giancotti, F.G., and Ruoslahti, E. (1999). Integrin Signaling. *Science* *285*, 1028.
- Gingras, A.C., Kennedy, S.G., O'Leary, M.A., Sonenberg, N., and Hay, N. (1998). 4E-BP1, a repressor of mRNA translation, is phosphorylated and inactivated by the Akt(PKB) signaling pathway. *Genes & development* *12*, 502-513.
- Gonzalez, E., and McGraw, T.E. (2009). The Akt kinases: isoform specificity in metabolism and cancer. *Cell cycle (Georgetown, Tex.)* *8*, 2502-2508.
- Gravalos, C., and Jimeno, A. (2008). HER2 in gastric cancer: a new prognostic factor and a novel therapeutic target. *Annals of oncology : official journal of the European Society for Medical Oncology* *19*, 1523-1529.
- Grothey, A., Hashizume, R., Ji, H., Tubb, B.E., Patrick, C.W., Jr., Yu, D., Mooney, E.E., and McCrea, P.D. (2000). C-erbB-2/ HER-2 upregulates fascin, an actin-bundling protein associated with cell motility, in human breast cancer cell lines. *Oncogene* *19*, 4864-4875.
- Grover, G., DeLuca, K., Quirin, S., DeLuca, J., and Piestun, R. (2012). Super-resolution photon-efficient imaging by nanometric double-helix point spread function localization of emitters (SPINDLE). *Optics express* *20*, 26681-26695.
- Groves, J.T., and Kuriyan, J. (2010). Molecular mechanisms in signal transduction at the membrane. *Nature structural & molecular biology* *17*, 659-665.
- Hall, A. (1998). Rho GTPases and the actin cytoskeleton. *Science* *279*, 509-514.

- Harburger, D.S., and Calderwood, D.A. (2009). Integrin signalling at a glance. *J Cell Sci* *122*, 159-163.
- Hay, N., and Sonenberg, N. (2004). Upstream and downstream of mTOR. *Genes & development* *18*, 1926-1945.
- Hayashi, Y., Osanai, M., and Lee, G.H. (2011). Fascin-1 expression correlates with repression of E-cadherin expression in hepatocellular carcinoma cells and augments their invasiveness in combination with matrix metalloproteinases. *Cancer science* *102*, 1228-1235.
- Hellyer, N.J., Cheng, K., and Koland, J.G. (1998). ErbB3 (HER3) interaction with the p85 regulatory subunit of phosphoinositide 3-kinase. *The Biochemical journal* *333 (Pt 3)*, 757-763.
- Hellyer, N.J., Kim, M.S., and Koland, J.G. (2001). Heregulin-dependent activation of phosphoinositide 3-kinase and Akt via the ErbB2/ErbB3 co-receptor. *J Biol Chem* *276*, 42153-42161.
- Hess, S.T., Girirajan, T.P., and Mason, M.D. (2006). Ultra-high resolution imaging by fluorescence photoactivation localization microscopy. *Biophys J* *91*, 4258-4272.
- Holbro, T., and Hynes, N.E. (2004). ErbB receptors: directing key signaling networks throughout life. *Annual review of pharmacology and toxicology* *44*, 195-217.
- Holzer, T., Liffers, K., Rahm, K., Trageser, B., Özbek, S., and Gradl, D. (2012). Live imaging of active fluorophore labelled Wnt proteins. *FEBS Letters* *586*, 1638-1644.
- Hommelgaard, A.M., Lerdrup, M., and van Deurs, B. (2004). Association with membrane protrusions makes ErbB2 an internalization-resistant receptor. *Molecular biology of the cell* *15*, 1557-1567.

- Hood, J.D., and Cheresch, D.A. (2002). Role of integrins in cell invasion and migration. *Nat Rev Cancer* 2, 91-100.
- Hsiung, F., Ramirez-Weber, F.A., Iwaki, D.D., and Kornberg, T.B. (2005). Dependence of *Drosophila* wing imaginal disc cytonemes on Decapentaplegic. *Nature* 437, 560-563.
- Huang, B., Wang, W., Bates, M., and Zhuang, X. (2008). Three-dimensional Super-resolution Imaging by Stochastic Optical Reconstruction Microscopy. *Science (New York, N.Y.)* 319, 810-813.
- Huang, F., Schwartz, S.L., Byars, J.M., and Lidke, K.A. (2011). Simultaneous multiple-emitter fitting for single molecule super-resolution imaging. *Biomedical Optics Express* 2, 1377-1393.
- Huang, F.K., Han, S., Xing, B., Huang, J., Liu, B., Bordeleau, F., Reinhart-King, C.A., Zhang, J.J., and Huang, X.Y. (2015). Targeted inhibition of fascin function blocks tumour invasion and metastatic colonization. *Nat Commun* 6, 7465.
- Huttenlocher, A., and Horwitz, A.R. (2011). Integrins in cell migration. *Cold Spring Harbor perspectives in biology* 3, a005074.
- Hynes, N.E., and Lane, H.A. (2005). ERBB receptors and cancer: the complexity of targeted inhibitors. *Nat Rev Cancer* 5, 341-354.
- Hynes, N.E., and MacDonald, G. (2009). ErbB receptors and signaling pathways in cancer. *Curr Opin Cell Biol* 21, 177-184.
- Insall, R.H., and Machesky, L.M. (2009). Actin dynamics at the leading edge: from simple machinery to complex networks. *Developmental cell* 17, 310-322.
- Irish, J.M., Kotecha, N., and Nolan, G.P. (2006). Mapping normal and cancer cell signalling networks: towards single-cell proteomics. *Nat Rev Cancer* 6, 146-155.

- Jacob, T., Agarwal, A., Ramunno-Johnson, D., O'Hare, T., Gonen, M., Tyner, J.W., Druker, B.J., and Vu, T.Q. (2016). Ultrasensitive proteomic quantitation of cellular signaling by digitized nanoparticle-protein counting. *Sci Rep* 6, 28163.
- Jacquemet, G., Hamidi, H., and Ivaska, J. (2015). Filopodia in cell adhesion, 3D migration and cancer cell invasion. *Current Opinion in Cell Biology* 36, 23-31.
- Jain, S., Wheeler, J.R., Walters, R.W., Agrawal, A., Barsic, A., and Parker, R. (2016). ATPase-Modulated Stress Granules Contain a Diverse Proteome and Substructure. *Cell* 164, 487-498.
- Jaiswal, Bijay S., Kljavin, Noelyn M., Stawiski, Eric W., Chan, E., Parikh, C., Durinck, S., Chaudhuri, S., Pujara, K., Guillory, J., Edgar, Kyle A., Janakiraman, V., Scholz, R.-P., Bowman, Krista K., Lorenzo, M., Li, H., Wu, J., Yuan, W., Peters, Brock A., Kan, Z., Stinson, J., Mak, M., Modrusan, Z., Eigenbrot, C., Firestein, R., Stern, Howard M., Rajalingam, K., Schaefer, G., Merchant, Mark A., Sliwkowski, Mark X., de Sauvage, Frederic J., and Seshagiri, S. (2013). Oncogenic ERBB3 Mutations in Human Cancers. *Cancer cell* 23, 603-617.
- Jans, D.A. (1992). The mobile receptor hypothesis revisited: a mechanistic role for hormone receptor lateral mobility in signal transduction. *Biochimica et Biophysica Acta (BBA) - Reviews on Biomembranes* 1113, 271-276.
- Jaqaman, K., and Grinstein, S. (2012). Regulation from within: the cytoskeleton in transmembrane signaling. *Trends in cell biology* 22, 515-526.
- Jaqaman, K., Kuwata, H., Touret, N., Collins, R., Trimble, W.S., Danuser, G., and Grinstein, S. (2011). Cytoskeletal control of CD36 diffusion promotes its receptor and signaling function. *Cell* 146, 593-606.

- Jaqaman, K., Loerke, D., Mettlen, M., Kuwata, H., Grinstein, S., Schmid, S.L., and Danuser, G. (2008). Robust single-particle tracking in live-cell time-lapse sequences. *Nat Methods* 5, 695-702.
- Jeong, J., Kim, W., Kim, L.K., VanHouten, J., and Wysolmerski, J.J. (2017). HER2 signaling regulates HER2 localization and membrane retention. *PLOS ONE* 12, e0174849.
- Jeong, J., VanHouten, J.N., Dann, P., Kim, W., Sullivan, C., Yu, H., Liotta, L., Espina, V., Stern, D.F., Friedman, P.A., and Wysolmerski, J.J. (2016). PMCA2 regulates HER2 protein kinase localization and signaling and promotes HER2-mediated breast cancer. *Proc Natl Acad Sci U S A* 113, E282-290.
- Jorgens, D.M., Inman, J.L., Wojcik, M., Robertson, C., Palsdottir, H., Tsai, W.-T., Huang, H., Bruni-Cardoso, A., López, C.S., Bissell, M.J., Xu, K., and Auer, M. (2017). Deep nuclear invaginations are linked to cytoskeletal filaments – integrated bioimaging of epithelial cells in 3D culture. *Journal of Cell Science* 130, 177.
- Junttila, T.T., Li, G., Parsons, K., Phillips, G.L., and Sliwkowski, M.X. (2011). Trastuzumab-DM1 (T-DM1) retains all the mechanisms of action of trastuzumab and efficiently inhibits growth of lapatinib insensitive breast cancer. *Breast cancer research and treatment* 128, 347-356.
- Kerber, M.L., and Cheney, R.E. (2011). Myosin-X: a MyTH-FERM myosin at the tips of filopodia. *J Cell Sci* 124, 3733-3741.
- Kholodenko, B.N. (2006). Cell-signalling dynamics in time and space. *Nat Rev Mol Cell Biol* 7, 165-176.
- Khurana, S., and George, S.P. (2011). The role of actin bundling proteins in the assembly of filopodia in epithelial cells. *Cell Adhesion & Migration* 5, 409-420.
- Kobayashi, M., Ooi, A., Oda, Y., and Nakanishi, I. (2002). Protein overexpression and gene amplification of *c-erbB-2* in breast carcinomas: A comparative study of

- immunohistochemistry and fluorescence in situ hybridization of formalin-fixed, paraffin-embedded tissues. *Human Pathology* *33*, 21-28.
- Kornberg, T.B., and Roy, S. (2014). Cytonemes as specialized signaling filopodia. *Development* *141*, 729-736.
- Kovesi, P. (2000). Phase congruency: a low-level image invariant. *Psychological research* *64*, 136-148.
- Krause, M., and Gautreau, A. (2014). Steering cell migration: lamellipodium dynamics and the regulation of directional persistence. *Nat Rev Mol Cell Biol* *15*, 577-590.
- Kusumi, A., Fujiwara, T.K., Morone, N., Yoshida, K.J., Chadda, R., Xie, M., Kasai, R.S., and Suzuki, K.G. (2012). Membrane mechanisms for signal transduction: the coupling of the meso-scale raft domains to membrane-skeleton-induced compartments and dynamic protein complexes. *Seminars in cell & developmental biology* *23*, 126-144.
- Kusumi, A., Nakada, C., Ritchie, K., Murase, K., Suzuki, K., Murakoshi, H., Kasai, R.S., Kondo, J., and Fujiwara, T. (2005). Paradigm shift of the plasma membrane concept from the two-dimensional continuum fluid to the partitioned fluid: high-speed single-molecule tracking of membrane molecules. *Annual review of biophysics and biomolecular structure* *34*, 351-378.
- Le Clainche, C., and Carlier, M.F. (2008). Regulation of actin assembly associated with protrusion and adhesion in cell migration. *Physiol Rev* *88*, 489-513.
- Lee-Hoeflich, S.T., Crocker, L., Yao, E., Pham, T., Munroe, X., Hoeflich, K.P., Sliwkowski, M.X., and Stern, H.M. (2008). A central role for HER3 in HER2-amplified breast cancer: implications for targeted therapy. *Cancer Res* *68*, 5878-5887.
- Leijnse, N., Oddershede, L.B., and Bendix, P.M. (2015). An updated look at actin dynamics in filopodia. *Cytoskeleton (Hoboken, N.J.)* *72*, 71-79.

- Lenferink, A.E., Pinkas-Kramarski, R., van de Poll, M.L., van Vugt, M.J., Klapper, L.N., Tzahar, E., Waterman, H., Sela, M., van Zoelen, E.J., and Yarden, Y. (1998). Differential endocytic routing of homo- and hetero-dimeric ErbB tyrosine kinases confers signaling superiority to receptor heterodimers. *The EMBO journal* *17*, 3385-3397.
- Lerdrup, M., Bruun, S., Grandal, M.V., Roepstorff, K., Kristensen, M.M., Hommelgaard, A.M., and van Deurs, B. (2007). Endocytic down-regulation of ErbB2 is stimulated by cleavage of its C-terminus. *Molecular biology of the cell* *18*, 3656-3666.
- Lidke, D.S., Lidke, K.A., Rieger, B., Jovin, T.M., and Arndt-Jovin, D.J. (2005a). Reaching out for signals: filopodia sense EGF and respond by directed retrograde transport of activated receptors. *The Journal of Cell Biology* *170*, 619-626.
- Lidke, D.S., Nagy, P., Heintzmann, R., Arndt-Jovin, D.J., Post, J.N., Grecco, H.E., Jares-Erijman, E.A., and Jovin, T.M. (2004). Quantum dot ligands provide new insights into erbB/HER receptor-mediated signal transduction. *Nat Biotech* *22*, 198-203.
- Lidke, K.A., Rieger, B., Lidke, D.S., and Jovin, T.M. (2005b). The role of photon statistics in fluorescence anisotropy imaging. *IEEE Trans Image Process* *14*, 1237-1245.
- Lippincott-Schwartz, J. (2004). Dynamics of secretory membrane trafficking. *Annals of the New York Academy of Sciences* *1038*, 115-124.
- Liu, B., Ordonez-Ercan, D., Fan, Z., Edgerton, S.M., Yang, X., and Thor, A.D. (2007). Downregulation of erbB3 abrogates erbB2-mediated tamoxifen resistance in breast cancer cells. *International journal of cancer* *120*, 1874-1882.
- Lohrisch, C., and Piccart, M. (2001). An overview of HER2. *Seminars in Oncology* *28*, 3-11.
- Low-Nam, S.T., Lidke, K.A., Cutler, P.J., Roovers, R.C., van Bergen en Henegouwen, P.M.P., Wilson, B.S., and Lidke, D.S. (2011). ErbB1 dimerization is promoted by domain co-

- confinement and stabilized by ligand-binding. *Nature structural & molecular biology* *18*, 1244-1249.
- Luz, M., Spann-Muller, S., Ozhan, G., Kagermeier-Schenk, B., Rhinn, M., Weidinger, G., and Brand, M. (2014). Dynamic association with donor cell filopodia and lipid-modification are essential features of Wnt8a during patterning of the zebrafish neuroectoderm. *PLoS One* *9*, e84922.
- Lyakhov, I., Zielinski, R., Kuban, M., Kramer-Marek, G., Fisher, R., Chertov, O., Bindu, L., and Capala, J. (2010). HER2- and EGFR-specific affiprobe: novel recombinant optical probes for cell imaging. *Chembiochem : a European journal of chemical biology* *11*, 345-350.
- Machesky, L.M. (2008). Lamellipodia and filopodia in metastasis and invasion. *FEBS Lett* *582*, 2102-2111.
- Machesky, L.M., and Li, A. (2010). Fascin: Invasive filopodia promoting metastasis. *Communicative & integrative biology* *3*, 263-270.
- Manning, B.D., and Toker, A. (2017). AKT/PKB Signaling: Navigating the Network. *Cell* *169*, 381-405.
- Marone, R., Hess, D., Dankort, D., Muller, W.J., Hynes, N.E., and Badache, A. (2004). Memo mediates ErbB2-driven cell motility. *Nature cell biology* *6*, 515-522.
- Mattila, P.K., Batista, F.D., and Treanor, B. (2016). Dynamics of the actin cytoskeleton mediates receptor cross talk: An emerging concept in tuning receptor signaling. *J Cell Biol* *212*, 267-280.
- Mattila, P.K., and Lappalainen, P. (2008). Filopodia: molecular architecture and cellular functions. *Nat Rev Mol Cell Biol* *9*, 446-454.

- Mellor, H. (2010). The role of formins in filopodia formation. *Biochimica et Biophysica Acta (BBA) - Molecular Cell Research* *1803*, 191-200.
- Menard, S., Casalini, P., Campiglio, M., Pupa, S., Agresti, R., and Tagliabue, E. (2001). HER2 overexpression in various tumor types, focussing on its relationship to the development of invasive breast cancer. *Annals of oncology : official journal of the European Society for Medical Oncology* *12 Suppl 1*, S15-19.
- Michalet, X., Pinaud, F.F., Bentolila, L.A., Tsay, J.M., Doose, S., Li, J.J., Sundaresan, G., Wu, A.M., Gambhir, S.S., and Weiss, S. (2005). Quantum Dots for Live Cells, in Vivo Imaging, and Diagnostics. *Science* *307*, 538.
- Miller, J., Fraser, S.E., and McClay, D. (1995). Dynamics of thin filopodia during sea urchin gastrulation. *Development* *121*, 2501-2511.
- Mitchison, T.J., and Cramer, L.P. (1996). Actin-based cell motility and cell locomotion. *Cell* *84*, 371-379.
- Moasser, M.M. (2007). The oncogene HER2; Its signaling and transforming functions and its role in human cancer pathogenesis. *Oncogene* *26*, 6469-6487.
- Mullins, R.D., Heuser, J.A., and Pollard, T.D. (1998). The interaction of Arp2/3 complex with actin: nucleation, high affinity pointed end capping, and formation of branching networks of filaments. *Proc Natl Acad Sci U S A* *95*, 6181-6186.
- Murphy, D.A., and Courtneidge, S.A. (2011). The 'ins' and 'outs' of podosomes and invadopodia: characteristics, formation and function. *Nat Rev Mol Cell Biol* *12*, 413-426.
- Nagy, S., Ricca, B.L., Norstrom, M.F., Courson, D.S., Brawley, C.M., Smithback, P.A., and Rock, R.S. (2008). A myosin motor that selects bundled actin for motility. *Proceedings of the National Academy of Sciences of the United States of America* *105*, 9616-9620.

- Nahta, R., and Esteva, F.J. (2006). HER2 therapy: molecular mechanisms of trastuzumab resistance. *Breast cancer research : BCR* 8, 215.
- Nan, X., Sims, P.A., Chen, P., and Xie, X.S. (2005). Observation of individual microtubule motor steps in living cells with endocytosed quantum dots. *The journal of physical chemistry. B* 109, 24220-24224.
- Nickerson, A., Huang, T., Lin, L.-J., and Nan, X. (2014). Photoactivated Localization Microscopy with Bimolecular Fluorescence Complementation (BiFC-PALM) for Nanoscale Imaging of Protein-Protein Interactions in Cells. *PLoS ONE* 9, e100589.
- Nobes, C.D., and Hall, A. (1995). Rho, rac, and cdc42 GTPases regulate the assembly of multimolecular focal complexes associated with actin stress fibers, lamellipodia, and filopodia. *Cell* 81, 53-62.
- Nobes, C.D., and Hall, A. (1999). Rho GTPases control polarity, protrusion, and adhesion during cell movement. *J Cell Biol* 144, 1235-1244.
- Ovesny, M., Krizek, P., Borkovec, J., Svindrych, Z., and Hagen, G.M. (2014). ThunderSTORM: a comprehensive ImageJ plug-in for PALM and STORM data analysis and super-resolution imaging. *Bioinformatics (Oxford, England)* 30, 2389-2390.
- Parakh, S., Gan, H.K., Parslow, A.C., Burvenich, I.J.G., Burgess, A.W., and Scott, A.M. (2017). Evolution of anti-HER2 therapies for cancer treatment. *Cancer treatment reviews* 59, 1-21.
- Parsons, J.T., Horwitz, A.R., and Schwartz, M.A. (2010). Cell adhesion: integrating cytoskeletal dynamics and cellular tension. *Nature reviews. Molecular cell biology* 11, 633-643.
- Parthasarathy, R. (2012). Rapid, accurate particle tracking by calculation of radial symmetry centers. *Nat Meth* 9, 724-726.

- Patterson, G., Davidson, M., Manley, S., and Lippincott-Schwartz, J. (2010). Superresolution imaging using single-molecule localization. *Annual review of physical chemistry* *61*, 345-367.
- Pavani, S.R.P., Thompson, M.A., Biteen, J.S., Lord, S.J., Liu, N., Twieg, R.J., Piestun, R., and Moerner, W.E. (2009). Three-dimensional, single-molecule fluorescence imaging beyond the diffraction limit by using a double-helix point spread function. *Proceedings of the National Academy of Sciences* *106*, 2995-2999.
- Paz, H., Pathak, N., and Yang, J. (2014). Invading one step at a time: the role of invadopodia in tumor metastasis. *Oncogene* *33*, 4193-4202.
- Peckys, D.B., Korf, U., and de Jonge, N. (2015). Local variations of HER2 dimerization in breast cancer cells discovered by correlative fluorescence and liquid electron microscopy. *Science Advances* *1*.
- Pelosi, G., Pastorino, U., Pasini, F., Maissonneuve, P., Frassetto, F., Iannucci, A., Sonzogni, A., De Manzoni, G., Terzi, A., Durante, E., Bresaola, E., Pezzella, F., and Viale, G. (2003). Independent prognostic value of fascin immunoreactivity in stage I nonsmall cell lung cancer. *British journal of cancer* *88*, 537-547.
- Peng, G.E., Wilson, S.R., and Weiner, O.D. (2011). A pharmacological cocktail for arresting actin dynamics in living cells. *Molecular biology of the cell* *22*, 3986-3994.
- Pinkas-Kramarski, R., Soussan, L., Waterman, H., Levkowitz, G., Alroy, I., Klapper, L., Lavi, S., Seger, R., Ratzkin, B.J., Sela, M., and Yarden, Y. (1996). Diversification of Neu differentiation factor and epidermal growth factor signaling by combinatorial receptor interactions. *The EMBO journal* *15*, 2452-2467.
- Plotnikov, S.V., and Waterman, C.M. (2013). Guiding cell migration by tugging. *Curr Opin Cell Biol* *25*, 619-626.

- Pollard, T.D., and Borisy, G.G. (2003). Cellular motility driven by assembly and disassembly of actin filaments. *Cell* 112, 453-465.
- Polsky, D., and Cordon-Cardo, C. (2003). Oncogenes in melanoma. *Oncogene* 22, 3087-3091.
- Prols, F., Sagar, and Scaal, M. (2016). Signaling filopodia in vertebrate embryonic development. *Cellular and molecular life sciences : CMLS* 73, 961-974.
- Purich, D.L., and Allison, R.D. (1999). *Handbook of biochemical kinetics: a guide to dynamic processes in the molecular life sciences*. Academic Press.
- Qiu, X.B., and Goldberg, A.L. (2002). Nrdp1/FLRF is a ubiquitin ligase promoting ubiquitination and degradation of the epidermal growth factor receptor family member, ErbB3. *Proc Natl Acad Sci U S A* 99, 14843-14848.
- Rajan, S.S., Liu, H.Y., and Vu, T.Q. (2008). Ligand-bound quantum dot probes for studying the molecular scale dynamics of receptor endocytic trafficking in live cells. *ACS Nano* 2, 1153-1166.
- Redd, M.J., Cooper, L., Wood, W., Stramer, B., and Martin, P. (2004). Wound healing and inflammation: embryos reveal the way to perfect repair. *Philosophical Transactions of the Royal Society of London. Series B: Biological Sciences* 359, 777.
- Relich, P.K., Olah, M.J., Cutler, P.J., and Lidke, K.A. (2016). Estimation of the diffusion constant from intermittent trajectories with variable position uncertainties. *Phys Rev E* 93, 042401.
- Reth, M. (2013). Matching cellular dimensions with molecular sizes. *Nature immunology* 14, 765-767.
- Ridley, A.J. (2011). Life at the leading edge. *Cell* 145, 1012-1022.
- Ridley, A.J. (2015). Rho GTPase signalling in cell migration. *Current Opinion in Cell Biology* 36, 103-112.

- Ridley, A.J., Paterson, H.F., Johnston, C.L., Diekmann, D., and Hall, A. (1992). The small GTP-binding protein rac regulates growth factor-induced membrane ruffling. *Cell* 70, 401-410.
- Ridley, A.J., Schwartz, M.A., Burridge, K., Firtel, R.A., Ginsberg, M.H., Borisy, G., Parsons, J.T., and Horwitz, A.R. (2003). Cell Migration: Integrating Signals from Front to Back. *Science* 302, 1704.
- Rovensky, Y.A. (2011). Pseudopodia and Adhesion Structures. In: Adhesive Interactions in Normal and Transformed Cells, Totowa, NJ: Humana Press, 37-56.
- Roy, S., Huang, H., Liu, S., and Kornberg, T.B. (2014). Cytoskeleton-mediated contact-dependent transport of the Drosophila decapentaplegic signaling protein. *Science* 343, 1244624.
- Rubin, I., and Yarden, Y. (2001). The basic biology of HER2. *Annals of oncology : official journal of the European Society for Medical Oncology* 12 Suppl 1, S3-8.
- Rust, M.J., Bates, M., and Zhuang, X. (2006). Sub-diffraction-limit imaging by stochastic optical reconstruction microscopy (STORM). *Nat Meth* 3, 793-796.
- Sahai, E. (2007). Illuminating the metastatic process. *Nat Rev Cancer* 7, 737-749.
- Sanders, T.A., Llagostera, E., and Barna, M. (2013). Specialized filopodia direct long-range transport of SHH during vertebrate tissue patterning. *Nature* 497, 628-632.
- Saurabh, S., Beck, L.E., Maji, S., Baty, C.J., Wang, Y., Yan, Q., Watkins, S.C., and Bruchez, M.P. (2014). Multiplexed modular genetic targeting of quantum dots. *ACS Nano* 8, 11138-11146.
- Schneider, C.A., Rasband, W.S., and Eliceiri, K.W. (2012). NIH Image to ImageJ: 25 years of image analysis. *Nat Methods* 9, 671-675.

- Schwartz, S.L., Yan, Q., Telmer, C.A., Lidke, K.A., Bruchez, M.P., and Lidke, D.S. (2015). Fluorogen-activating proteins provide tunable labeling densities for tracking FcepsilonRI independent of IgE. *ACS Chem Biol* *10*, 539-546.
- Scott, J.D., and Pawson, T. (2009). Cell Signaling in Space and Time: Where Proteins Come Together and When They're Apart. *Science* *326*, 1220-1224.
- Shibue, T., Brooks, M.W., Inan, M.F., Reinhardt, F., and Weinberg, R.A. (2012). The outgrowth of micrometastases is enabled by the formation of filopodium-like protrusions. *Cancer discovery* *2*, 706-721.
- Singh, J.C., Jhaveri, K., and Esteva, F.J. (2014). HER2-positive advanced breast cancer: optimizing patient outcomes and opportunities for drug development. *British journal of cancer* *111*, 1888-1898.
- Slamon, D.J., Godolphin, W., Jones, L.A., Holt, J.A., Wong, S.G., Keith, D.E., Levin, W.J., Stuart, S.G., Udove, J., Ullrich, A., and et al. (1989). Studies of the HER-2/neu proto-oncogene in human breast and ovarian cancer. *Science* *244*, 707-712.
- Smith, C.S., Joseph, N., Rieger, B., and Lidke, K.A. (2010). Fast, single-molecule localization that achieves theoretically minimum uncertainty. *Nat Meth* *7*, 373-375.
- Sorkin, A., Di Fiore, P.P., and Carpenter, G. (1993). The carboxyl terminus of epidermal growth factor receptor/erbB-2 chimerae is internalization impaired. *Oncogene* *8*, 3021-3028.
- Sousa, A.D., and Cheney, R.E. (2005). Myosin-X: a molecular motor at the cell's fingertips. *Trends in cell biology* *15*, 533-539.
- Spector, I., Shochet, N.R., Kashman, Y., and Groweiss, A. (1983). Latrunculins: novel marine toxins that disrupt microfilament organization in cultured cells. *Science* *219*, 493.

- Steeg, P.S., Camphausen, K.A., and Smith, Q.R. (2011). Brain metastases as preventive and therapeutic targets. *Nat Rev Cancer* *11*, 352-363.
- Steffen, A., Stradal, T.E., and Rottner, K. (2017). Signalling Pathways Controlling Cellular Actin Organization. *Handbook of experimental pharmacology* *235*, 153-178.
- Sundara Rajan, S., and Vu, T.Q. (2006). Quantum dots monitor TrkA receptor dynamics in the interior of neural PC12 cells. *Nano Lett* *6*, 2049-2059.
- Svitkina, T.M., Verkhovskiy, A.B., McQuade, K.M., and Borisy, G.G. (1997). Analysis of the Actin–Myosin II System in Fish Epidermal Keratocytes: Mechanism of Cell Body Translocation. *The Journal of Cell Biology* *139*, 397.
- Szent-Gyorgyi, C., Schmidt, B.F., Creeger, Y., Fisher, G.W., Zakel, K.L., Adler, S., Fitzpatrick, J.A., Woolford, C.A., Yan, Q., Vasilev, K.V., Berget, P.B., Bruchez, M.P., Jarvik, J.W., and Waggoner, A. (2008). Fluorogen-activating single-chain antibodies for imaging cell surface proteins. *Nat Biotechnol* *26*, 235-240.
- Tada, H., Higuchi, H., Wanatabe, T.M., and Ohuchi, N. (2007). In vivo real-time tracking of single quantum dots conjugated with monoclonal anti-HER2 antibody in tumors of mice. *Cancer Res* *67*, 1138-1144.
- Tan, V.Y., Lewis, S.J., Adams, J.C., and Martin, R.M. (2013). Association of fascin-1 with mortality, disease progression and metastasis in carcinomas: a systematic review and meta-analysis. *BMC medicine* *11*, 52.
- Tebbutt, N., Pedersen, M.W., and Johns, T.G. (2013). Targeting the ERBB family in cancer: couples therapy. *Nat Rev Cancer* *13*, 663-673.
- Treanor, B., Depoil, D., Gonzalez-Granja, A., Barral, P., Weber, M., Dushek, O., Bruckbauer, A., and Batista, F.D. (2010). The membrane skeleton controls diffusion dynamics and signaling through the B cell receptor. *Immunity* *32*, 187-199.

- Tzahar, E., Waterman, H., Chen, X., Levkowitz, G., Karunakaran, D., Lavi, S., Ratzkin, B.J., and Yarden, Y. (1996). A hierarchical network of interreceptor interactions determines signal transduction by Neu differentiation factor/neuregulin and epidermal growth factor. *Molecular and cellular biology* *16*, 5276-5287.
- Valley, C.C., Arndt-Jovin, D.J., Karedla, N., Steinkamp, M.P., Chizhik, A.I., Hlavacek, W.S., Wilson, B.S., Lidke, K.A., and Lidke, D.S. (2015). Enhanced dimerization drives ligand-independent activity of mutant epidermal growth factor receptor in lung cancer. *Molecular biology of the cell* *26*, 4087-4099.
- Venter, D.J., Tuzi, N.L., Kumar, S., and Gullick, W.J. (1987). Overexpression of the c-erbB-2 oncoprotein in human breast carcinomas: immunohistological assessment correlates with gene amplification. *Lancet (London, England)* *2*, 69-72.
- Vermehren-Schmaedick, A., Krueger, W., Jacob, T., Ramunno-Johnson, D., Balkowiec, A., Lidke, K.A., and Vu, T.Q. (2014). Heterogeneous Intracellular Trafficking Dynamics of Brain-Derived Neurotrophic Factor Complexes in the Neuronal Soma Revealed by Single Quantum Dot Tracking. *PLOS ONE* *9*, e95113.
- Vicario, R., Peg, V., Morancho, B., Zacarias-Fluck, M., Zhang, J., Martínez-Barriocanal, Á., Navarro Jiménez, A., Aura, C., Burgues, O., Lluch, A., Cortés, J., Nuciforo, P., Rubio, I.T., Marangoni, E., Deeds, J., Boehm, M., Schlegel, R., Tabernero, J., Mosher, R., and Arribas, J. (2015). Patterns of HER2 Gene Amplification and Response to Anti-HER2 Therapies. *PLOS ONE* *10*, e0129876.
- Vignjevic, D., Kojima, S., Aratyn, Y., Danciu, O., Svitkina, T., and Borisy, G.G. (2006). Role of fascin in filopodial protrusion. *J Cell Biol* *174*, 863-875.
- Vignjevic, D., Schoumacher, M., Gavert, N., Janssen, K.P., Jih, G., Lae, M., Louvard, D., Ben-Ze'ev, A., and Robine, S. (2007). Fascin, a novel target of beta-catenin-TCF signaling, is expressed at the invasive front of human colon cancer. *Cancer Res* *67*, 6844-6853.

- Vivanco, I., and Sawyers, C.L. (2002). The phosphatidylinositol 3-Kinase AKT pathway in human cancer. *Nat Rev Cancer* 2, 489-501.
- Vu, T., and Claret, F.X. (2012). Trastuzumab: Updated Mechanisms of Action and Resistance in Breast Cancer. *Frontiers in Oncology* 2, 62.
- Vu, T.Q., Lam, W.Y., Hatch, E.W., and Lidke, D.S. (2015). Quantum dots for quantitative imaging: from single molecules to tissue. *Cell and tissue research* 360, 71-86.
- Wakatsuki, T., Schwab, B., Thompson, N.C., and Elson, E.L. (2001). Effects of cytochalasin D and latrunculin B on mechanical properties of cells. *J Cell Sci* 114, 1025-1036.
- Wang, D., Agrawal, A., Piestun, R., and Schwartz, D.K. (2017a). Enhanced information content for three-dimensional localization and tracking using the double-helix point spread function with variable-angle illumination epifluorescence microscopy. *Applied Physics Letters* 110, 211107.
- Wang, Y., Ballou, B., Schmidt, B.F., Andreko, S., St Croix, C.M., Watkins, S.C., and Bruchez, M.P. (2017b). Affibody-targeted fluorogen activating protein for in vivo tumor imaging. *Chemical communications (Cambridge, England)* 53, 2001-2004.
- Wang, Y., Telmer, C.A., Schmidt, B.F., Franke, J.D., Ort, S., Arndt-Jovin, D.J., and Bruchez, M.P. (2015). Fluorogen activating protein-affibody probes: modular, no-wash measurement of epidermal growth factor receptors. *Bioconjug Chem* 26, 137-144.
- Watanabe, T.M., Tokuo, H., Gonda, K., Higuchi, H., and Ikebe, M. (2010). Myosin-X induces filopodia by multiple elongation mechanism. *J Biol Chem* 285, 19605-19614.
- Wood, W., Jacinto, A., Grose, R., Woolner, S., Gale, J., Wilson, C., and Martin, P. (2002). Wound healing recapitulates morphogenesis in *Drosophila* embryos. *Nature cell biology* 4, 907-912.

- Wu, X., Liu, H., Liu, J., Haley, K.N., Treadway, J.A., Larson, J.P., Ge, N., Peale, F., and Bruchez, M.P. (2003). Immunofluorescent labeling of cancer marker Her2 and other cellular targets with semiconductor quantum dots. *Nat Biotechnol* 21, 41-46.
- Xu, K., Babcock, H.P., and Zhuang, X. (2012). Dual-objective STORM reveals three-dimensional filament organization in the actin cytoskeleton. *Nat Methods* 9, 185-188.
- Yamaguchi, H., and Condeelis, J. (2007). Regulation of the actin cytoskeleton in cancer cell migration and invasion. *Biochimica et biophysica acta* 1773, 642-652.
- Yamaguchi, H., Wyckoff, J., and Condeelis, J. (2005). Cell migration in tumors. *Current Opinion in Cell Biology* 17, 559-564.
- Yang, C., and Svitkina, T. (2011). Filopodia initiation: focus on the Arp2/3 complex and formins. *Cell Adh Migr* 5, 402-408.
- Yang, S., Huang, F.K., Huang, J., Chen, S., Jakoncic, J., Leo-Macias, A., Diaz-Avalos, R., Chen, L., Zhang, J.J., and Huang, X.Y. (2013). Molecular mechanism of fascin function in filopodial formation. *J Biol Chem* 288, 274-284.
- Yarden, Y. (2001). Biology of HER2 and its importance in breast cancer. *Oncology* 61 *Suppl* 2, 1-13.
- Yarden, Y., and Sliwkowski, M.X. (2001). Untangling the ErbB signalling network. *Nat Rev Mol Cell Biol* 2, 127-137.
- Yokotsuka, M., Iwaya, K., Saito, T., Pandiella, A., Tsuboi, R., Kohno, N., Matsubara, O., and Mukai, K. (2011). Overexpression of HER2 signaling to WAVE2-Arp2/3 complex activates MMP-independent migration in breast cancer. *Breast cancer research and treatment* 126, 311-318.

Zanet, J., Jayo, A., Plaza, S., Millard, T., Parsons, M., and Stramer, B. (2012). Fascin promotes filopodia formation independent of its role in actin bundling. *J Cell Biol* *197*, 477-486.

Zhang, Q., Park, E., Kani, K., and Landgraf, R. (2012). Functional isolation of activated and unilaterally phosphorylated heterodimers of ERBB2 and ERBB3 as scaffolds in ligand-dependent signaling. *Proc Natl Acad Sci U S A* *109*, 13237-13242.

Zhuravlev, P.I., Der, B.S., and Papoian, G.A. (2010). Design of Active Transport Must Be Highly Intricate: A Possible Role of Myosin and Ena/VASP for G-Actin Transport in Filopodia. *Biophysical Journal* *98*, 1439-1448.

Ziegler, Wolfgang H., Gingras, Alex R., Critchley, David R., and Emsley, J. (2008). Integrin connections to the cytoskeleton through talin and vinculin. *Biochemical Society Transactions* *36*, 235.

Zimmerberg, J., and Hess, S.T. (2011). Elongated membrane zones boost interactions of diffusing proteins. *Cell* *146*, 501-503.